THE EFFECTS OF ASPHALT BINDER OXIDATION ON HOT MIX ASPHALT CONCRETE MIXTURE RHEOLOGY AND FATIGUE PERFORMANCE

A Dissertation

by

SUNG HOON JUNG

Submitted to the Office of Graduate Studies of
Texas A&M University
in partial fulfillment of the requirements for the degree of

DOCTOR OF PHILOSOPHY

August 2006

Major Subject: Chemical Engineering

THE EFFECTS OF ASPHALT BINDER OXIDATION ON HOT MIX ASPHALT CONCRETE MIXTURE RHEOLOGY AND FATIGUE PERFORMANCE

A Dissertation

by

SUNG HOON JUNG

Submitted to the Office of Graduate Studies of
Texas A&M University
in partial fulfillment of the requirements for the degree of

DOCTOR OF PHILOSOPHY

Approved by:

Chair of Committee, Charles J. Glover
Committee Members, Richard R. Davison
Amy Epps Martin
M. Sam Mannan
Head of Department, Kenneth R. Hall

August 2006

Major Subject: Chemical Engineering

ABSTRACT

The Effects of Asphalt Binder Oxidation on Hot Mix Asphalt Concrete Mixture Rheology and Fatigue Performance. (August 2006)

Sung Hoon Jung, B.E., Soongsil University;

M.E., Texas A&M University

Chair of Advisory Committee: Dr. Charles J. Glover

Asphalt oxidation causes major changes to binder properties and is hypothesized to be a major contributor to age-related pavement failure such as fatigue cracking. Extensive laboratory aging research has been done to assess the effects of oxidation on binder properties. Previous work shows binder oxidation makes the binder stiffer and more brittle, leading to higher binder stresses under a given deformation. Failure occurs when these stresses exceed the strength of the binder. However, binder oxidation in pavements has not been studied in the same detail as laboratory aging of neat binders. The impact of binder oxidation on long-term pavement performance has been either underestimated or ignored.

This research includes studies of binder oxidation in Texas pavements to compare the field aging with laboratory neat binder aging, the impact of binder oxidation on HMAC mixture aging and HMAC mixture fatigue performance, and fundamental rheological property changes of the binder and the mixture.

Binder oxidation is studied in fifteen pavements from locations across Texas. Results indicate that unmodified binders in pavements typically oxidize and harden to a degree that exceeds generally accepted pavement aging assumptions. This hardening may also extend much deeper into the pavement than has been previously assumed or documented. Data suggest that pavements can oxidize at rates surprisingly uniform with depth once early oxidation occurs, and that these rates continue for an extended time.

Laboratory-aged HMAC mixtures and binders were tested and analyzed for fatigue resistance and their rheological properties. Mixture aging shows the same aging

mechanisms as neat binder aging. Both binder and mixture have a higher modulus with aging and a good rheological correlation. The decline in mixture fatigue life (determined using the calibrated mechanistic fatigue analysis approach with surface energy measurement) due to oxidation is significant. Pavement service life is dependent on the mixture, but can be estimated by a cumulative damage approach that considers binder oxidation and pavement loading rate simultaneously. The differences in expected pavement life arise from differences in the rate of binder stiffening due to oxidation and the impact of this stiffening on the decline of fatigue life.

DEDICATION

First, I would like to announce my appreciation to God for His grace, guidance and protection of my family and me during my Ph.D. study. I dedicate this dissertation to my parents, Moo-young and Gyung-ja, my wife, Ryung, and my two daughters, Hamin and Soomin, for their love, encouragement and support.

ACKNOWLEDGMENTS

I would like to express my deep gratitude to my advisor, Dr. Charles J. Glover, for his support and guidance through my graduate studies; I could not have completed this work without his help. Simply watching him and how he manages his time and work has increased my learning and understanding of research as well as life itself. I would also like to thank Dr. Richard R. Davison for all his contributions to our research group and his amazing ability which has served as an inspiration to me. I also appreciate Dr. Amy Epps Martin for showing me how to organize and solve our research problems and Dr. M. Sam Mannan for his encouragement and support.

It is impossible for me to forget mentioning my appreciation of my research group members. I owe a great debt to Wonjun Woo, Nikornpon Prapaitrakul, Tyner Devine, Yonghong Ruan, Nasser Al-Azri, Pramitha Juristyarini, Lubinda Walubita and Richard Canatella. I also would like to thank Dr. Rayford G. Anthony, Dr. William Rogers, Dr. David Ford and Mrs. Towanna Hubacek for their help and support.

I also want to thank my friends who have shared ideas, fun and inspiration: Jun-Yen Tewg, Sukjoon Yoo, Josh Bush, Jin-soo Uh, Roger Lo, Sungmun Lee, Sehoon Kim, Jon Lunn, Kunwoo Han, Seunguk Yeu, Sung Hyun Kim, Won Jae Lee, Seoung-ju Lee, Won-huyk Jang, Kyosik Park and Sung Gil Kim. I also hope God would bless my church family: Pastor Tim Owens, David Scott Wilson and his family, Travis Angel and his family, Mr. and Mrs. Lancaster, and Sara Cutshall. Furthermore, I would like to thank my TAMU Kumdo (Kendo) Club members for their devotions and prayers.

Finally, I appreciate my parents-in-law for giving me an amazing wife and my brother, Sehoon, who has taken my responsibilities along with his own, to serve our parents in my absence.

All the support from these precious people made my study and achievement possible. Thank God for letting me have such blessings.

NOMENCLATURE

$a_T(T)$	Shift Factor at Temperature T relative to the Reference Temperature
E(t)	Time Dependent Elastic Modulus
f_c	Fraction of a Consumed Pavement Service Life
f_r	Fraction of a Remaining Pavement Service Life (1- f_c)
G_1	Initial Shear Modulus
G'(ω)	Elastic (storage) Dynamic Shear Modulus
G"(ω)	Viscous (loss) Dynamic Shear Modulus
G*(ω)	Complex Dynamic Shear Modulus
G'/(η'/G')	DSR Function
N_i	Number of Load Cycles to Crack Initiation
N_f	Fatigue Life or Number of Load Cycles to Fatigue Failure
N_p	Number of Load Cycles to Crack Propagation
Pc	Aggregate Contact Volume
r_η	Binder Hardening Rate
r_{CA}	Binder Oxidation Rate (Rate of Carbonyl Area Formation)
R_L	Pavement Loading Rate
S_{mix}	Initial Mixture Stiffness
SF_a	Shift Factor due to Anisotropy
SF_h	Shift Factor due to Healing Effects
t_r	Reduced Time
ε	Strain
Γ	Gamma Function.
η'(ω)	Dynamic Shear Viscosity
υ	Poisson's Ratio
σ_t	Tensile Stress
ω	Angular Frequency

TABLE OF CONTENTS

CHAPTER Page

CHAPTER Page

Page

LIST OF FIGURES

Page

Page

LIST OF TABLES

Page

CHAPTER I
INTRODUCTION

Dissertation Outline

This dissertation consists of six chapters. It begins with a general introduction and research background in the Chapter I. In the following chapters, the results from this research about the binder oxidation in pavements, and the effects of binder oxidation on the HMAC mixture fatigue performance, pavement service life and rheological properties are described. Chapter II contains a study of binder oxidative aging in Texas pavements. Chapter III compares the laboratory aging with mixture aging and shows the impact of binder oxidation on mixture fatigue performance. Chapter IV provides a method of estimating the effect of binder oxidation on a pavement service life by using cumulative damage approach. Chapter V describes the binder-mixture characterization with binder oxidation. Chapter VI summarizes the findings and conclusions of this study.

Introduction

Asphalt binder is man's oldest engineering material; its adhesive and waterproofing properties were known at the dawn of civilization (Barth, 1962). Before the patriarchal age, it was used as water proofing material. Noah as a ship builder used pitch for sealing his Ark in Genesis 6: 14 (NIV). An ancient civilization in the Indus Valley used asphalt binder in the construction of large public baths or tanks about 3000 B.C (Roberts et al., 1996). The first use of asphalt as a road building material was in Babylon around 625 B.C., in the reign of King Nebuchadnezzar (Gillespie and Crawford, 1992).

The dissertation follows the style of the *AIChE Journal*.

The first true asphalt pavement was laid in the United States, a sand mix in front of the City Hall in Newark, New Jersey, in 1870. Now, there are more than 2.5 million miles of paved roads in the United States (FHWA, 2001). According to the National Asphalt Pavement Association (NAPA), asphalt binder is used in more than 94 percent of the paved roads in the United States.

In spite of this remarkable growth and development in the use of asphalt pavement, engineers face many obstacles to building long-term durable asphalt pavements. Typical problems in asphalt pavements are rutting, thermal cracking and fatigue cracking. Rutting is the permanent deformation occurring due to heavy traffic at higher temperature several years after pavement construction (Huber and Decker, 1995) and thermal cracking results from thermal stresses generated by pavement shrinkage at cold temperature (Hardin, 1995). Fatigue cracking is generally believed to result from repeated loading. However, binder oxidation may play a significant role.

The impact of binder oxidation has been either underestimated or ignored in its role in pavement long-term fatigue performance. Most of HMAC mixture fatigue study depends on notable conclusions by Coons and Wright (1968). They concluded that most of the aging occurred in the top quarter inch of the pavement but at 1.5 inches below the surface, very little hardening occurred after the initial increase at placement, which is contrary to recent studies (Al-Azri et al., 2006; Glover et al., 2005). More details are presented in the chapter two.

Over the past fifteen years, much has been learned about binder oxidation and its impact on binder hardening and durability. In the laboratory, binder oxidation hardening and reaction kinetics in thin films have been determined for a large number of asphalt binders (Lau et al., 1992, Liu et al., 1996, Domke et al., 2000). The description of hardening susceptibility has been further developed using a rheological function of the binder's elastic and viscous properties (Glover et al., 2005; Juristyarini, 2003). The latter function, also called DSR Function has been shown to relate to binder brittleness under elongation (Ruan et al., 2003b). The studies show that binder oxidative hardening

continues indefinitely and binder oxidation is a major contributor to age-related pavement failure.

While laboratory aging of asphalt binders has been studied extensively, aging of binders in pavements is much less well understood because of a number of complications. Such complications include suitable extraction and recovery methods; uncontrolled variables and unknowns such as mixture characteristics (air voids, e.g.), maintenance treatments, traffic, and climate; sustaining a research effort to study a given pavement over an appropriate time frame (in excess of one decade); and cost. Binder oxidation in the field is studied to find the level of hardening reached in pavements and to compare with laboratory binder aging.

In addition to the binder studies, extensive studies have been performed to predict mixture resistance to fatigue under repeated loads. However, there is no study to explain the effects of binder oxidation on HMAC mixture fatigue performance. It is necessary to study the influence of binder oxidation on HMAC mixture fatigue performance to determine the binder aging effects on pavement fatigue performance. Therefore, a method of measuring the impact of binder oxidation on pavement service life is studied to provide a more reasonable estimation of pavement service time for the development of mixture design, pavement construction and maintenance.

While binder oxidation has a great potential impact on HMAC mixture fatigue performance, the fundamental properties of binders and mixtures which affect HMAC mixture fatigue performance are unknown. In this study, the fundamental rheological properties of binders and their mixtures were investigated to establish binder-mixture relationships with binder oxidation.

In short, this research concentrates on the impact of binder oxidation on binder aging in the field to compare with that in the laboratory. The impact of binder oxidation on HMAC mixture fatigue performance is studied. A new method of estimating the effect of binder oxidation in the pavement service life is provided. The fundamental rheological relationships between binders and HMAC mixtures due to binder oxidation are investigated.

Objectives

This research focused on the effect of binder oxidation on binder hardening in asphalt pavements, HMAC mixture fatigue performance and fundamental rheological properties of both binders and mixtures. The specific objectives of the research were:

1. To determine the state of binder in field pavements over time and with depth
2. To determine the impact of binder oxidation on the fatigue performance of HMAC mixtures
3. To describe the effect of binder oxidation on field fatigue performance using a cumulative damage approach
4. To develop relationships between the fundamental rheological properties of HMAC mixtures and binders

The research background for the above research objectives is divided into four sections. The first section describes binder oxidation hardening and reaction kinetics. The second section reviews binder oxidation and embrittlement. The third section discusses fatigue prediction models of asphalt mixtures. The last section presents binder mixture characterization.

Binder Oxidation Hardening and Reaction Kinetics

Binder oxidation greatly affects the physical and chemical properties of binders and over time makes binders harder and stiffer (Lau et al., 1992; Liu et al., 1998a; Martin et al., 1990). As binders oxidize, carbonyl (– C=O) groups are formed that increase the polarity of their host compounds and make them much more likely to associate with other polar compounds (Liu et al., 1998a; Liu et al., 1998b). As they form these associations, they create less soluble asphaltene materials, the formation of which leads to asphalt hardening.

The binder hardening rate can be expressed as follows:

$$r_\eta = \frac{\partial \ln \eta}{\partial t} = \frac{\partial \ln \eta}{\partial AS} \cdot \frac{\partial AS}{\partial \mathrm{CA}} \cdot \frac{\partial \mathrm{CA}}{\partial t} \tag{I-1}$$

Three terms in Equation I-1 are important characteristics of asphalt binder that are dependent on its chemical composition. $\partial \ln \eta / \partial AS$ is the effect of asphaltene (*AS*) increase on increasing viscosity and is affected by asphaltene size (Lin et al., 1996). $\partial AS / \partial \mathrm{CA}$ is the asphaltene formation susceptibility (AFS) that is a measure of the capacity of the maltene to produce new asphaltenes with aging. $\partial \mathrm{CA} / \partial t$ is the rate of carbonyl area (CA) formation, also called binder oxidation rate (Lin et al., 1996; Lin et al., 1995).

CA is the area under the absorption band from 1650 to 1820 cm^{-1} and relates directly to the oxygen content in the asphalt binder. The increases in CA are used to quantify oxidative aging (Jemison et al., 1990; Liu et al., 1998a). The increase of binder oxidation as well as binder hardening has a linear correlation with oxidation time after the early rapid aging stage that is called the initial jump (Lau et al., 1992). These relationships are in Equations I-2 and I-3.

$$\mathrm{CA} = \mathrm{CA}_0 + r_{\mathrm{CA}} t \tag{I-2}$$

$$\ln \eta^* = \ln \eta_0^* + r_\eta t \tag{I-3}$$

where CA is carbonyl area; CA_0 is the carbonyl area intercept at t=0; r_{CA} is the binder oxidation rate; η^* is the limiting complex viscosity; η_0^*= is the limiting complex viscosity intercept at t=0; r_η= binder hardening rate; t= the time of oxidation. Both binder hardening rate and oxidation rate also followed an Arrhenius equation (Domke et al., 2000; Lin et al., 1996; Liu et al., 1996):

$$r_n = \frac{\partial n}{\partial t} = AP^{\alpha} Exp(-E_n / RT) \quad \text{(I-4)}$$

where subscript n is CA or η, A is the pre-exponential factor, P is the pressure, α is the reaction order with respect to oxygen pressure, E_n is the activation energy, R is the gas Constant, and T is the absolute temperature.

Combining the first two terms in Equation I-1 gives $\partial \ln \eta / \partial CA$ which is defined as Hardening susceptibility (HS) (Domke et al., 1999; Lau et al., 1992). HS is the impact of CA growth on the binder viscosity. Equation I-1 can be simplified as:

$$r_\eta = HS \cdot r_{CA} \quad \text{(I-5)}$$

HS is independent of oxidation temperature below about 100-110 ^{o}C and is a characteristic parameter for asphalt binder with aging process under constant pressure (Lau et al., 1992).

Binder oxidation hardening and kinetic in laboratory aging has been reviewed in this section. The following section introduces the previous study of relationships between binder oxidation and Embrittlement.

Binder Oxidation and Embrittlement

As briefly introduced in the general introduction section, binder oxidation has a significant impact on age-related pavement failure. Through oxidation, the binder becomes stiffer and more brittle and thus reduces the performance of flexible pavements (Domke et al., 2000; Petersen et al., 1993). The process is relentless and thus, over time, can destroy the pavement.

The composition change of binder due to oxidation, taken far enough, results in orders-of-magnitude increases in both the binder's viscous and elastic properties (Ruan et al., 2003b). Thus the oxidized binder sustains high shear stress with deformation (high

elastic stiffness) and simultaneously the material cannot relieve the stress by flow (high viscosity), resulting in a pavement that is very brittle and susceptible to fatigue and thermal cracking.

A literature review emphasizes the importance of a binder's ductility to pavement durability (Clark, 1958; Doyle, 1958; Halstead, 1963; Kandhal, 1977; Kandhal and Koehler, 1984; Kandhal and Wenger, 1975). This previous research indicates that asphalt binder ductility correlates quite well with pavement cracking, provided it is measured at the low temperature (15 ^{o}C). Several studies report that a value of the 15 °C ductility at 1 cm/min in the range of 2 to 3 cm corresponds to a critical level for age-related cracking in pavements (Doyle, 1958; Kandhal, 1977; Kandhal and Koehler, 1984; Kandhal and Wenger, 1975).

Even though ductility correlates well with cracking failure of asphalt pavements, the ductility test is time consuming and needs about 20 grams of binder, which is not always practical for binders recovered from laboratory mixtures. Thus, a correlation between ductility and Dynamic Shear Rheometer (DSR) measurement was investigated (Ruan et al., 2003b).

Maxwell Model

The Maxwell model is a very simple way of explaining, in a qualitative sense, the essence of the impact of this increase in both elastic stiffness and viscosity on elongational flow of a binder. The model is that of an elastic spring in series with a viscous dashpot element as shown in Figure I-1.

The stress that builds in the combined element is the result of the balance between the elastic modulus and the viscosity. Upon elongation, the stress versus elongation response rises in response to the elastic spring but then goes through a maximum value before decaying over time in response to viscous flow. The value of the maximum stress depends upon the relative values of the elastic modulus and the viscosity. The higher their values, the higher the maximum stress; the lower the values,

the lower the maximum stress. If the maximum stress exceeds the failure stress of the material, then failure occurs.

$$\sigma_t + \frac{\eta_e}{E}\frac{d\sigma_t}{dt} = \eta_e \frac{d\varepsilon}{dt}$$

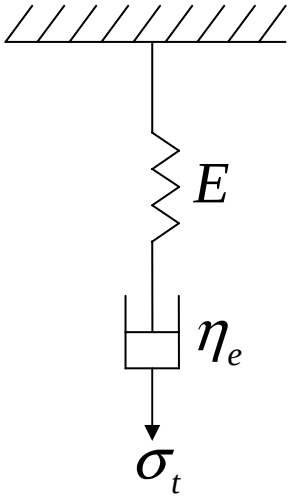

Figure I-1. The Maxwell Model.

This Maxwell model is very simple and certainly is too simple to quantitatively characterize asphalt materials, but it still captures the basic elements that are important to determining binder failure that occurs due to oxidation and embrittlement. As asphalts oxidize, they harden, and this is a process that simultaneously increases its elastic stiffness and its viscosity.

Consequently, in the context of the Maxwell model, with aging and consequent hardening, a binder cannot take as much deformation without building to a stress level that results in its failure stress being exceeded. So, as binders age harden, their ductilities decrease dramatically. The binder ductility for a newly constructed pavement may be of the order of 30 cm (15 °C, 1 cm/min) whereas the binder ductility of a heavily aged pavement will be much lower, down to 3 cm or less.

To correlate the ductility to DSR measurement, the equation in Figure I-1 was converted to Equation I-6 by transforming the independent variable time to the elongation ratio.

$$\left(\frac{L_0}{U_0}\right)\left(\frac{E}{\eta_e}\right)\sigma_t + \frac{d\sigma_t}{d\left(L/L_0\right)} = \frac{E}{\left(L/L_0\right)} \tag{I-6}$$

where σ_t is the total tensile stress since the ductility test is a tensile test, L_0 is the initial length of the binder, L/L_0 is the elongation ratio, U_0 is the constant elongation ratio rate (dL/dt= 1cm/min), E is the elastic modulus and η_e is the elongational viscosity.

The elastic modulus (E) is converted to shear modulus (G) by equation I-7, assuming Poisson's ratio (υ) is 0.5 for an incompressible material (Ferry, 1980; Glover and Jones, 1996; Rosen, 1993).

$$E = 2G\left(1+\upsilon\right) \tag{I-7}$$

The elongational viscosity (η_e) is converted to shear viscosity (η) by Trouton's rule (η_e=3η). Then, Equation I-6 becomes Equation I-8 where α is the elongation ratio (L/L_0). This equation shows binder ductility is not only related to just one parameter like the shear modulus G, but both parameters, G and η/G.

$$\left(\frac{L_0}{U_0}\right)\left(\frac{G}{\eta}\right)\sigma_t + \frac{d\sigma_t}{d\alpha} = \frac{3G}{\alpha} \tag{I-8}$$

DSR Function

The embrittlement of binders had been captured with the discovery of a correlation between binder ductility (measured at 15 °C, 1 cm/min) and binder DSR properties (dynamic elastic shear modulus, G' and dynamic shear viscosity, η') (Glover et al., 2005; Ruan et al., 2003b). In Figure I-2, a very good correlation exists between binder ductility and DSR function (G'/(η'/G')) for ductilities less than 10 cm, demonstrating the interplay between elastic stiffness and ability to flow in determining binder brittleness, as discussed above in the context of the Maxwell model (Glover et al., 2005; Ruan et al., 2003b).

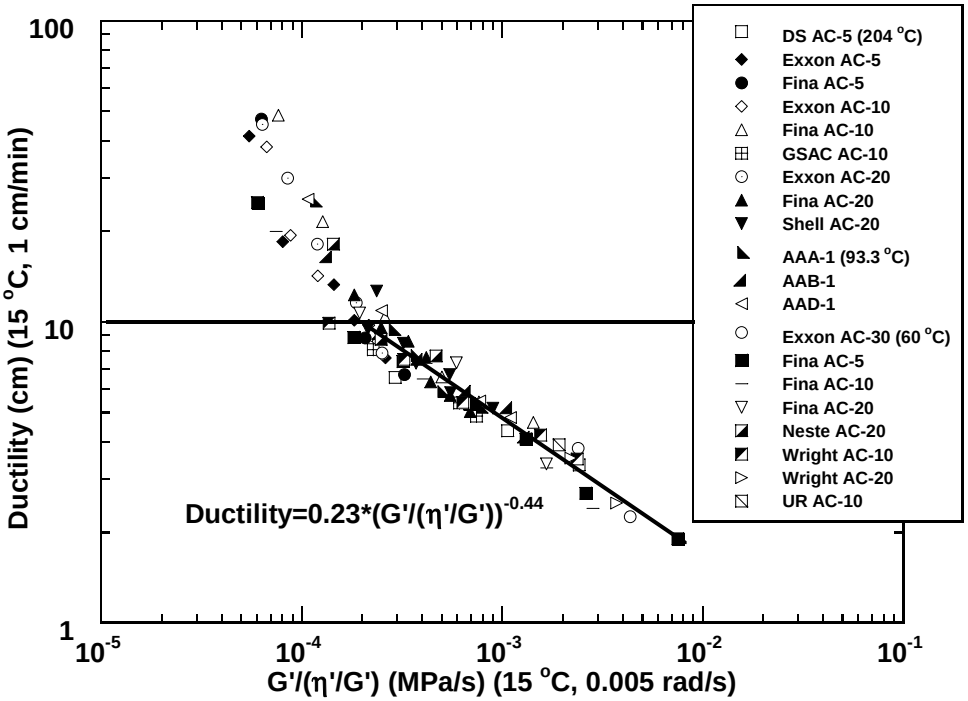

Figure I-2. Correlation of Aged-Binder Ductility with the DSR Function G'/(η'/G') for Unmodified Binders.

This correlation is depicted on a "DSR map" of G' versus η'/G' in Figure I-3 which shows the data with each material identified at different levels of aging (Ruan, 2002; Ruan et al., 2003b). The general trend is apparent. With increased aging, a binder moves from the lower right toward the upper left as the result of increases in both the elastic stiffness and viscosity but note that G' increases more than viscosity, η', because movement is toward the left to smaller values of η'/G'.

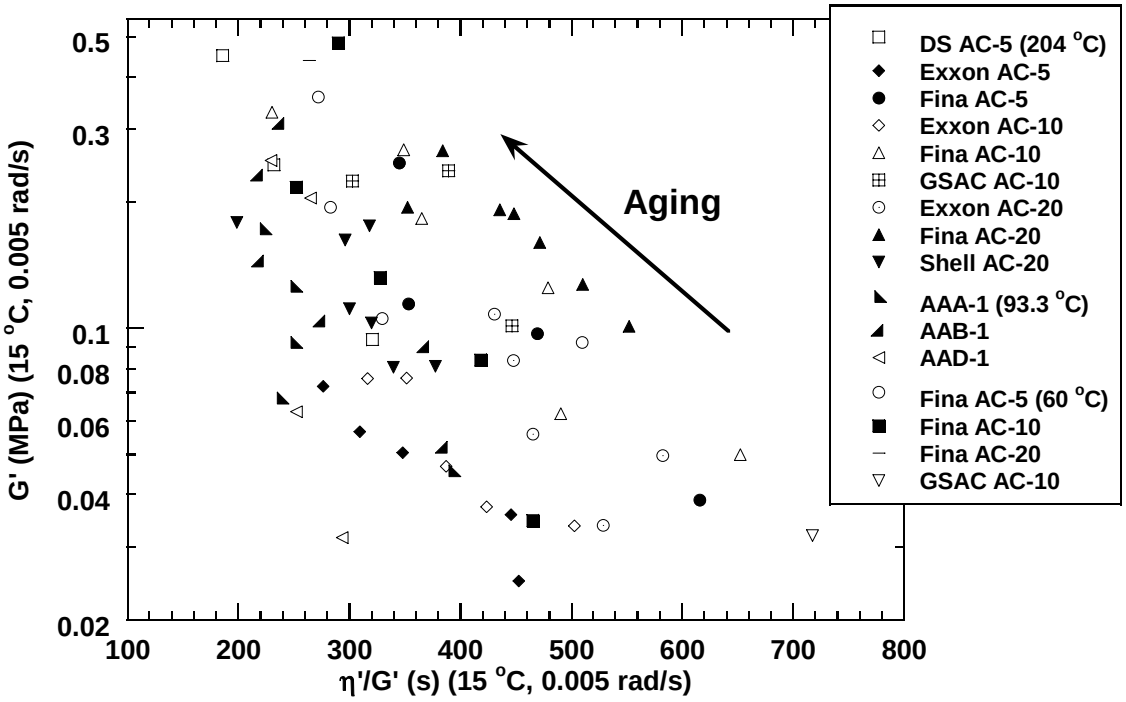

Figure I-3. DSR Map for Unmodified Binders.

Briefly, DSR function (G'/(η'/G')) is a rheological function combining two fundamental rheological parameters, G' and η'/G', and with DSR map, provides a new method to track the level of binder oxidation related to binder durability in asphalt pavements.

Fatigue Prediction Models of Asphalt Mixtures

Traditional Fatigue Analysis Models

The fatigue life of an asphalt mixture represents its ability to sustain its service life or resist repeated loading without fatigue failure. The fatigue characteristics of asphalt mixtures are commonly defined as relationships between the strain (or stress) and the number of load cycles to failure (fatigue life) through the following Equation I-9 (Monismith et al., 1985; Monismith et al., 1970). According to this power law, the fatigue life is related to the applied strain (representing loading level).

$$N_f = a\left(\varepsilon\right)^{-b} \tag{I-9}$$

where N_f is the number of load cycles to fatigue failure or fatigue life, ε is the applied strain and a and b are experimentally determined coefficients.

In addition to the fatigue life-strain relation, Monismith et al. (1985) noticed that the number of fatigue life cycles (N_f) decreased with the increase in asphalt mixture stiffness in a strain-controlled fatigue test. They included the effects of the stiffness of asphalt mixtures on asphalt mixture fatigue performance at an applied strain and characterized the fatigue life by the following model:

$$N_f = a\left(\varepsilon\right)^{-b}\left(S_{mix}\right)^{-c} \tag{I-10}$$

where S_{mix} is the initial asphalt mixture stiffness and a, b and c are experimentally determined coefficients.

This model can partly explain the effect of binder oxidation on asphalt mixture fatigue performance by relating binder oxidative hardening to mixture stiffening. As the binder in an asphalt mixture is hardened due to binder oxidation, the asphalt mixture is

stiffened and the fatigue life of the asphalt mixture decreases. However, this model is not sufficient to describe the impact of binder oxidation on the pavement fatigue performance.

While the stiffness of asphalt mixtures is an important parameter for the asphalt mixture fatigue performance, more parameters such as HMAC mixture design parameters, binder hardening rate, pavement structures, traffic conditions and environmental conditions should be considered to explain the impact of binder oxidation on the HMAC pavement fatigue performance. In the following section, a fatigue analysis approach which considers fundamental material properties and field conditions are described.

Calibrated Mechanistic (CMSE) Fatigue Analysis Model with Surface Energy

The CMSE fatigue analysis model is based on the fundamental theories which are the visco-elatic correspondence principle, Paris' Law fracture mechanics, Schapery's work potential theory and energy concepts to characterize HMAC mixture fatigue resistance (Kim et al., 1997a; Lytton et al., 1993; Schapery, 1984; Si, 2001). This approach utilizes fundamental material properties such as asphalt mixture tensile strength, stiffness, relaxation modulus in tension and compression, dissipated pseudo strain energy and surface energies for both binders and aggregates to characterize HMAC mixture fatigue resistance (Lytton et al., 1993).

In this CMSE approach, crack initiation and propagation processes for fatigue failure are related to stress-strain constitutive relations. Equation I-11 represents the CMSE model that relates field fatigue life to the number of load cycles to crack initiation and crack propagation with shift factors due to anisotropy and binder healing effects,

$$N_f = SF_a \times SF_h \left(N_i + N_p \right) \tag{I-11}$$

where SF_a is the shift factor due to anisotropy, ranging between 1 and 5, SF_h is the shift factor due to binder healing effects, ranging between 1 and 10, N_i is the number of load cycles to crack initiation, N_p is the number of load cycles to crack propagation and N_f is the number of load cycles to fatigue failure or fatigue life.

In Equation I-11, the summation of N_i and N_p produces the laboratory fatigue life and the shift factors product provides the field fatigue life. Because this approach measures fundamental asphalt mixture properties, it can be used to measure the asphalt mixture material properties at each aging level to estimate the field fatigue life with binder oxidation.

Binder Mixture Characterization

In addition to the impact of binder oxidation on the asphalt mixture fatigue performance, the impact of binder oxidation on the asphalt mixture rheological properties has been studied to understand the relationship of these mixture properties to changes in binder properties. In the next two sub-sections, previous studies of binder and mixture characterizations are described.

Binder Characterization

The storage (elastic) dynamic shear modulus (G'(ω)), loss dynamic shear modulus (G"(ω)) and complex dynamic shear modulus (G*(ω)) are fundamental rheological properties of which master curves have been used to characterize asphalt rheological behaviors (Lu and Isacsson, 1998; Lu and Isacsson, 1999; Palade et al., 2000; Ruan, 2002). The time-temperature superposition (TTSP) principle is used to create these rheological master curves.

TTSP was first developed by Williams, Landel, and Ferry in 1955 to describe the effect of time and temperature on the viscoelastic properties of amorphous polymers (Williams et al., 1955). The log shift factor is described as a function of the temperature

difference between measured and reference temperature in Equation I-12 (Ferry, 1980; Williams, 1971; Williams et al., 1955):

$$\log a_T = \frac{-C_1(T - T_{ref})}{(C_2 + T - T_{ref})} \tag{I-12}$$

where a_T is the shift factor at temperature (T) relative to the reference temperature (T_{ref}) and C_1 and C_2 are empirically determined coefficients.

HMAC Mixture Characterization

For HMAC mixture viscoelastic characterization, TTSP procedures and the power law model has been used in Equation I-13 (Lytton et al., 1993; Roque et al., 1994).

$$E(t_r) = E_\infty + E_1 t_r^{-m} \cong E_1 t_r^{-m} = E_1 \left(\frac{t}{a_T(T)} \right)^{-m} \tag{I-13}$$

where $E(t_r)$ is the time dependent elastic modulus at reduced time t_r, E_1 is the initial elastic modulus (t_r=1), t is time, T is temperature and $a_T(T)$ is the shift factor at temperature T relative to the T_{ref} .

The elastic modulus obtained by the relaxation modulus (RM) test is a function of time because of the viscoelastic nature of the HMAC mixture. Under deformation, the stress builds because of the mixture's elastic nature but then relaxes at fixed strain because of its ability to undergo viscous flow. This relaxation is reflected in the decrease of $E(t_r)$ over time. Therefore, storage (elastic) and loss (viscous) moduli can be calculated from the $E(t_r)$ master curve.

The elastic modulus $E(t_r)$ is converted to a shear modulus $G(t_r)$ according to Equation I-14 where υ is Poisson's ratio for the HMAC mixture (≅ 0.33) (Huang, 1993; Lytton et al., 1993), E_1 is the initial elastic modulus and G_1 is the initial shear modulus.

$$G(t_r) = \frac{E(t_r)}{2(1+\upsilon)},\ G_1 = \frac{E_1}{2(1+\upsilon)} \tag{I-14}$$

According to Lytton et al. (1993), the reduced time (t_r) is converted to an angular frequency (ω) according to Equation I-15.

$$\omega \cong \frac{1}{2t_r} \tag{I-15}$$

The elastic (storage) dynamic shear modulus (G'(ω)), viscous (loss) dynamic shear modulus (G"(ω)) and complex dynamic shear modulus (G*(ω)) can be calculated by Equations I-16 to I-18 where Γ is the Gamma function and m is the exponential stress relaxation rate (Lytton et al., 1993; Schapery, 1973).

$$G'(\omega) = G_1 \frac{\Gamma(1-m)}{\omega^{-m}} cos\left(\frac{m\pi}{2}\right) \tag{I-16}$$

$$G''(\omega) = G_1 \frac{\Gamma(1-m)}{\omega^{-m}} sin\left(\frac{m\pi}{2}\right) \tag{I-17}$$

$$G^*(\omega) = \sqrt{G'(\omega)^2 + G''(\omega)^2} \tag{I-18}$$

In this section, the study of the rheological master curves of asphalt binders and mixtures are reviewed to correlate rheological properties with binder oxidation

Summary

Binder oxidation changes physical and chemical properties of binders and makes binders harder and more susceptible to the brittle failure. DSR function (G'/(η'/G')) provides a good relation with binder's ductility which correlates quite well with long-term pavement durability, and with DSR map, a new method to track binder oxidation in field asphalt pavements. This study tries to determine the state of binders in field pavements over time.

The CMSE fatigue approach estimates the field fatigue life based on fundamental properties of asphalt mixtures. It is also utilized to calculate the field fatigue life with binder oxidation since it measures fundamental material properties. The impact of binder oxidation on HMAC mixture fatigue performance and a new way of estimating the effect of binder oxidation in field fatigue performance are studied in this research.

Asphalt binders and mixtures are viscoelastic materials. The rheological master curves of asphalt binders and mixtures have been used to characterize their material behaviors. In this study, the impact of binder oxidation on the other HMAC mixture properties besides fatigue is of interest in explaining HMAC mixture fatigue changes due to binder oxidation. The fundamental rheological relationships between binders and HMAC mixtures due to binder oxidation are investigated.

CHAPTER II
BINDER OXIDATIVE AGING IN TEXAS PAVEMENTS: HARDENING RATES, HARDENING SUSCEPTIBILITIES, AND THE IMPACT OF PAVEMENT DEPTH*

Synopsis

Aging of binders in pavements is much less well understood than laboratory aging of neat binders because of a number of complications including suitable extraction and recovery methods; uncontrolled variables and unknowns such as mixture characteristics (air voids, e.g.), maintenance treatments, traffic, and climate; sustaining a research effort to study a given pavement over an appropriate time frame (in excess of one decade); and cost.

An ongoing research effort sponsored by the Texas DOT studied fifteen pavements across Texas with respect to binder oxidative hardening. Results indicate that unmodified binders in pavements typically oxidize and harden to a degree that exceeds generally accepted pavement aging assumptions. This hardening also may extend much deeper into the pavement than has been previously assumed or documented. Data suggest that pavements can oxidize at surprisingly uniform rates with depth once early oxidation occurs, and that these rates continue for an extended time. As a rough measure, one month environmental room aging of 1 mm neat binder films at 60 °C was equivalent to about 15 months in SH 21 after the early higher hardening rate period.

* Reprinted with permission of TRB from "Binder Oxidative Aging in Texas Pavements: Hardening Rates, Hardening Susceptibilities, and the Impact of Pavement Depth," coauthored with N. A. Al-Azri, K. M. Lunsford, A. Ferry, J. A. Bullin, R. R. Davison, and C. J. Glover, Presented at the 85th Annual Meeting of the Transportation Research Board, January 22, 2006, Washington, D.C., and accepted for publication in the 2006 series of the *Transportation Research Record: Journal of the Transportation Research Board* (forthcoming). (See Appendix C)

Introduction

Many laboratory investigations have led to a detailed understanding of asphalt binder hardening in response to oxidation. The reaction kinetics as it relates to temperature and pressure, and the asphaltene growth that leads to this hardening are quite well understood (Lau et al., 1992; Lin et al., 1996; Lin et al., 1995). Physicochemical aspects have been studied as well (Domke et al., 1999; Domke et al., 2000; Lin et al., 1996; Petersen et al., 1993). The low shear rate viscosity hardening in response to oxidation (as measured by FTIR carbonyl growth) has been termed the hardening susceptibility (Martin et al., 1990; Petersen et al., 1993). Recently, unmodified binder decline in ductility with oxidation has been correlated to DSR property changes so that a binder's increase in brittleness due to oxidation can be estimated from the easier DSR measurements (Ruan et al., 2003b). All of this work provides significant tools for measuring and understanding binder oxidation and hardening.

Yet, in spite of all that is understood about the character of neat binder oxidation, much remains unknown about hardening in mixtures and its impact on pavement performance. That binders oxidize and harden in pavements is an accepted fact. That this hardening is related to performance characteristics such as fatigue cracking also has been reported. Perhaps the best correlations to pavement durability use ductility of the recovered binder to characterize the binder hardening (Clark, 1958; Doyle, 1958; Halstead, 1963; Kandhal, 1977; Kandhal and Koehler, 1984; Kandhal and Wenger, 1975). But what is not well characterized is the extent to which binders in pavements harden, the rates at which they harden, and the pavement depth to which significant hardening occurs.

One noted paper provides data on hardening versus depth to 1.75 inches for pavements that ranged in age from four to 151 months (Coons and Wright, 1968). The authors concluded that most of the aging occurred in the top quarter inch of the pavement and that at 1.5 inches below the surface, very little hardening occurred beyond the initial increase at placement.

These conclusions are adopted in the Global Aging Model (GAM) of Mirza and Witczak (Mirza and Witczak, 1995) and subsequently incorporated into the NCHRP mechanistic-empirical design guide (AASHTO, 2004). Furthermore, the GAM assumes a hyperbolic aging function so that the great bulk of the hardening occurs in the first 10 years of service.

One difficulty of the data upon which the above assumptions are based is that the solvent recovery process likely left enough solvent in the recovered binder to soften its properties significantly (Burr et al., 1990). Mirza and Witczak note that the recovery method for the materials in their master database typically was not noted in the reference sources, implying that needed modifications were not employed. Residual solvent levels will be greater for the more heavily aged binders. Thus, stiffer binders will be more affected by residual solvent, leading to a compression of binder properties and thus erroneously small relative viscosity values when tracking binder properties over time.

Finally, there have been few data that correlate laboratory binder aging to corresponding field properties or that assess the effect of aggregate. Actual field aging data are needed to relate field aging to laboratory rates, to determine if aging mechanisms are the same in both situations, and to establish the level of field aging that can be tolerated before failure occurs.

Objectives

This work represents a comprehensive effort conducted over more than a decade to address several significant issues of binder oxidation in pavements. Of specific interest was the level of hardening reached in pavements, both near the surface and four to six inches below the surface, the corresponding rates of hardening and hardening susceptibilities for field aging compared to laboratory aging of neat binders. Additionally, the march of a binder across the ductility-DSR map (Ruan et al., 2003b) with increasing oxidation in pavements was of interest to provide insight into the state of the binder over time.

Methodology

Field Pavements

Data were obtained from Texas Highway 21 between Bryan and Caldwell, ten Strategic Highway Research Program (SHRP) long-term pavement performance (LTPP) general pavement study (GPS) sites, and two other TxDOT pavements. In all, 15 pavements are reported and one (Texas Highway 21) was evaluated at eight different stations over a 15-year period.

Texas Highway 21

Texas Highway 21 (SH 21) is the most investigated pavement of this study. The construction of this road, a four-lane divided highway, began on July 22, 1986, and was completed on July 21, 1988. The tank asphalt used in this road was an Exxon AC-20. The hotmix was produced at Young Brothers hotmix plant in Bryan, Texas. The aggregate was Texas crushed limestone and field sand. The pavement was placed in three, two-inch lifts. The highway was seal coated and over laid in July 2000, 24 months before 2002 cores were taken.

The westbound lanes of this road were cored several times during the 13-month construction period between the Brazos River and Caldwell, Texas. Also, stations were sampled in 1989 (nine locations), 1992 (seven locations), 1996 (six locations) and 2002 (six locations). The various locations are designated by station number.

SHRP LTPP GPS Sites

Ten long-term pavement performance (LTPP) general pavement studies (GPS) sites from across Texas were evaluated. Cores were obtained by the LTPP program during the 1989-1990 time period and stored at the materials reference library (MRL)

without temperature control. No doubt there was some further aging once removed from the pavement, but the rate of aging certainly was slower compared to pavement aging in Texas.

Other Pavements

Other Texas pavements included the northbound and southbound frontage roads to IH 10 near Beaumont. Both pavements were 2 inches of asphalt hotmix pavement over a box beam overpass and 15 years old. However, the northbound lane visually appeared to be significantly more oxidized than the southbound lane. Additionally, newly recovered binder data from 1993 cores of a previously-reported test section study (Martin et al., 1990) are included.

Extraction and Recovery

The pavement cores (after separating the lifts either by sawing or cleaving) were broken into small pieces before solvent extracting the binder from the aggregate. The extraction used three successive washes: one wash of 100% toluene followed by two washes of a more powerful asphalt solvent, a mixture of 15% ethanol plus 85% toluene by volume (Burr et al., 1993). After the extraction, the solvent was filtered to remove all aggregate particles from the binder solution.

The binder was recovered from the solvent with a Büchi, RE 111 rotovap (Burr et al., 1993). During recovery, nitrogen carried off solvent and prevented contact with oxygen. During solvent removal, the bath temperature was kept at 100 °C to avoid hardening or softening of the asphalt in dilute solution (Burr et al., 1994; Burr et al., 1991). When no more condensing solvent could be detected visually, the temperature was increased to 173.9 °C for an additional 30 minutes to ensure sufficient solvent removal (Burr et al., 1993).

Size Exclusion Chromatography (SEC)

After the binder was extracted and recovered, it was analyzed by SEC to ensure complete solvent removal (Leicht et al., 2001). Without this feedback, it is likely that residual solvent will be left in aged binders (Burr et al., 1990). Incomplete solvent removal results in a peak located at 38 minutes on the chromatogram.

Dynamic Shear Rheometer (DSR)

After complete solvent removal, the rheological properties of the binder were determined using a Carri-Med CSL 500 Controlled Stress Rheometer. The rheological properties of interest were the complex viscosity (η^*_0) measured at 60 °C and 0.1 rad/s (approximately equal to the low-shear rate limiting viscosity, also called the zero shear viscosity, ZSV) and the storage modulus (G') and the dynamic viscosity (η'), both at 44.7 °C and 10 rad/s in time sweep mode. These temperature and frequency conditions are readily accessible to standard asphalt testing rheometers and correspond approximately to 15 ^{o}C and 0.005 rad/s through time-temperature superposition (Ruan et al., 2003b). A 2.5-cm composite parallel plate geometry was used with a 500 μm gap between the plates.

DSR measurement was also important for deciding whether the binder was changed in some way by the extraction and recovery process (Burr et al., 1990; Burr et al., 1994; Burr et al., 1991; Cipione et al., 1991). If two replicate extraction and recovery processes yielded binders with matching SEC chromatograms but significantly different complex viscosities, then at least one of the binders was suspected of having undergone solvent hardening or softening.

Fourier Transform Infrared (FTIR) Spectrometer

Carbonyl area (CA), reported in arbitrary units, was measured using a Galaxy 5000 FTIR spectrometer with an attenuated total reflectance (ATR) zinc selenide prism (Jemison et al., 1992). The absorption band from 1650 to 1820 cm^{-1} relates directly to oxygen content (Liu et al., 1998a), providing a good measure of binder oxidation.

Results and Discussion

Texas Highway 21

Experimental Data

Binder was extracted and recovered from each of the three lifts of the pavement cores, analyzed by several methods, and the results compared to laboratory aging of the same binder sampled during construction. From the cores of different age, we determined binder hardening rates, carbonyl growth rates, and binder hardening susceptibilities. Each of these values was compared to laboratory values to evaluate similarities of field and laboratory aging, and relative rates of aging. A second issue was how aging rates in the top 2-inch lift compared to aging rates in the other lifts. Data on the top and bottom lifts (0 to 2 inches and 4 to 6 inches below the surface) were obtained to address this issue.

A hardening susceptibility plot is shown in Figure II-1. For each station and lift for which we have sufficient data, η^*_0 is plotted versus the CA. The slope of each line is the hardening susceptibility (HS) and indicates how much the binder hardens in response to aging (increase in CA) and as such, serves as a valuable consistency check. Note that of the six correlations shown, half have a HS of approximately four, and half of about six (the top-to-bottom order of the regression equations is the same as the legend order). The laboratory-aged binder shows an HS of from 4.0 to 4.7 and agrees well with one

group of the recovered binders. The HS is characteristic of a binder and the value of six for three of the lift/station combinations is significantly outside the bounds of measurement error, leading to the conclusion that a different binder was used in some portions of the paving project. This result is not surprising, given the different lifts and the thirteen-month construction time span.

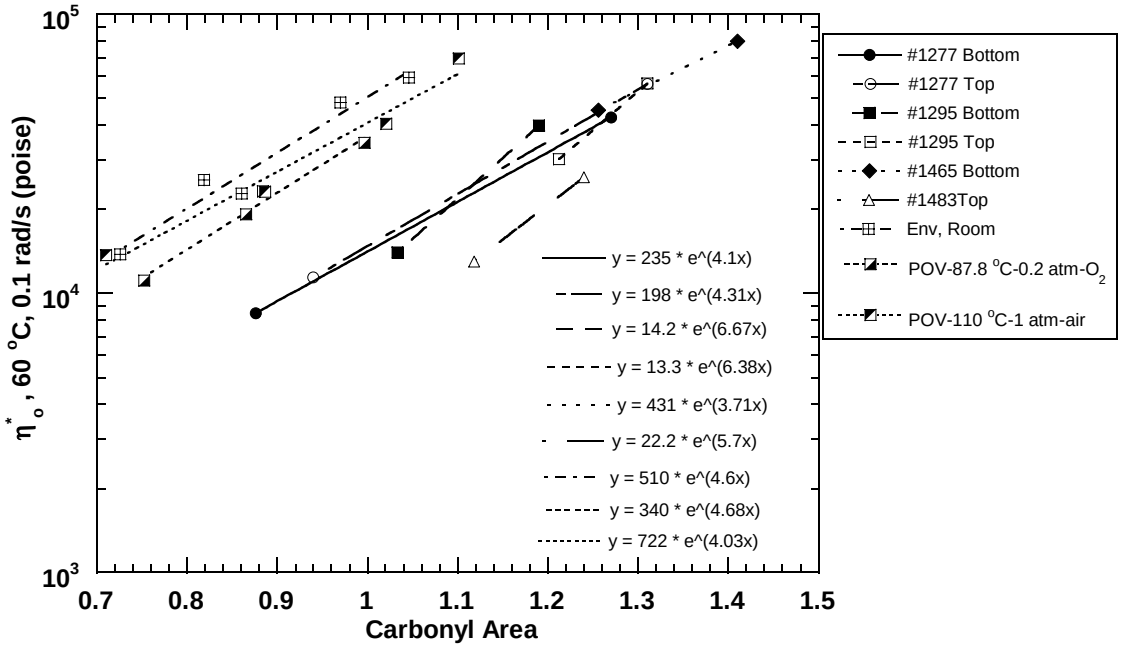

Figure II-1. Hardening Susceptibilities from Lab- and Field-Aged Binder.

Figure II-1 also shows the hardening susceptibility of Exxon AC-20 aged in the laboratory under candidate conditions for an aging test and those SH 21 binders recovered from 1989, 1992, and1996 cores that are considered to be the same Exxon AC-20. The pressure oxidation vessel (POV) was reported in a previous binder kinetic

study (Lau et al., 1992). Note the very good agreement between the lab- and pavement-aged binder HS values in spite of the offset of several sets of data.

In addition to η^*_0, the dynamic shear modulus (G') and dynamic viscosity (η') were measured on binders recovered from the 1996 and 2002 cores. These properties, measured at 44.7 °C and 10 rad/s and time-temperature superposition shifted to 15 °C and 0.005 rad/s, were of interest in view of the excellent correlation between ductility at15 °C and 1 cm/min and the DSR function G'/(η'/G') at 15 °C and 0.005 rad/s (Ruan et al., 2003b).

Thus G', η', and the DSR function could be used to track the pavement aging of a binder in a way that should relate to the long-term pavement cracking performance of the binder (Ruan et al., 2003b). Table II-1 reports measured values of η^*_0. Also shown are the measured values of the DSR function (G'/(η'/G')) for the 1996 and 2002 cores and an estimated value of ductility, calculated from the ductility-DSR function correlation reported for unmodified binders stiffened to a 15 °C, 1 cm/min ductility less than 10 cm (Ruan et al., 2003b):

$$\text{Ductility}(cm) = 0.23\left(G'/\left(\eta'/G'\right)\right)^{-0.44} \qquad \text{(II-1)}$$

Experimentally, binders recovered from pavement replicates produce estimated ductility values to within approximately 1cm.

In order to add binder data to this figure from earlier measurements of the 1989 and 1992 cores (for which the more complete DSR measurements were not available), estimates of the DSR function were made based upon the asphalt-dependent correlation of function values to the low-shear-rate complex viscosity. As a binder oxidizes, its ZSV increases but so does its DSR function. The correlation for the SH21 binder was obtained from recovered core binders, environmental-room aging, and temperature-accelerated aging at atmospheric air pressure.

Table II-1. Values of η^*_0 and the DSR Function for the SH 21 Cores

Station	Lift	1989[a]			1992[a]			1996 Wheel Path			2002 Wheel Path			2002 Center Path		
		η^*_o	DSR Func.	Est. Duct.	η^*_o	DSR Func.	Est. Duct.	η^*_o	DSR Func.	Est. Duct.	η^*_o	DSR Func.	Est. Duct.	η^*_o	DSR Func.	Est. Duct.
1277	Top	11400	0.000064	16.1	-	-	-	56230	0.001135	4.54	78190	0.001724	3.78	67130	0.001294	4.29
	Middle	8200	0.000036	20.8	18200	0.0001477	11.15	-	-	-	-	-	-	-	-	-
	Bottom	8500	0.000038	20.3	-	-	-	42685	0.000698	5.63	56705	0.000977	4.85	52020	0.001021	4.76
1295	Top	-	-	-	30200	0.0003648	7.49	56420	0.00091	5.01	85165	0.001998	3.54	45050	0.000753	5.44
	Middle	-	-	-	45480	0.0007575	5.43	-	-	-	-	-	-	-	-	-
	Bottom	-	-	-	14000	0.000093	13.7	39900	-	6.58	26600	0.000269	-	35565	0.000517	-
1392	Top	-	-	-	-	-	-	42700	0.000619	5.93	47235	0.000646	5.82	42785	0.000581	6.1
	Middle	-	-	-	-	-	-	23000	-	-	-	-	-	-	-	-
	Bottom	-	-	-	-	-	-	19540	0.000131	11.75	11875	0.000044	18.99	12172	0.000046	18.63
1394	Top	-	-	-	20800	0.0001875	10.04	-	-	-	-	-	-	-	-	-
	Middle	-	-	-	15800	0.0001148	12.46	-	-	-	-	-	-	-	-	-
	Bottom	-	-	-	30000	0.0003605	7.53	-	-	-	-	-	-	-	-	-
1465	Top	-	-	-	-	-	-	52335	0.000822	5.24	34690	0.000429	6.97	40945	0.000519	6.41
	Middle	-	-	-	22500	0.0002157	9.44	-	-	-	-	-	-	-	-	-
	Bottom	-	-	-	45300	0.0007522	5.45	80160	0.001225	4.39	21090	0.000175	10.35	27220	0.000275	8.48
1483	Top	-	-	-	13000	0.000081	14.52	26060	0.000241	8.99	30080	0.000203	9.69	-	-	-
	Middle	-	-	-	15500	0.0001109	12.65	-	-	-	-	-	-	-	-	-
	Bottom	-	-	-	24300	0.002475	8.9	33285	0.000374	7.41	34940	0.000432	6.95	-	-	-
1500	Top	-	-	-	-	-	-	43600	0.000344	7.68	40350	0.000527	6.37	-	-	-
	Middle	-	-	-	-	-	-	-	-	-	-	-	-	-	-	-
	Bottom	-	-	-	-	-	-	24690	0.000189	10.01	32640	0.000376	7.39	-	-	-
1518	Top	-	-	-	-	-	-	-	-	-	-	-	-	-	-	-
	Middle	-	-	-	15000	0.0001046	12.98	-	-	-	-	-	-	-	-	-
	Bottom	-	-	-	-	-	-	-	-	-	-	-	-	-	-	-

[a] The DSR function of the 1989 and 1992 cores were estimated from the G'/(η'/G') versus η^*_o correlation.

Comparison of Field and Laboratory Hardening Rates

Of particular interest to this project is the rate at which pavement binders harden due to oxidation. Hardening results in an embrittlement of the binder that decreases its ability to sustain deformation without cracking. Three questions are especially relevant: 1) How quickly does hardening occur on the road? 2) How do hardening rates vary with pavement depth? and 3) How do pavement hardening rates compare to laboratory hardening rates? From the data reported above, we reviewed two hardening rate parameters (in both the top and bottom lifts) and compared them to their corresponding laboratory hardening rates.

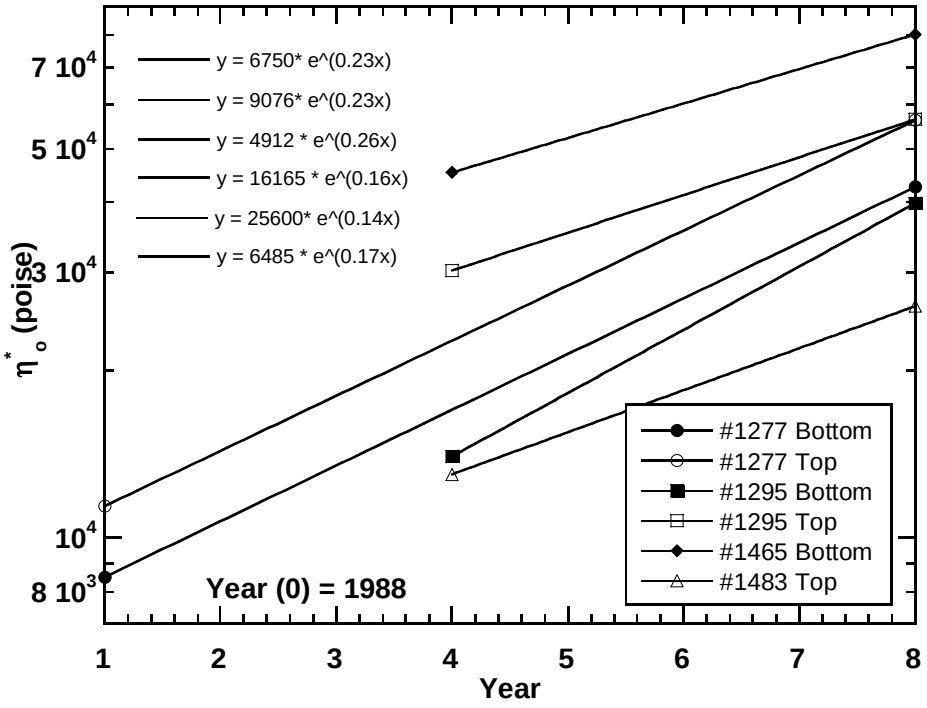

Figure II-2. Binder η^*_0 Hardening Over Time in SH 21.

The first two questions are addressed by the data of Figure II-2 which shows changes in η^*_0 over time for several pavement stations and both bottom and top lifts. As

was noted before from Figure II-1 and based on common HS, the top and bottom lifts of station 1277 are likely constructed from the same asphalt. The same can be said for the bottom and top lifts of station 1295. However, the binders at these two stations do not appear to be the same asphalt because of their different hardening susceptibilities. Thus, some care is warranted in comparing their hardening rates. With that caution, note that the 1277 bottom and top lifts have the same hardening rates from 1989 to 1996 (0.23 ln poise/year). Recall that the top lift is 0 to 2 inches from the surface of the pavement and the bottom lift having 4 to 6 inches below the surface. A layer that deep into the pavement having the same hardening rate as the top 2 inches is a surprise. However, the 1465 bottom lift, apparently the same binder because of its HS, appears to have a lower hardening rate, 0.14. However, for the two lifts at station 1295, the bottom lift rate is actually higher than that of the top lift (0.26 ln poise/year versus 0.16) and these rates vary by the same amounts as the 1277 rates and the 1465 rate. Further, lift 1483 top, which has approximately the same hardening susceptibility as the 1295 bottom and top lifts, has essentially the same hardening rates as the 1295 top lift (0.17 versus 0.16 ln poise/year). Hardening rates also were assessed using the DSR function $G'/(\eta'/G')$, and follow the same trends as the ZSV.

So, while there is some uncertainty to the data that is complicated by a fairly limited data set, the indications are that asphalt hardening is not impeded as much as has been previously reported (Coons and Wright, 1968; Mirza and Witczak, 1995), by a few inches (4 inches in this work) of dense-graded pavement above it. This result may seem contrary to intuition, based on the dual assumptions of limited access to oxygen by pavement at deeper levels and lower maximum summertime temperatures below the surface. However, pavements do breathe (assuming reasonable air voids permeability) as daily temperature fluctuations pump air in and out of the pavement and temperatures below the surface are not cooled as quickly as the surface by nighttime decreases in air temperature. Even though more data are needed to add statistical weight to this conclusion, it is a result that bears on the issues of pavement performance, pavement maintenance and rehabilitation, and perpetual pavements.

The third question to be addressed was how pavement binder hardening rates compare to the laboratory. For this calculation, we used the data of Table II-1 and Figure

II-2, stations 1277 (both top and bottom lifts) and 1465 bottom as these binders had the same hardening susceptibility as the binder sampled during pavement construction and studied in the laboratory. Laboratory aging beyond RTFOT equivalent aging was conducted in 0.86 mm thick films in an environmental room at atmospheric air pressure controlled to 60 ^{o}C and 25 percent relative humidity. At these laboratory conditions, the ZSV hardening rate was 0.0088 ln Poise/day compared to the field rate of 0.00055 and the DSR function laboratory and field hardening rates were 0.014 (ln MPa/s/day) and 0.00091, respectively. Thus, we estimate that the environmental room constant-rate aging is about 15 times faster than in the pavement, or, in other words, one month aging in the environmental room is equivalent to about 15 months aging in the pavement, once the initial jump is past. (At constant temperature and oxygen pressure, asphalt binders oxidize in two stages (Lau et al., 1992). The first stage is a rapid but decelerating rate period; the second stage is a slower, constant-rate period. In SH 21, the end of the first period occurred approximately two years after mixture and laydown, i.e., in 1989.) This relative hardening rate is about the same whether viscosity or the DSR function is adopted as the measure of hardening. It should be noted that this estimate is valid only for SH 21 and subject to considerable error. Nevertheless, it is probably the best comparison that exists between field and laboratory aging rate.

Tracking Pavement Aging

A relationship between ductility and DSR properties was reported that provides a rationale for tracking binder pavement aging to the point of road performance failure (Ruan et al., 2003b). All unmodified asphalts that have been studied (twenty to date) follow this same correlation, in spite of having rather distinct DSR properties as indicated by their decidedly different aging paths across a G' versus η'/G' map. Furthermore, literature reports suggest that a value of 15 °C ductility in the range of 3 cm is a danger threshold for pavement failure (Kandhal, 1977; Kandhal and Koehler, 1984; Kandhal and Wenger, 1975). Thus, tracking pavement binder properties across this DSR map could be expected to relate to age-related pavement performance.

Figure II-3 gives such a view of binder pavement aging over an extended period of time. The dashed curves are lines of equal ductility with their values (cm) shown on the graph. This figure includes all top and bottom lift data in Table 1 for station 1277, but for the pre-1996 data the points are plotted based on estimates. It was previously explained that pre-1996 values of the DSR function were estimated from ZSV values.

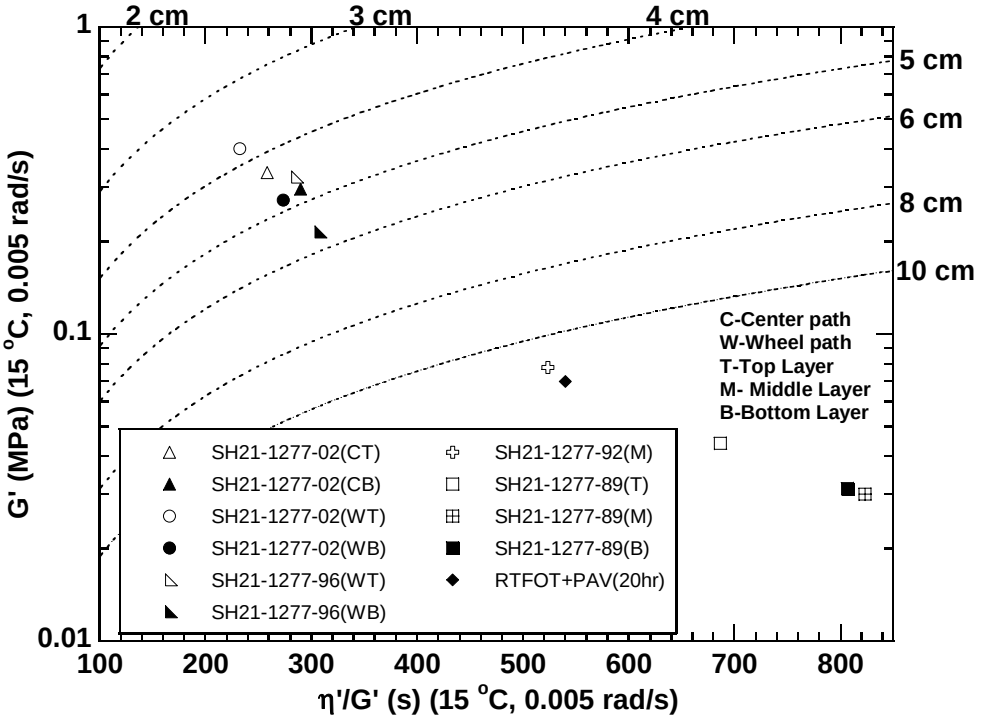

Figure II-3. Movement of Binder Across the DSR Map, Station 1277.

However, these estimates are not sufficient for plotting points on the DSR map because the separate values of G' and η'/G' are not known. However, by using the known path for this binder across the DSR map (determined by 1996, 2002 cores and environmental-room aged binders), these individual values can be determined (for the estimated value of the DSR function) by trial and error and then the point located on the map. The Exxon AC-20 standard PAV-aged (100 °C, 20 hour, 3mm thick, after RTFOT)

sample also is plotted (using its ZSV value of 16,000 poise) by the same estimation procedure.

During service, the binder from these 1277 lifts moves from the lower right to the upper left on the DSR map. The binder recovered from the 1989 cores is at the lower right in Figure II-3, and the binder from the 2002 cores is at the upper left where calculated ductility values range from 4 to 5 cm. In 1992, the binder was near 10 cm, and by 1996, it was between 5 and 6 cm. For the most part, the recovered binders from these 1277 lifts show a relentless track across the DSR map. For comparison, the RTFOT plus standard PAV point is aged to about 12 cm, close to the 1992 recovered binder value. It should be noted that the 2002 binders likely were softened by the seal coat placed in 2000, accounting for the relatively small decrease in calculated ductility from 1996 to 2002, compared to the changes observed in prior years.

From these results, we conclude that for this binder and this pavement, the RTFOT plus 20-hour PAV aging corresponded to about four years in the pavement after hot-mix plant and placement aging. Also, 14 years in the pavement aged the binder to a ductility of approximately 4 cm, short of the 3 cm level that might suggest approaching failure, but note again possible softening by the seal coat.

Texas LTPP Pavements

The LTPP sites studied in this project were from various locations across Texas, including the panhandle, west Texas, the gulf coast and east Texas. The thinnest pavement is 1.8 inches and the thickest is 12.9 inches. The LTPP site numbers are given in Figure II-4 and Figure II-5.

Experimental Data

For each core, one layer was targeted for study, the original surface layer (OSL) at the time the pavement was first constructed. In all but one case, this was the surface layer at the time of the 1989 or 1990 coring; for the other location, it was buried below 10.5

inches of additional layers (48-1046, US-66, was converted to I 40 in 1971, requiring a much thicker pavement).

Each core was either sawn or cleaved into lifts (while frozen), and the target lift was further broken into pieces. Then, in two replicates (A and B) the broken core was sampled, extracted, and recovered, and the binder analyzed.

Tracking Pavement Aging

The DSR properties for both replicate extractions for each core are plotted on the DSR function map in Figure II-4. For easy reference, the date that the pavement OSL was placed is noted in parentheses in the legend for the 1989-1990 cores. Replicate samples generally gave very similar results with the estimated ductility differing by less than 1 cm. Generally, these binders follow the trend that the older binder is stiffer and thus appears more towards the upper left in the figure. Of course, this generalization is not universally true, as binders in pavements will age at different rates depending upon climate, air voids, binder content, binder oxidation kinetic parameters, and binder hardening susceptibility. That these different binders all follow roughly the same path across the DSR map is coincidence.

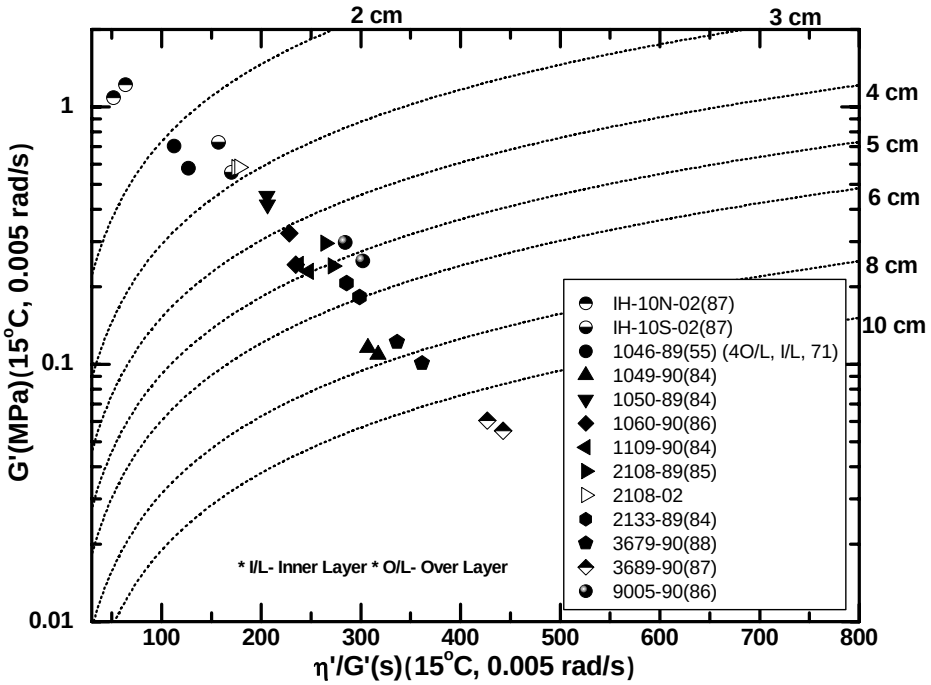

Figure II-4. DSR Function Map for the LTPP and IH-10 Binders.

Other Pavements

Other pavements were evaluated during the course of this work. Two pavements were the northbound and southbound lanes of an IH 10 frontage road in Beaumont, Texas. Both pavements were stated as having been constructed in approximately 1987.

These binder DSR properties also are shown in Figure II-4. Both recovered binders in fact, were quite aged, with the northbound binder (calculated ductility of 1.3 cm) somewhat more hardened than the southbound (ductility of 2.7 cm). In fact, the northbound lane's binder was stiffer than any other pavement binder tested. Based upon the preceding discussion, we might expect that this binder would be too brittle to hold up without cracking. However, the box beam construction of the overpass likely provides an extremely stiff system that prevents excessive deformation.

All Pavements - Summary of Aging Levels

Figure II-5 summarizes the level of oxidative hardening that was reached by the various pavements studied in this work. The low shear rate viscosity at 60 °C for each recovered binder is shown versus the time in the pavement when the core was obtained. The SH 21 pavements are shown for both the top lifts (0 to 2 inches deep) and the bottom lifts (4 to 6 inches below the surface), offset in time slightly so that the symbols do not overlay each other. The other pavement binders were all recovered from the entire pavement thickness but for pavements that were only from one to three inches thick.

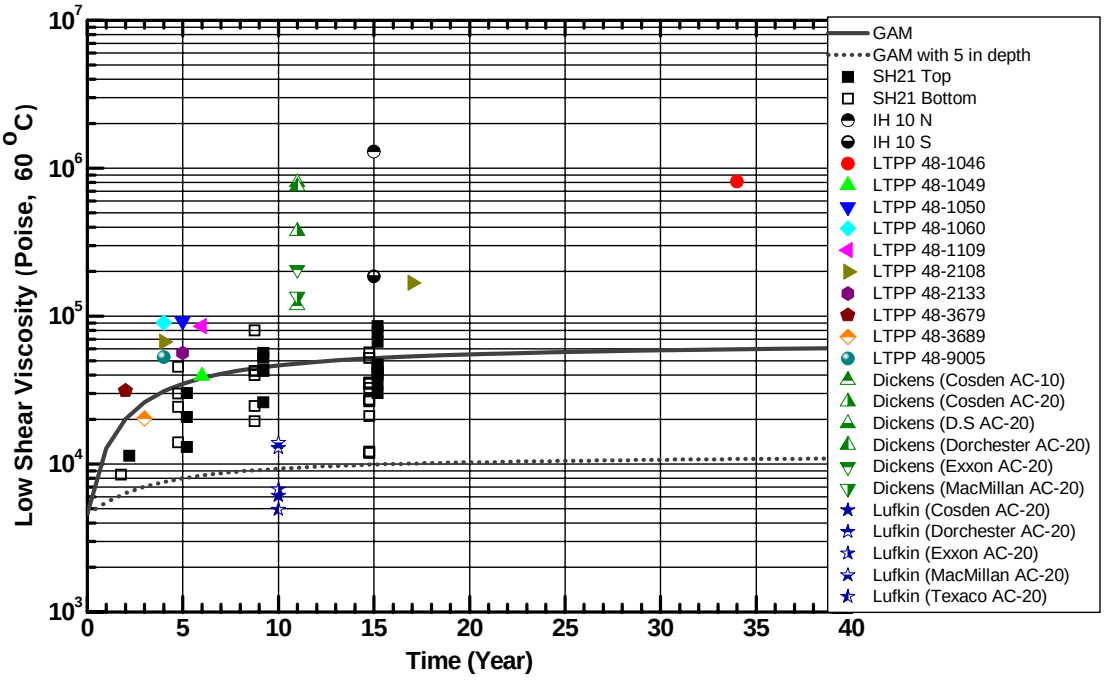

Figure II-5. Binder Aging in the Various Texas Pavements.

Also shown in the figure for comparison are 60 °C low shear rate viscosities versus time for the pavement surface (top 0.25 in) and for five inches below the surface, calculated using the Global Aging Model (GAM) of Mirza and Witczak at 60 °C (Mirza and Witczak, 1995; AASHTO, 2004). For this calculation, a mean annual air temperature

of 70 °F and an initial (mix/laydown) viscosity of 4,600 poise were used. The effect of air void changes over time on this calculation was not considered. To do so would have resulted in even lower GAM estimates of binder aging.

Some observations are evident. First, the great majority of the recovered surface binders lie above (or only slightly below) the GAM calculation for the surface. Most of them are significantly above the GAM and some are in excess of an order of magnitude above the GAM. The SH 21 surface cores span above and below the GAM. These results are in spite of the fact that these binders include much more than just the top 0.25 in of the pavement. Second, one pavement (Lufkin) falls well under the surface GAM calculation and in fact, is in line with the 5-in deep calculation. This clear aberration to the low side is almost certainly the result of very low air voids for this pavement (typically less than three percent, compared to seven percent (SH 21) and from 8 to 12 percent for the Dickens pavement; air voids for the other pavements were not measured). It has been noted previously that low air voids correlate with reduced oxidative hardening (Martin et al., 1990).

A third observation is that the SH 21 binders from the bottom lift (4 to 6 in below the surface) exceed the GAM calculation for five inches below the surface to a very significant degree, nearly by an order of magnitude in some cases, even exceeding the GAM calculation for the pavement surface. In fact, the top and bottom core binder values are very much in agreement with the possible exception of the 2002 data which may have been softened by a seal coat placed in 2000.

Finally, comparing the data for those pavements that were sampled in more than one year (notably 48-2108 and SH 21), the rates of binder hardening do not appear to have leveled out, even after 10 to 15 years, contrary to the GAM. The high level of aging for some of the other pavements also suggests that the pavement aging function does not level out.

Summary and Conclusions

Extensive investigations of selected Texas highway pavements have provided new information about changes in unmodified binder properties over time. These studies

included SH 21 plus 10 LTPP GPS pavements, two test sections, and two other pavements sampled late in their life. They were conducted to provide information on pavement performance as it relates to recovered binder properties and also to provide data on comparisons between pavement and laboratory binder oxidation rates and changes in physical properties. From these studies, a number of conclusions concerning unmodified binder aging are tentatively offered:

1. Binders in pavements can oxidize at surprisingly uniform rates with depth once early oxidation occurs, even for dense-graded mixtures, and these rates may continue for an extended period of time, virtually unabated.
2. The DSR function map provides a very useful method of tracking pavement aging over time. The coordinates on the map correlate quite well to binder ductility for unmodified binders, a binder characteristic that is reported to relate well to cracking failure.
3. The level of hardening reached in pavement binders significantly exceeds estimated values calculated by the Global Aging Model, both at the pavement surface and at 5 in below the surface.
4. The Superpave RTFOT plus PAV procedure ages binders at Texas conditions to a level that is approximately equal to hot-mix aging plus four years on the road, based on SH 21 data. This is not a very severe level of aging in the context of pavement life in Texas. It also is only one data point and many others are needed.
5. One month of aging in the 60 °C environmental room was equivalent to approximately 15 months on SH 21 after the initial jump region of the oxidation is past. This calibration will vary with climate, binder composition, binder content and air voids.
6. On SH 21, aggregate altered neither the oxidation hardening susceptibility nor the path followed on the G' versus η'/G' map, compared to laboratory aging of the neat binder.

CHAPTER III
MIXTURE VERSUS NEAT-FILM BINDER OXIDATION AND HARDENING AND THE IMPACT OF BINDER OXIDATION ON MIXTURE FATIGUE

Synopsis

Asphalt oxidation causes major changes to binder properties and is hypothesized to be a major contributor to age-related pavement failure such as fatigue cracking. Neat film asphalt oxidative aging stiffens the binder, leading to higher binder stresses under a given deformation; when these stresses exceed the strength of the binder, failure occurs. Thus, heavily-aged binders exhibit a significantly reduced failure strain (e.g. in direct tension,) compared to less aged binders. However, the impact of binder oxidation in HMAC mixtures on fatigue lives has not been adequately addressed.

In this study, we have investigated the effect of binder oxidation on the HMAC mixture fatigue performance. Binder aging was characterized by FT-IR carbonyl area growth and by changes in the DSR function hardening (G'/(η'/G'). HMAC Mixture fatigue life was estimated by a calibrated mechanistic with surface energies (CMSE) fatigue approach. Binders recovered from aged mixtures track across the DSR function map (G' versus η'/G'), following the same path as neat binder aged in a 60°C environmental room, a path that previous study has shown correlates well with significant decreases in binder ductility. Mixture fatigue resistance also decreases dramatically in direct relation to binder oxidative hardening.

Introduction

Asphalt binder oxidation is one of the major contributors to age-related pavement failure, including fatigue cracking. However, its impact has been underestimated or ignored in most hot mix asphalt concrete (HMAC) mixture fatigue studies of fatigue failure in asphalt pavements.

An HMAC mixture is a heterogeneous complex composite material of air voids, aggregates, and asphalt binder. The physico-chemical properties of binders are mainly

changed by binder oxidation. A recent study shows that binder oxidation can affect the binder hardening and embrittlement six inches below the surface of asphalt pavements (Al-Azri et al., 2006). It indicated that binder hardening rates of the top two inches of the sampled cores are almost the same as the two inch layer that is four inches below the surface. The findings have an important conclusion: the effects of binder oxidation are not limited to the asphalt pavement surface but penetrate the HMAC layer, making the HMAC layer stiffer and more brittle.

Previous studies (Clark, 1958; Doyle, 1958; Halstead, 1963; Kandhal, 1977; Kandhal and Koehler, 1984) point out that pavement long term durability has a good correlation with asphalt binder ductility. Ruan et al. (2003b) found a good correlation between a fundamental rheological function, called the DSR function (G'/(η'/G')), and ductility below ductilities of 10 cm. They found that binder long-term durability is not dependent on a single rheological property such as the dynamic elastic shear modulus, G' or the dynamic shear viscosity, η' but rather both of them in the form of G' and η'/G'. The DSR function quantifies binder durability change with binder oxidative hardening, and the DSR map (G' versus η'/G') provides a convenient tool to track durability changes of binders in neat aged binders, HMAC mixtures and pavements.

The detrimental impact of binder oxidation on binder durability and asphalt pavement cannot be ignored and must be included in fatigue analysis in addition to repeated traffic loading. This study focuses on how binder oxidation affects binder properties in HMAC mixtures and the HMAC fatigue performance.

While extensive studies of asphalt pavement fatigue performance have been conducted, successful characterization of HMAC mixtures to ensure adequate fatigue performance is not well established and fundamental fatigue predictive models still remain to be developed. The conventional way of measuring asphalt pavement fatigue life is testing laboratory HMAC mixtures and then applying a shift factor which relates laboratory conditions to field conditions.

In this study, the calibrated mechanistic with surface energy (CMSE) fatigue approach is utilized to measure laboratory HMAC fatigue life cycles and subsequently estimate field fatigue life. The CMSE fatigue analysis model uses fundamental theories (the visco-elastic correspondence principle, Paris' Law fracture mechanics, Schapery's

work potential theory and energy concepts) to characterize HMAC mixture fatigue resistance (Kim et al., 1997a; Kim et al., 1997b; Lytton et al., 1993; Schapery, 1984; Si, 2001). This approach is applied in this current study and is used to determine the impact of binder oxidation on the field fatigue performance because of its ability to measure fundamental material properties such as asphalt mixture tensile strength, stiffness, relaxation modulus in tension and compression, dissipated pseudo strain energy and surface energy for binder and aggregates to characterize HMAC mixture fatigue resistance (Lytton et al., 1993).

Objectives

This research investigated the impact of binder oxidation on HMAC mixtures and their fatigue resistance. The objectives of the study were 1) to compare neat-film binder aging to laboratory compacted mixture binder aging, 2) to determine the effect of oxidative binder aging on controlled-strain HMAC mixture fatigue, 3) to investigate the effect of different binders and their contents in HMAC mixtures on their fatigue performances.

Methodology

This section describes materials, aging processes, binder and mixture tests and the CMSE fatigue approach. The materials were neat binders aged in thin films, binders recovered from aged HMAC mixtures, and seven different types of HMAC mixtures. Binder tests included: gel permeation chromatography (GPC) using a refractive index (RI) detector to insure complete solvent removal in the binder recovery process; dynamic shear rheometry (DSR) to measure the rheological properties of the binder; and Fourier transform infrared (FTIR) spectroscopy to measure the carbonyl content in the binder. Mixture tests for the CMSE approach involve the use of Whilhelmy plate (WP), the universal sorption device (USD), and other instruments to determine tensile strength (TS), uniaxial relaxation modulus (RM) and dissipated pseudo strain energy (DPSE). These materials and methods are described in further detail in the following paragraph.

Materials

Binders

Three different binders were used in this study: a conventional binder (performance grade (PG) 64-22), a styrene-butadiene-styrene (SBS) polymer modified binder (PG 76-22 SBS) and a tire rubber/SBS polymer modified binder (PG 76-22 TR). Aged neat binders as well as recovered binders from aged HMAC mixtures were used to compare neat binder aging with mixture aging and to determine the impact of binder oxidation on HMAC fatigue performance.

HMAC Mixtures

Seven different types of mixtures were prepared in the mixture study. Table III-1 is a summary of HMAC mixtures and binders (Lubinda et al., 2005, Lubinda et al., 2006). With the three different binders, two aggregate types (limestone, river gravel), and two binder content levels (optimum, optimum plus 0.5 percentage point binder contents), are used. Note that the binder contents in Table III-1 are on a binder free weight basis, and the values in parentheses are on a total weight basis.

The mixtures were made based on two commonly used TxDOT mixture designs. The first mixture design is a basic mixture design, defined as Bryan mixture, which is a dense graded TxDOT type C mixture design with PG 64-22 binder and limestone aggregate (TxDOT, 2003). The second mixture design is a rut resistant mixture design, also referred to in this work as the Yoakum mixture, which is a 12.5 mm Superpave mixture designed with a polymer modified PG 76-22 SBS binder and crushed river gravel aggregate with 14 percent limestone screenings and 1 percent hydrated lime. Five more types of mixtures were made based on a rut resistant mixture design to determine the impact of binder type and content on fatigue performance. Note that the target air void (AV) of all HMAC mixtures is 7 ± 0.5 percent to simulate the in-situ AV field compaction during HMAC pavement construction. The standard Superpave Gyratory

Compactor (SGC) was used for compacting cylindrical HMAC specimens for CMSE testing (AASHTO, 1996b; AASHTO, 1996c; TxDOT, 2003).

Table III-1. List of HMAC Mixtures

Basic Mixture Design with Optimum Binder Content		
HMAC Mixture	Binder + Aggregate	Binder Content (%)
Bryan	PG 64-22 + Limestone	4.6[a] (4.4%)[b]
Rut Resistant Mixture Design with Optimum Binder Content		
HMAC Mixture	Binder + Aggregate	Binder Content (%)
A1	PG 64-22 + Gravel	5.3 (5.0)
Yoakum (B1)	PG 76-22 SBS + Gravel	5.6 (5.3)
C1	PG 76-22 TR+ Gravel	5.5 (5.2)
Rut Resistant Mixture Design with Optimum + 0.5 Percentage Point Binder Content		
HMAC Mixture	Binder + Aggregate	Binder Content (%)
A2	PG 64-22 + Gravel	5.8 (5.5)
B2	PG 76-22 SBS + Gravel	6.1 (5.8)
C2	PG 76-22 TR+ Gravel	6.0 (5.7)

[a] Binder-free weight basis
[b] Total weight basis

Aging Processes

Binder aging in pavements follows short-term (hotmix and placement) and long-term aging (pavement in-service) processes. A stirred air flow test (SAFT), which stimulates the hot mix process, was used for short-term aging (Vassiliev et al., 2001; Vassiliev et al., 2002). The standard pressure aging vessel (PAV) aging procedure (AASHTO, 1996a), modified PAV aging procedure (PAV*), and the environmental room (ER) were used for long-term aging (Glover et al., 2005; Juristyarini, 2003). The ER (60 ^{o}C room) is used as an approximation to field aging in Texas; one month in the ER was found approximately equal to 15 months in the field for one pavement in Texas (Glover et al. 2005, Al-Azri et al., 2006). PAV (AASHTO PP1) is used for comparison with ER because PAV is a standard long-term binder aging process. PAV* is used to test a different accelerated long-term aging process (Juristyarini et al., 2003). The conditions of binder and HMAC mixture aging processes are shown in Table III-2.

Table III-2. Aging Processes

Binder Aging Process	Aging Conditions
SAFT	163 ^{o}C, 1 atm, 35 min
PAV	100 ^{o}C, 2.1 MPa, 3 mm film thickness, 20 hours
PAV*	90 ^{o}C, 2.1 MPa, 1 mm film thicknes, 16, 32 hours
ER (60 ^{o}C room)	60 ^{o}C, 1 atm, 50 % relative humidity, 0.86 mm film thickness, 0, 3, 6, and 9 months
Mixture Aging Process	**Aging Conditions**
PP2 (AASHTO PP2)	135 ^{o}C, 1 atm, 4 hours
ER (60 ^{o}C room)	60 ^{o}C, 1 atm, 50 % relative humidity, 0, 3, and 6 months

Like binder aging processes, two different methods of HMAC mixture aging were used in this study. All loose HMAC mixtures were subjected to the AASHTO PP2 short-oven aging process (PP2) for 4 hours at 135 °C prior to compaction (AASHTO, 1996b). After compaction, the HMAC mixtures were aged for 0, 3, and 6 months) at 60 °C room.

The Calibrated Mechanistic with Surface Energy (CMSE) Fatigue Model

The CMSE approach points out that HMAC fatigue damage consists of two components; resistance to fracture under repeated loading and the ability to heal during rest periods, processes that both change over time. According to the approach, fatigue life (N_f) is controlled by two processes; crack initiation represented by the number of repetitive load cycles to crack initiation (N_i) and crack propagation represented by the number of repetitive load cycles for macrocrack propagation through the HMAC layer thickness (N_p) in Equation III-1.

$$N_f = SF_i\left[N_i + N_p\right] \geq Q \times \text{TrafficDesign}_{\text{ESALs}} \quad \text{(III-1)}$$

$$SF_i = SF_a \times SF_h \quad \text{(III-2)}$$

The CMSE approach considers the fact that HMAC is not an isotropic material and introduces an anisotropic shift factor SF_a to account for the differences in the vertical and lateral elastic modulus due to the differences in the particle orientation during compaction/construction.

Due to traffic rest periods and temperature variations, the binder has a tendency to heal, which often results in improvement in the HMAC mixture fatigue performance. A SF_h shift factor is thus introduced in the analysis to account for this healing process. This SF_h is a function of the rest periods, pavement design life, field temperature correction factor, HMAC elastic relaxation modulus in compression, surface energy due to healing (ΔG_h), and fatigue field calibration constants.

N_i is defined as the number of load cycles required to initiate and grow a

microcrack of 7.5 mm in length in the HMAC layer. It is a function of crack density, specimen cross-sectional area, Paris' Law fracture coefficients (A and n), and the rate of damage accumulation (b) as indicated by DPSE in the uniaxial repeated-direct tension test. Crack density calculations in this study were based on the cavitation analysis by Marek and Herrin (Marek and Herrin, 1968) assuming a brittle-adhesive mode of crack failure for the HMAC specimens.

N_p refers to the number of load cycles required to propagate a 7.5 mm microcrack through the HMAC layer thickness. N_p is calculated as a function of the maximum microcrack length, HMAC layer thickness, shear modulus, Paris' Law fracture coefficients (A and n), and a design shear strain (γ) (Cheng, 2002; Lytton et al., 1993; Si, 2001). Other CMSE input parameters include non-linearity correction factor ($\psi(t)$), stress intensity, regression and shear coefficient factors, HMAC brittle-ductile failure characterization, healing constants, and field calibration constants.

Q is a reliability factor that accounts for mixture and traffic prediction variability and the anticipated uncertainties in the mixture fatigue performance during service. A Q value of 1.0 was used in this study. However, further CMSE research should inevitably explore the derivation of Q as a function of reliability level so as to adequately account for HMAC mixture and traffic prediction variability in N_f analysis.

Table III-3. Summary of CMSE Laboratory Tests

Test	Loading Configuration,	Test Parameters, and Output Data
Whilmey Plate	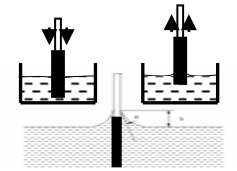	Automatic immersion and withdrawal of binder coated glass plates into/from liquid solvents up to approx. 5 mm depth @ 20±2 °C. Test time: ≅45 minutes. Measurable & output data is dynamic contact angle (θ) and surface energy (SE) components for the binder ($\Gamma_{i\text{-}binder}$) HMAC mixture fracture (ΔG_f) and healing (ΔG_h) bond strengths determination
Universal Sorption Device (USD)	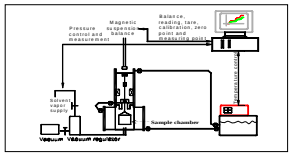	Clean oven dried 50 g aggregate of fraction size (4.75 mm < aggregate size < 2.63 mm) . Measurable parameters are vapor pressure & adsorbed gas mass of liquid solvents @ 25±2 °C. Test time: 60 to 70 hrs. Output data is SE components for the aggregates ($\Gamma_{j\text{-}aggregate}$) for HMAC mixture fracture (ΔG_f) and healing (ΔG_h) bond strengths determination
Anisotropic (AN)	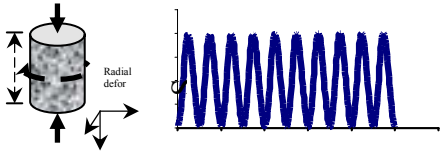	Sinusoidal compressive stress-controlled @ 1 Hz, 20 °C & 690 kPa stress level for 200 load cycles. Test time: ≅5 minutes Output data is HMAC mixture vertical (E_z) and (E_x) lateral elastic modulus shift factor due to anisotropy (SF_a).
Tensile Strength (TS)	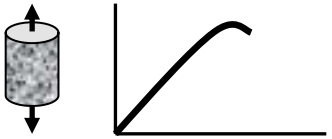	Tensile loading till break @ 0.05 mm/min @ 20 °C. Test time: ≅5 minutes. Output data is HMAC mixture tensile strength (σ_t) and failure strain (ε_f) for determining Paris' Law fracture coefficient A
Uniaxial Relaxation Modulus (RM)	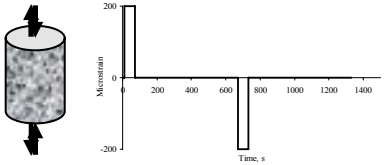	Trapezoidal shaped strain-controlled @ 200 microstrain (tension & compression), 60 s loading & 600 s rest period @ 10, 20, & 30 °C. Test time: ≅ 25 minutes. Output data is HMAC mixture elastic relaxation modulus (E_i), stress relaxation rate (m), and temperature correction factors (a_T) for determining the healing shift factor (SF_h) and Paris' Law fracture coefficients A and n.
Uniaxial Repeated Direct-Tension (RDT)		Haversine strain-controlled @ 1 Hz, 30 °C, & 350 microstrain level for 1, 000 load cycles. Test time: ≅20 minutes. Output data is dissipated pseudo strain energy (DPSE) and rate of fracture damage accumulation (b) necessary to calculate the number of load cycle to crack initiation (N_i).

HMAC Mixture Tests

The CMSE laboratory tests conducted in this study are summarized in Table III-3. For each test type, at least two replicate HMAC specimens were tested per aging condition per mixture type. For simplicity and because HMAC fatigue cracking is generally more prevalent at intermediate pavement service temperatures, most of the laboratory tests were conducted at 20 °C. Otherwise, the data were normalized to a reference temperature, 20 °C using a time temperature superposition shift during the analysis.

Output data from these laboratory tests served as input data for predicting the fatigue life in Equation III-1 (Cheng, 2002; Lytton et al., 1993; Si, 2001). Fatigue failure for the CMSE approach was defined as crack initiation and propagation through the HMAC layer thickness with a 7.5 mm microcrack length as the selected failure threshold value based on the work by Tseng and Lytton. (Lytton et al., 1993).

Field Condition

For hypothetical field conditions, a standard TxDOT pavement structure consisting of 150 mm HMAC (3,447 MPa, $\upsilon = 0.33$), 350 mm flex (granular) base (194 MPa, $\upsilon = 0.40$), and a subgrade with an elastic modulus of 63 MPa ($\upsilon = 0.45$) was utilized. Typical traffic conditions consisted of an 80 kN axle load, 690 kPa tire pressure, and 5 million equivalent single axle loads (ESALs) with about 25% trucks over a design life of 20 years and a 95% reliability level in a Wet-Warm (WW) Texas environment considered critical to HMAC pavement fatigue performance (Huang, 1993; TxDOT, 2003). Shear strains (γ) which constitute the input failure load-response parameters for the CMSE fatigue analysis approach were computed using an elastic multi-layered ELSYM5 software, but were adjusted based on Finite Element (FEM) simulations to account for more realistic HMAC behavior (Park, 2004; Walubita et al., 2005).

Binder Tests

Extraction and Recovery

The extraction used three successive washes: one wash of 100% toluene followed by two washes of a mixture of 15% ethanol plus 85% toluene by volume. After the extraction, the solvent was filtered to remove all aggregate particles from the binder solution using a centrifuge. The binder was recovered from the solvent with a Büchi, RE 111 rotovap (Burr et al., 1993). During recovery, nitrogen gas was introduced to the vessel to drive off any remaining solvent and to prevent contact with oxygen. Before the removal of the solvent from the last batch of the solution, the bath temperature was kept at 100 °C to avoid hardening or softening of the asphalt in dilute solution((Burr et al., 1994; Burr et al., 1991). When no more solvent could be detected visually, the temperature was increased to 173.9 °C for an additional 30 minutes to ensure sufficient solvent removal (Burr et al., 1990).

Size Exclusion Chromatography (SEC)

After the binder was extracted and recovered, it was analyzed by SEC to ensure complete solvent removal using previously reported methodology (Burr et al., 1990; Leicht et al., 2001). Without this feedback on the recovery process, it is likely that residual solvent will be left in the binder, especially the more heavily aged binders (Burr et al., 1990). Test samples were prepared by dissolving 0.2±0.005 g of binder in 10 mL of carrier. The sample of interest was then sonicated to ensure complete dissolution. The sonicated sample was then filtered through a 0.45 μm polytetrafluoro ethylene (PTFE) syringe filter. Samples of 100 μL were injected into 1000, 500, and 50 Å columns in series with tetrahydrofuran (THF) carrier solvent flowing at 1.0 mL/min. Incomplete solvent removal is indicated by a peak located at 38 minutes on the chromatogram.

Dynamic Shear Rheometer (DSR)

After complete solvent removal, the rheological properties of the binder were determined. The DSR used in this research was a Carri-Med CSL 500 Controlled Stress Rheometer.

The rheological properties of interest were the complex viscosity (η^*_0) measured at 60 °C and 0.1 rad/s (approximately equal to the low-shear rate limiting viscosity) and the storage modulus (G') and the dynamic viscosity (η'), both at 44.7 °C and 10 rad/s in time sweep mode. A 2.5-cm composite parallel plate geometry was used with a 500 μm gap between the plates.

DSR measurement was also important for deciding whether the binder was chemically altered in some way by the extraction and recovery process (Burr et al., 1990; Burr et al., 1994; Burr et al., 1991; Cipione et al., 1991). If two extraction and recovery processes yielded binders with matching SEC chromatograms but significantly different complex viscosities, then at least one of the binders was suspected of having undergone solvent hardening or softening.

Fourier Transform Infrared (FTIR) Spectrometer

Carbonyl area was measured using a Galaxy 5000 FTIR spectrometer with an attenuated total reflectance, ATR zinc selenide prism (Jemison et al., 1992). The absorption band from 1650 to 1820 cm^{-1} relates directly to oxygen content (Liu et al., 1998) and, thus, provides a good measure of binder oxidation.

Results and Discussion

The main goal of this study was to determine the impact of binder oxidation on the HMAC mixture fatigue performance. Two main results, the binder test results and the mixture fatigue results, are provided to achieve the goal. In the binder test results, mixture aging is compared with neat binder aging to understand the impact of binder oxidation on mixture physical properties. The binder test results consist of five sections to compare physico-chemical properties, binder aging mechanisms, and binder aging paths of both the neat binders and the recovered binders: 1) binder viscosity for the unmodified binders, 2) DSR function hardening, 3) carbonyl area growth, 4) DSR function hardening susceptibility and 5) DSR map. Then, the mixture results of the HMAC mixture fatigue performance from the different mixtures with binder oxidation are presented.

Mixture versus Neat-Film Binder Oxidation and Hardening

As noted earlier, mixtures were prepared using the PP2 short-term aging protocol and then compacted to produce one aging level (PP2+0M). Second and third levels were obtained by aging the compacted laboratory mixture in the ER for 3 and 6 months beyond PP2 conditioning (PP2+3M and PP2+6M). Here, the "0 months," "3 months," and "6 months" refer to environmental room aging beyond PP2 aging. Note that the mixture with an optimum binder content, the Yoakum (B1) mixture has one more aging level - 9 month beyond PP2 (PP2+9M) and the A1 and 2, B2 and C1and 2 mixtures do not have PP2+3M.

The two binders were extracted and recovered from their laboratory prepared mixtures at several levels of aging and evaluated. SEC was used to check whether solvent residue exist in the binder. SEC chromatograms for binders recovered from mixtures are shown in Figure III-1 and show that the recovered binders did not have

solvent residue, which, if present, would be detected as a peak at 38 minutes and would significantly affect the rheological properties.

Neat binders were aged in a HMAC simulation, the stirred air-flow test (Vassiliev et al., 2001, 2002) to give one level of aging (designated SAFT). Then these binders were further aged in the 60 °C (140 °F) environmental room in thin films (approximately 1 mm thick) for 3, 6 and 9 months to obtain second, third and fourth aging levels (SAFT+3M, SAFT+6M and SAFT+9M).

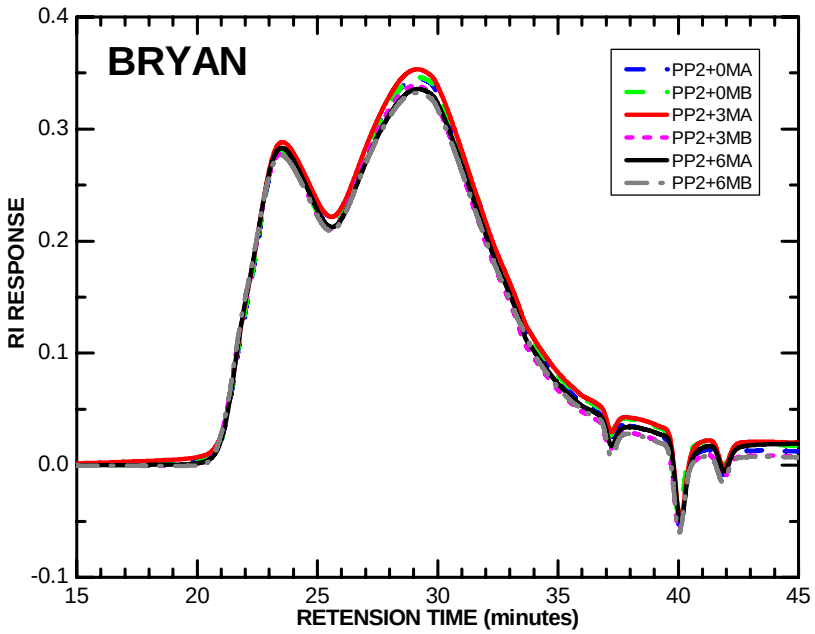

Figure III-1. SEC Chromatograms for Recovered Binders from Bryan Mixtures.

The aged binders were characterized by DSR and FTIR measurements. Oxidative aging increases carbonyl area (CA, oxygen content), viscosity (zero shear viscosity, η^*_0) and DSR function (G'/(η'/G')) for both neat binders and recovered binders. The data are shown in Table III-4. While there is a difference between neat binder aging and mixture aging due to diffusion resistance in the mixture, binder oxidation still significantly affects binder hardening, binder durability and the CA growth of the binder in the mixture.

Table III-4. Carbonyl Area and DSR Properties of Neat and Recovered Binders

ER									
				CA					
Aging	PG64-22	Bryan		PG76-22SBS	Yoakum		PG76-22TR	C1	
(months)	SAFT	PP2		SAFT	PP2		SAFT	PP2	
0	0.620	0.807	0.807	0.556	0.720	0.721	0.708	0.722	0.713
3	0.857	0.927	0.919	0.914	0.891	0.878	0.863	-	-
6	0.957	0.964	0.975	1.033	0.961	0.960	1.045	1.051	0.994
9	1.138	-	-	1.194	1.061	1.074	1.217	-	-
ER	η_0* (dPa-s @ 60 °C, 0.1 rad/s)								
Aging	PG64-22	Bryan							
(months)	SAFT	PP2							
0	10500	36900	38200						
3	45760	81000	75000						
6	106400	122600	115500						
9	-	-	-						
ER	DSR Function x 10^4 (MPa/s @ 15 °C, 0.005 rad/s)								
Aging	PG64-22	Bryan		PG76-22SBS	Yoakum		PG76-22TR	C1	
(months)	SAFT	PP2		SAFT	PP2		SAFT	PP2	
0	0.43	2.13	2.11	0.80	3.24	2.31	1.41	1.52	1.73
3	3.11	6.60	5.50	8.83	7.43	8.31	9.48	-	-
6	8.30	10.00	8.90	16.1	12.6	11.4	22.5	15.60	14.90
9	19.79	-	-	49.3	25.4	25.6	39.7	-	-
ER	DSR Function x 10^4 (MPa/s @ 15 °C, 0.005 rad/s)								
Aging	A1		A2		B2			C2	
(months)	PP2		PP2		PP2			PP2	
0	3.09	2.95	1.81	1.84	1.93	1.97		1.17	1.40
3	-	-	-	-	-	-		-	-
6	6.08	5.75	4.36	4.80	12.70	13.70		7.33	6.78
9	-	-	-	-	-	-		-	-

The following sections present additional details on the effects of binder oxidation in the neat binders and the HMAC mixtures.

Viscosity Comparison for the unmodified binders

The zero shear viscosity (η^*_0) has been widely used to represent unmodified binder hardening. The binder hardening rate (r_{η^*}) has a linear correlation with aging time after the early rapid aging stage that is called the initial jump (Lau et al., 1992). The initial jump period includes the hardening in the hot mix plant and during construction and the hardening in the early rapid aging stage (Glover et al., 2005, Juristyarini, 2003). The equations III-3 - III-5 represents the ideas:

$$\ln \eta^*(t) = \ln \eta^*(t_0) + \Delta\left(\ln \eta^*(t_{HMix})\right) + \left(\Delta \ln \eta^*(t_{IJ})\right) + r_{\eta^*} t \qquad \text{(III-3)}$$

$$\eta^*(t) = Ae^{Bt},\ t > \text{initial jump time period} \qquad \text{(III-4)}$$

$$r_{\eta^*} = \frac{\partial \ln \eta^*}{\partial t} = \text{const},\ t > \text{initial jump period} \qquad \text{(III-5)}$$

where t is the aging time; $\eta^*(t)$ is the viscosity at any time; $\eta^*(t_0)$ is the original viscosity; $\eta^*(t_{HMix})$ is the viscosity change at hot mix plant; $\eta^*(t_{IJ})$ is the viscosity change in the initial jump period and A and B are experimentally determined coefficients. Further, Juristyarini (2003) explains that the hardening rate in the initial jump period decreases with aging time until it reaches constant after the initial jump period.

The binder hardening represented by the zero shear viscosity (η^*_0) in both the neat binders and the recovered binders from the Bryan mixtures (PG64-22 + limestone) increases with aging time shown in Figure III-2. SAFT aging leaves the binder within the initial jump (higher aging rate) region because the aging rate between 0 and 3 months is still higher than between 3 and 6 months. While PP2 aging is more severe than SAFT

aging, binder hardening is still not in a linear region. PP2 aging data between 0 and 3 months show a higher aging rate (slope) than between 3 and 6 months. The neat binder aging is also approaching the mixture aging with aging time.

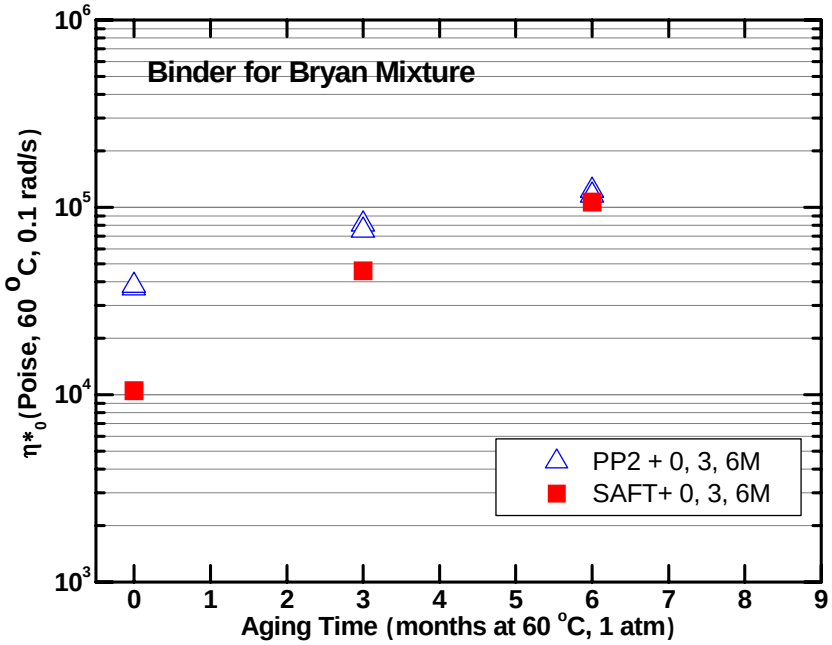

Figure III-2. η^*_0 Hardening Rate for Bryan Binders

The other binders used for the other mixtures are polymer modified binders, for which the zero shear viscosity is not appropriate for characterizing hardening rate because polymer modified binders typically do not exhibit a low shear rate limiting viscosity. Instead, the DSR function (at a defined temperature and frequency) hardening rate is used to represent changes of binder physical properties with aging.

DSR Function Hardening Comparison

The DSR function (G'/(η'/G')) represents binder hardening with its durability (Ruan et al., 2003; Al-Azri et al., 2006). The DSR function hardening rate ($r_{\text{DSR function}}$) is also constant with aging time after the initial jump period (Juristyarini et al., 2002)

$$\ln \text{DSR function} = \ln \text{DSR function}_0 + r_{\text{DSR function}} t \qquad \text{(III-6)}$$

$$r_{\text{DSR function}} = \frac{\partial(\text{DSR function})}{\partial t} = \text{const}, \text{ for } t > \text{initial jump time period} \qquad \text{(III-7)}$$

where t is the aging time and DSR function$_0$ is the intercept at t=0.

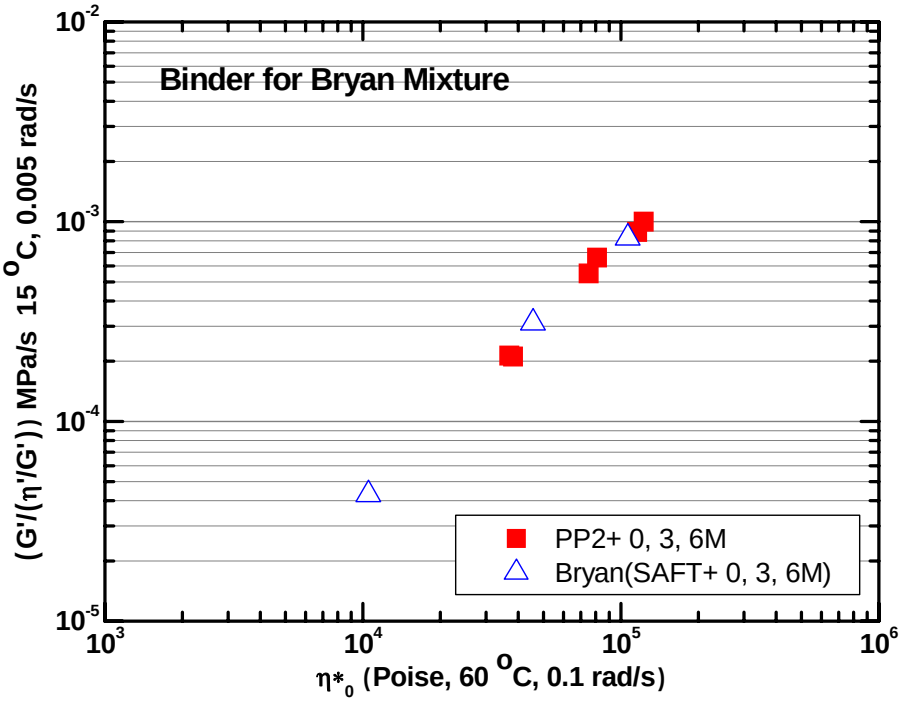

Figure III-3. DSR Function versus η*$_0$ for Bryan Binders.

The relation of DSR function and η^*_0 with aging time for the Bryan binder (PG 64-22) are shown in Figure III-3. The DSR function can be a good substitute for the zero shear viscosity because both the viscosity and the DSR function hardening have a very good linear correlation. In addition to that, as mentioned earlier, the DSR function increase due to binder oxidation relates to the binder's ductility decrease and its embrittlement increase, which will be shown graphically in the DSR map later.

Figures III-4 to III-6 show that both mixture aging and neat binder aging increase a binder's DSR function with aging time, which means the binder in the mixture also becomes harder and more brittle, as to neat binders with aging. The neat binder aging (SAFT+0, 3, 6, 9M) results indicate that all the neat binders aged at the SAFT aging level (SAFT+ 0M) are in the initial jump period and the more aged neat binders have a linear DSR function hardening rate from the 3 months in the 60 ^{o}C room after SAFT aging. The figures also show that the recovered binders at the PP2 aging level (PP2+0M) are more severely aged than the neat binders at the SAFT aging level (SAFT+0M) and the PP2 level aged binders (PP2+0M) do not completely pass the initial jump period. However, after 3, 6 and 9 months additional aging in the 60 ^{o}C room, the neat aged binders become harder than the mixture aged binders.

Figure III-4 shows the DSR function hardening of recovered binders from the three mixtures made with the PG 64-22 unmodified binder. With the PG 64-22 binder, limestone was used for the Bryan mixture and river gravel for the A1 and A2 mixtures to find the mixture design impact on the binder oxidative hardening and the HMAC fatigue performance. The A1 and A2 mixtures have different binder contents (optimum, optimum plus 0.5 percentage points) to understand the impact of binder contents on the binder oxidative hardening and the HMAC fatigue performance. The binders in the mixtures also become harder with aging time. The DSR function hardening rate between PP2+0M and 3M is higher than the hardening rate between PP2+3M and 6M. More aging levels are better for making a more accurate determination of the initial jump period; however, the small number of aging levels was necessary to reduce cost. The recovered A1 and A2 binders have two aging levels (PP2+0M, PP2+6M). The A1 binder

(recovered from the smaller binder content mixture) is harder than the A2 binder even with aging. Also, both the A1 and A2 binders show that binder oxidation can change the binder's rheological properties in the mixture with aging time. The comparison of hardening rate is not appropriate due to the limited data; PP2 + 3M data are not available for the A mixtures. Because of this, it is hard to determine whether the binder hardening has passed the initial jump period.

The recovered binders from the aged Yoakum mixtures with two binder contents are shown in Figure III-5. The figure also demonstrates that the binders in the mixtures become harder with aging time. In this case, the increase of 0.5 percentage points of the binder content does not affect binder hardening with aging time. Fortunately, the 9 month aged Yoakum mixtures with the optimum binder content after PP2 level aging were available (B1-PP2+9M). The figure also shows that the hardening rate of the recovered binders before PP2+3M is higher than the hardening rate among PP2+3M to PP2+9M.

The C1 and C2 binders are recovered binders from the mixtures which were made by the same mixture design as Yoakum mixture but with the PG 76-22 TR binder with two different binder contents. Figure III-6 shows that the binder content affects their hardening with the longer aging time of PP2+6M.

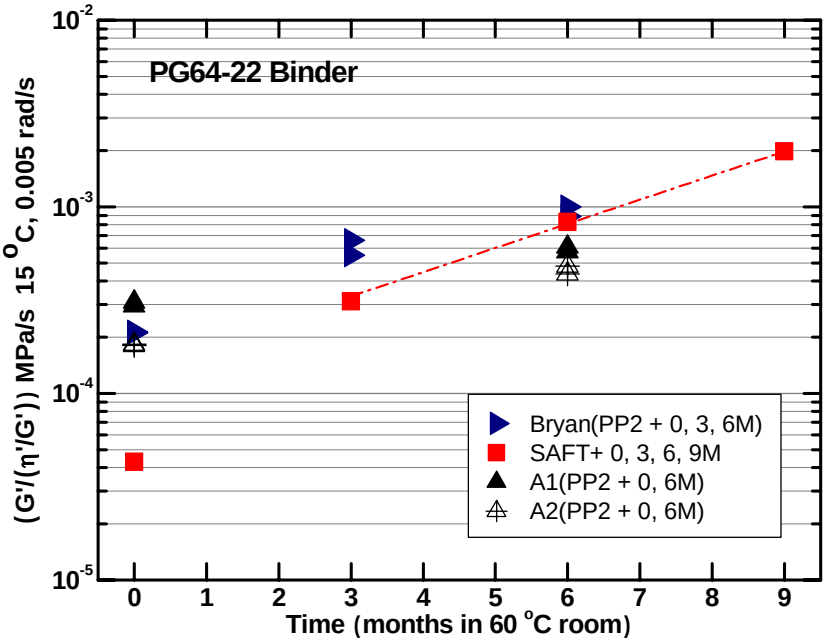

Figure III-4. DSR Function Hardening Rate for the Bryan Binder

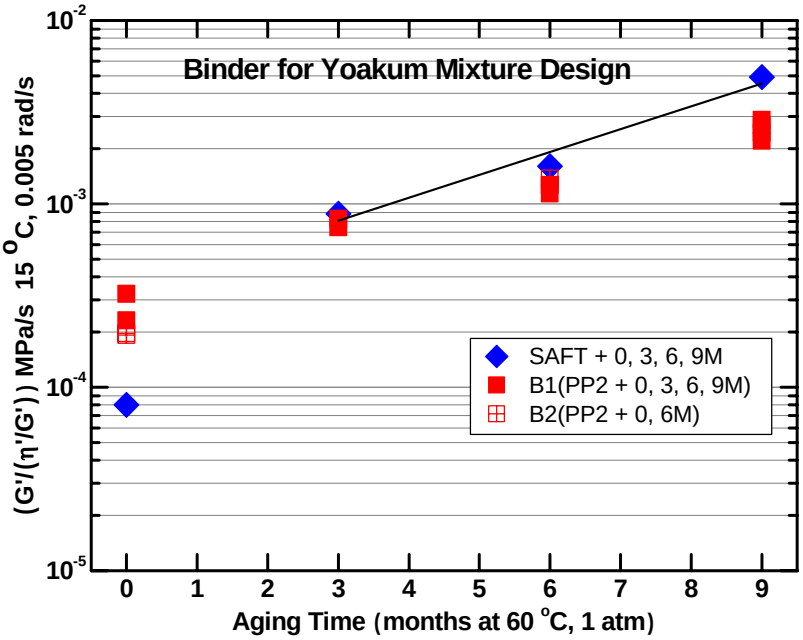

Figure III-5. DSR Function Hardening Rate for Yoakum Binder

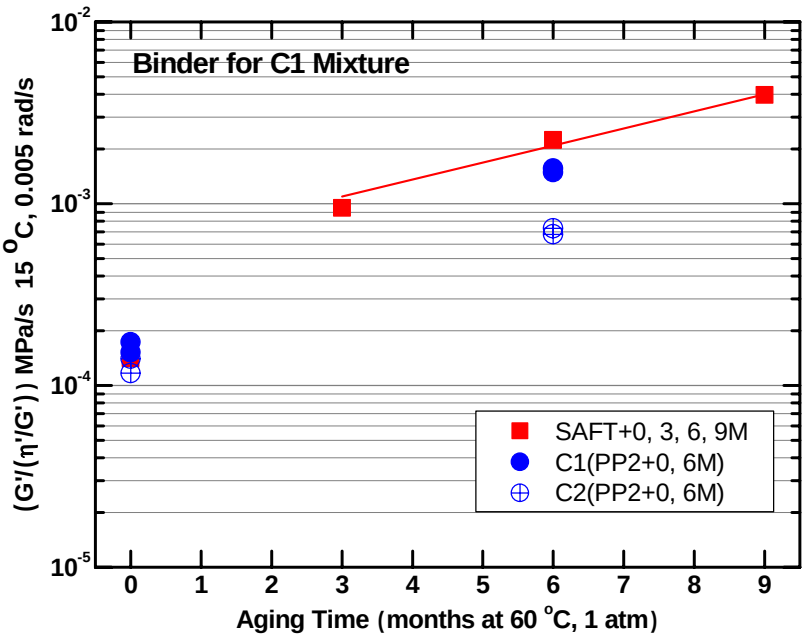

Figure III-6. DSR Function Hardening Rate for PG 76-22TR Binder

Carbonyl Area Growth Comparison

The oxidation rate (r_{CA}) can be described by Equation III-8 where *CA* is carbonyl area; CA_0 is extrapolated amount of carbonyl area at $t = 0$. The oxidation rate has a linear correlation with oxidation time after the initial jump period (Lau et al., 1992).

$$CA = CA_0 + r_{CA}t \qquad \text{(III-8)}$$

Figures III-7 to III-9 indicate that the CA also increases with aging for both the neat binders and for the recovered binders from the Bryan, the Yoakum and the C1 mixtures. These figures include all the CA data in Table III-4. The figures show that the CA increase with aging time follows the same trends as the DSR function increase: the binders at the PP2 aging level (PP2+0M) have the much higher CA than the binders at

the SAFT aging level (SAFT+0M); the PP2 aged binders did not pass the initial jump period; the binders have linear aging rates after initial jump and the neat thin film aged binders get the higher CA than the mixture aged binders after long term aging.

In Figure III-9, the binder modified with tire rubber and SBS (PG 76-22 TR for C mixtures) at the SAFT level aging shows different CA increases from the other two binders. The higher CA content at the SAFT aging level makes neat binder have a uniform oxidation rate from the SAFT aging level. The reason is unknown and more research is recommended. However, one previous study reports that one tire rubber/SBS modified binder has higher CA growth rate compared to its binder hardening rate with binder oxidation (Ruan et al., 2003a).

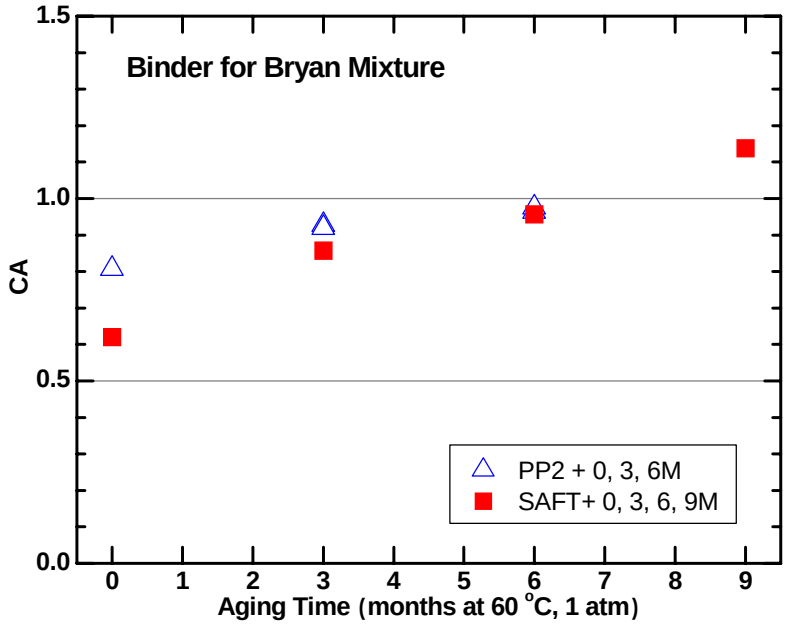

Figure III-7. Oxidation Rate for Bryan Binder.

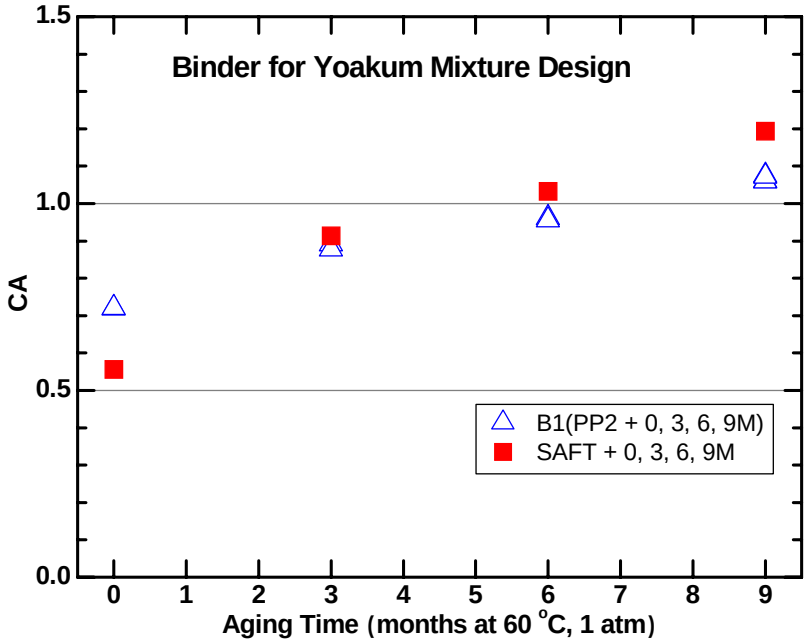

Figure III-8. Oxidation Rate for Yoakum Binder.

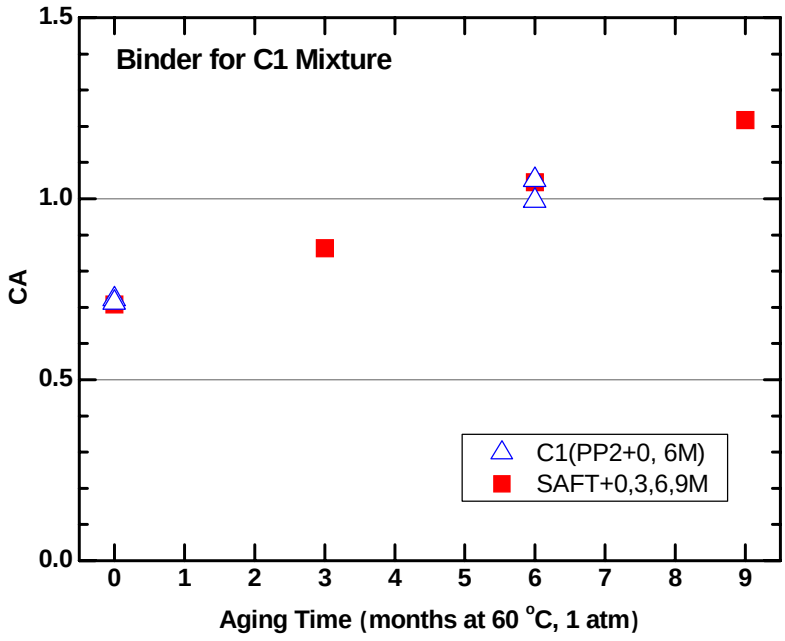

Figure III-9. Oxidation Rate for PG 76-22TR Binder.

DSR Function Hardening Susceptibility

The DSR function hardening susceptibility (HS) is a characteristic of the asphalt and is defined as the ratio of the ln DSR function increase to the CA growth. Previous studies indicated that DSR function HS is linear with binder oxidation at constant pressure (Juristyarini, 2003, Glover et al., 2005).

The DSR function hardening susceptibility for the Bryan binder is shown in Figure III-10. The DSR function is plotted on a logarithmic scale against the CA which represents the amount of aging. Thus, aging time is removed as a factor and both the PP2 aged binders and SAFT aged binders show the same linear relation between CA and DSR function.

Figure III-11 shows the increase in DSR function with CA for the Yoakum binder. Again, both the neat aged binders and the mixture aged binders show the same linear relation suggesting the same aging mechanism is followed in both cases.

The DSR function of the C1 mixture binder also increases with aging time, but the PP2 aging process (PP2 + 0 M) aged the C1 mixture binder slightly more than the SAFT process (SAFT+0M) in Figure III-12. Normally, SAFT aged binder is much less aged than PP2 aged binder. The C1 mixture binder has exceptionally high CA and DSR function hardening at SAFT aging level and slower hardening rate than the other two binders after the initial jump period. More data are recommended for certainty. However, this result provides possible criteria for designing more durable pavement. Higher initial stiffness could provide a high rut-resistant ability in early pavement service and slower hardening rate could improve long-term fatigue performance. More research is recommended to determine the fundamental reason for the different behavior of the C1 mixture binder. After 6 month additional aging in the 60 ^{o}C room, the neat thin film aged C1 mixture binder is harder than the mixture aged binder.

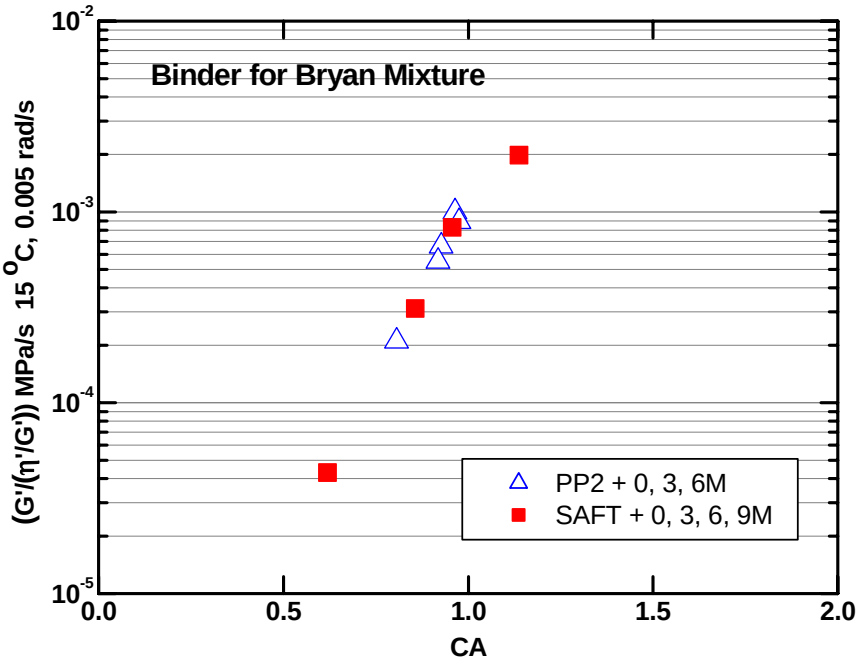

Figure III-10. DSR Function vs. Carbonyl Area of Bryan Binder (PG 64-22).

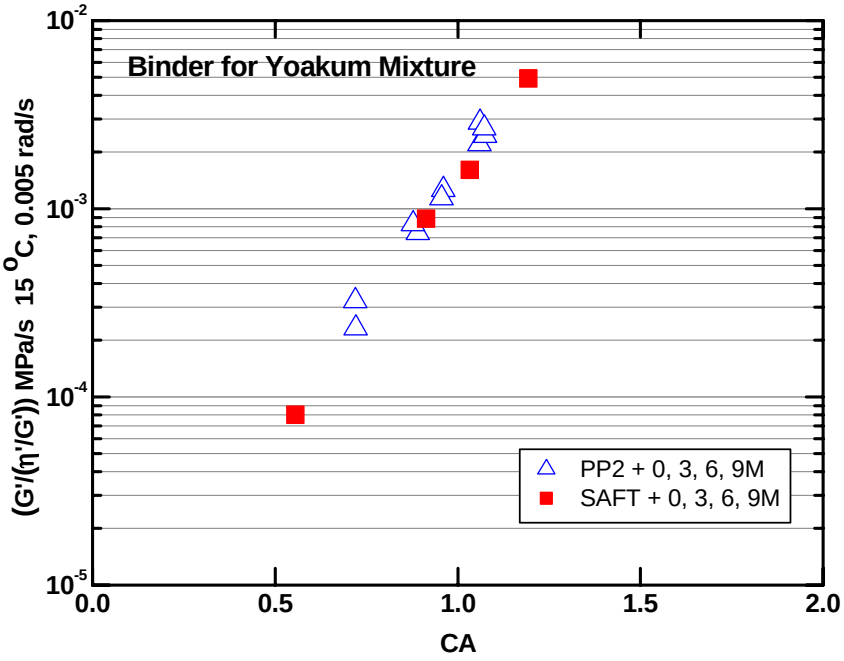

Figure III-11. DSR Function versus CA for Yoakum Binder (PG 76-22 SBS).

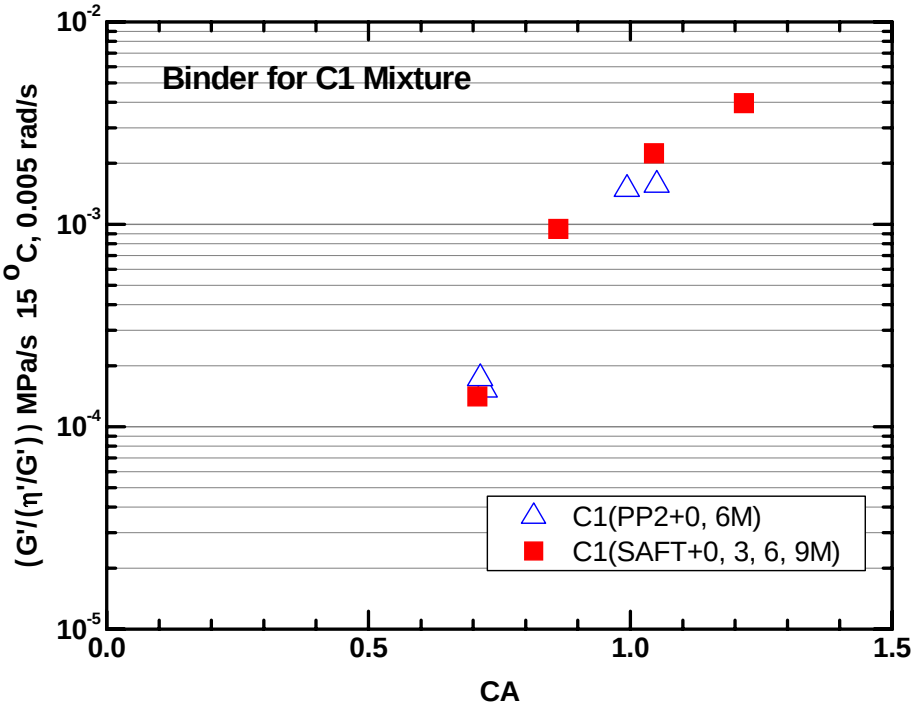

Figure III-12. DSR Function versus CA for C Mixture Binder (PG 76-22 TR).

DSR Map

DSR map (G' versus η'/G') aging paths for both the recovered binders from the aged mixtures and the neat-aged binders, are shown in Figures III-13 to III-15. In each case, all the binders move upward and to the left with aging, as has been observed previously (Ruan et al., 2003, Glover et al., 2005, Al-Azri et al., 2006).

The thin film binder aging catches up with the mixture binder partly because, after SAFT, it is still in the higher aging-rate initial jump period, but also because binder aging in thin films has more access to oxygen than binder in compacted mixtures. In the case of the Bryan binder, it appears that the same process is occurring but that the neat binder takes longer to catch up to the mixture-aged binder. Even though it is not very decisive to determine the exact starting point for a linear hardening rate slope, the SAFT+3M aging from the neat binder aging is surely beyond the initial rapid aging period.

DSR function values beyond SAFT+ 6 months (the neat binder aging) or PP2 +6 months (the mixture aging) are far more aged than standard PAV-aged binders. Note that only the Bryan binder has standard PAV data. However, Juristyarini et al (2003) showed that PAV aged binder hardening is close to PAV*16 hour in her study where the PAV*16 hour and PAV*32 hour procedures are considered in lieu of the standard PAV test as a field simulating aging process. PAV*16 and 32 hour aging results are also shown for comparison. Either PAV or PAV*16 aged binder after SAFT aging are approximately SAFT+3 months aging which is not long enough aging for the long-term binder aging conditions when compared to Texas field data in chapter II.

The curved, dashed lines shown are lines of costant ductility (cm at 15 ^{o}C, 1 cm/min) that were determined for unmodified binders by Ruan et al. (Glover et al., 2005, Ruan etal., 2003); as a binder ages, its ductility decreases. The previous studies suggest that a ductility of 3 cm at 15 ^{o}C is a value that corresponds well to age-related cracking failure in HMAC pavements (Kandhal, 1977, Dole, 1958, Vallerga 1971)

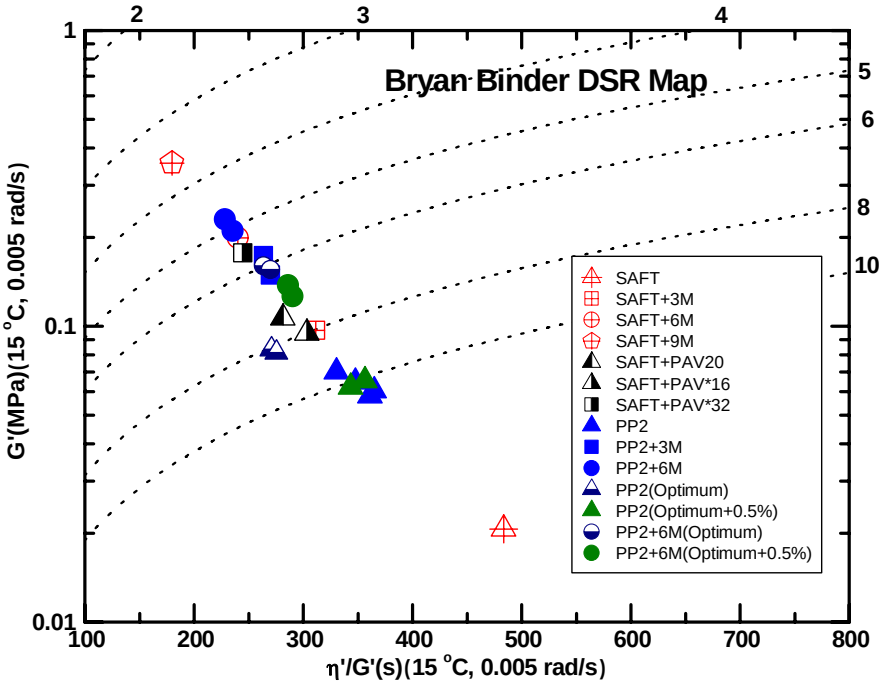

Figure III-13. DSR Map for Bryan Binder.

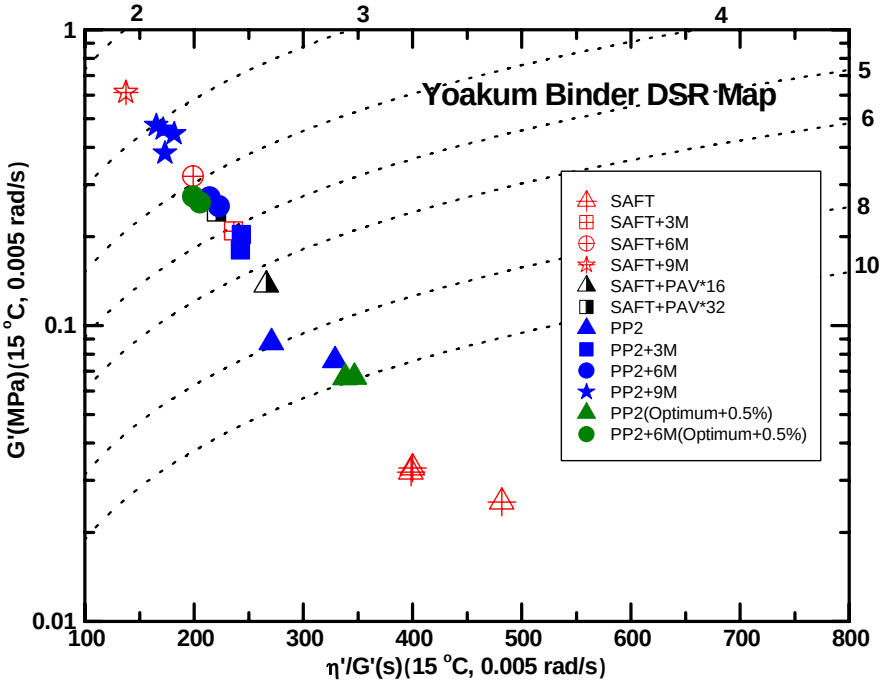

Figure III-14. DSR Map for Yoakum Binder.

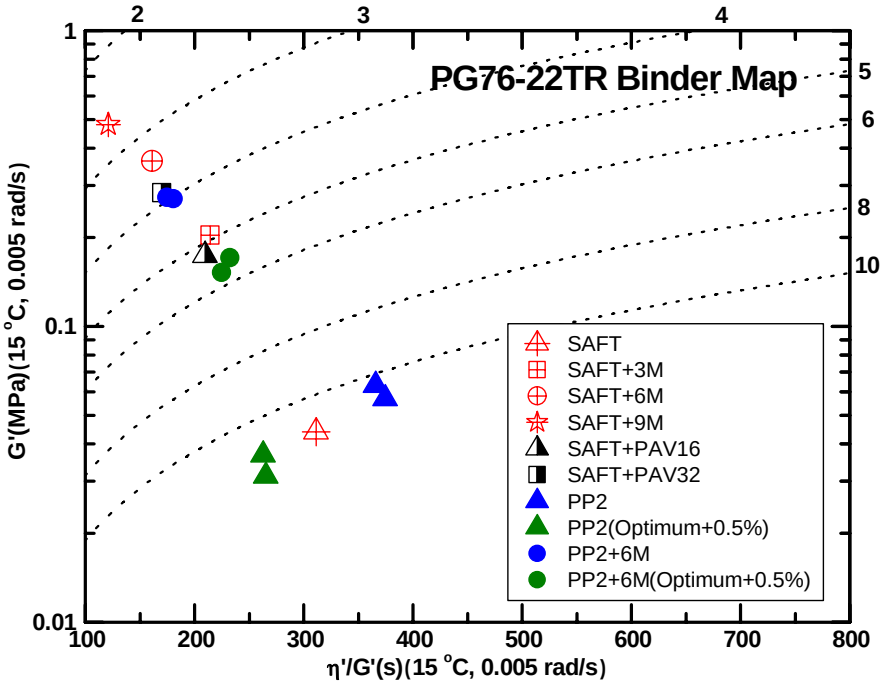

Figure III-15. DSR Map for C Mixture Binder

Mixture Oxidative Aging and Fatigue Resistance

As noted above, two mixtures were aged for 0, 3, and 6 months and 5 extra mixtures were aged for 0 and 6 months beyond PP2 conditioning in an environmental room (ER), temperature-controlled at 60 °C. These mixtures were subjected to the tests in Table III-3 to determine the various CMSE parameters from which mixture fatigue under strain-controlled testing was determined.

Table III-5 is a summary of the SF_i, the lab N_f (N_i + N_p), and the field N_f calculated from laboratory tested mixtures. While the Table shows some degree of SF_a dependence on mixture type due to the differences in the aggregate gradation, this parameter did not vary significantly as a function of aging condition based on a ±15% error tolerance. This SF_a insensitivity to aging was theoretically expected because anisotropy is predominantly controlled by particle orientation due to compaction and will therefore be insignificantly affected by aging. Therefore, the same SF_a for the other mixtures were used for the field N_f calculations.

SF_h on the other hand is dependent on both mixture type and aging condition. In terms of SF_h magnitude, the higher the value, the greater the potential to self heal. The Table shows that SF_h decreases with oxidative aging and increases with binder content at PP2 level aging. As mentioned earlier, the A1, B1 and C1 mixtures have optimum binder content and the A2, B2 and C2 mixtures have optimum + 0.5 percentage point binder content. Therefore, mixtures lose their healing ability with aging and show better SF_h with more binder content at the initial aging time. However, SF_h does not increase significantly with the increase of binder content at 6 months beyond the PP2 level aging.

Table III-5. Summary of Shift Factor, Lab N_f, and Field N_f Results*

Mixture	Parameter	Aging Condition (Months in 60 °C ER beyond PP2)		
		0	3	6
Bryan	SF_a	1.63	1.65	2.09
	SF_h	6.73	4.74	3.07
	Lab N_f	6.31 E+06	2.42 E+06	0.94 E+06
	Field N_f	69.2 E+06	18.9 E+06	6.03 E+06
Yoakum (or B1)	SF_a	2.10	2.08	2.40
	SF_h	7.26	4.76	3.81
	Lab N_f	7.88 E+06	4.95 E+06	3.23 E+06
	Field N_f	1.20 E+08	4.91 E+07	2.95 E+07
A1, A2, B2, C1, C2	SF_a	2.0	2.0	2.0
A1	SF_h	7.18	-	3.63
	Lab N_f	1.30E+07	-	4.98E+06
	Field N_f	1.86E+08	-	3.62E+07
A2	SF_h	7.28	-	3.66
	Lab N_f	1.49E+07	-	5.26E+06
	Field N_f	2.16E+08	-	3.85E+07
B2	SF_h	7.32	-	3.98
	Lab N_f	9.01E+06	-	4.12E+06
	Field N_f	1.32E+08	-	3.28E+07
C1	SF_h	5.91	-	2.97
	Lab N_f	4.92E+06	-	2.73E+06
	Field N_f	5.82E+07	-	1.62E+07
C2	SF_h	6.53	-	2.95
	Lab N_f	6.12E+06	-	2.71E+06
	Field N_f	7.99E+07	-	1.60E+07

* Lubinda Walubita in the Epps research group provided these data for this study

Binder oxidative aging in mixtures significantly decreases controlled-strain fatigue performance. Figure III-16 shows the decline of Field N_f as the result of binder aging and the deterioration is significant in all cases. Fatigue life decline with binder oxidation is also characteristic of each mixture type. The mixtures show different fatigue decline rates which are independent of field N_f at PP2 level aging. Even though the A mixture has the higher N_f than the other mixtures at PP2 level aging, the B and C mixtures have slower fatigue decline rates than the A mixture over the period of aging time. This difference is significant with respect to the expected pavement fatigue performance. The reasons for this difference are not as yet understood, but are important and merit further research.

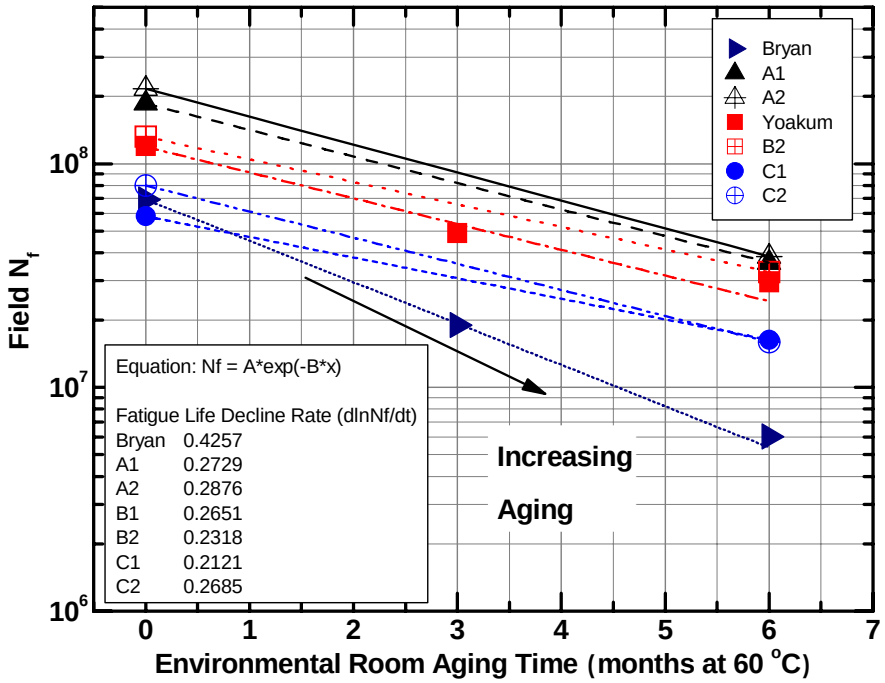

Figure III-16. Decline of Field N_f with Oxidative Aging.

Figure III-16 also shows the impact of binder type on the fatigue performance. Except for the Bryan mixtures, all the mixtures were made from the same mixture design where the only difference is the binder type. The mixtures with the different binder types give the different fatigue performance and decline rates. Compared to the binder types, binder content has a little impact on the fatigue performance.

Figure III-17 shows the fatigue performance results from the different mixture designs that used the same binder. Even though the binder type is the same, the different mixture design provided different initial fatigue life and different fatigue decline rate. The reason is not clear, but initial bond strength between the binder and the aggregate and change in bond strength with aging may play a role in the different fatigue performances.

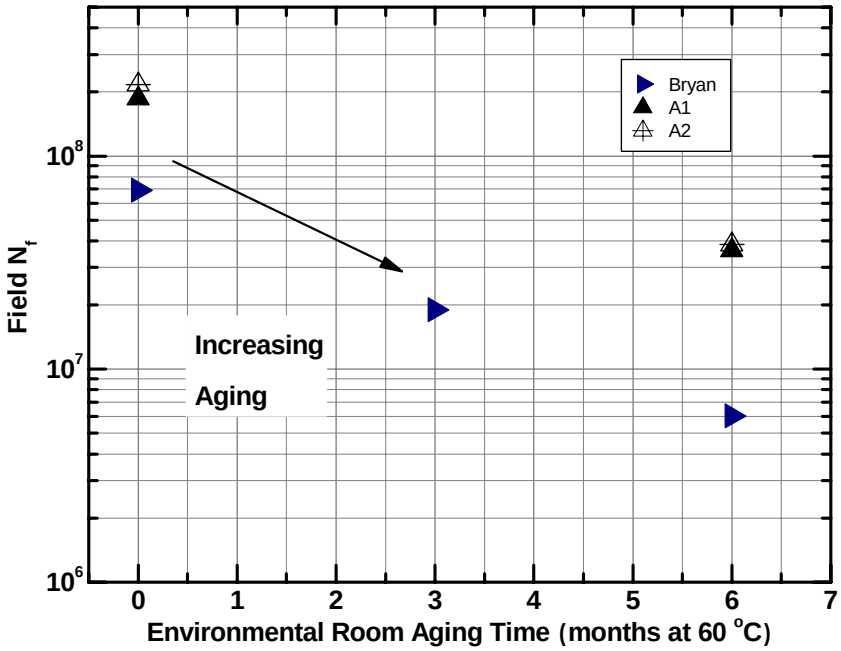

Figure III-17. Decline of Field N_f with Different Mixture Designs due to Binder Oxidation

Summary and Conclusions

Three types of binders and seven types of mixtures with different aging levels have been studied to determine the impact of binder oxidation on the HMAC fatigue performance. Mixture aging was compared to neat binder aging to determine whether the mixture aging follows the same aging mechanism as neat binder aging. The field fatigue was calculated from the measured laboratory fatigue at different binder oxidation levels. Following are the conclusions and recommendations from this study:

Findings

1) Binder oxidation significantly decreases the strain controlled fatigue life.
2) Binder oxidation in mixtures follows a similar path as neat binders (DSR function hardening rate, hardening susceptibility, DSR map) even though hardening rates in mixtures are slower than those in neat binder thin-films due to diffusion resistance.
3) The PP2 level aging process ages binders more severely than the SAFT level aging. However, the PP2 level aged binders for this study still are not out of the initial jump period.
4) DSR Function is a good rheological property for tracking binder durability due to oxidative hardening.
5) Standard PAV is not appropriate for measuring the long-term aging binder properties for Texas asphalt pavement.
6) HMAC mixture fatigue performance is a function of mixture design and binder type, and greatly affects the HMAC mixture fatigue performance. However, variability of binder content within normal construction ranges does not affect the fatigue life as much as binder type and mixture design.

Recommendations

1) A more fundamental study of binder hardening related to the mixture fatigue life is recommended. The relationship between the mixture fatigue and binder hardening needs better understanding.
2) The fatigue life at PP2 level aging is not a sufficient criterion to determine pavement fatigue performance. Therefore, the study of better fatigue performance criteria is recommended.
3) More research is recommended to find the threshold of a linear hardening period in mixture aging.
4) The reason why the tire rubber/SBS modified binder has a lower DSR function HS and a low hardening rate needs to be determined.

The impact of binder oxidation on mixture fatigue life has been studied. In the following chapter, a method of estimating a pavement service life by using cumulative damage approach is described.

CHAPTER IV
ESTIMATING THE EFFECT OF BINDER OXIDATION ON PAVEMENT SERVICE LIFE BY USING A CUMULATIVE DAMAGE APPROACH

Synopsis

Binders oxidize in laboratory mixtures, leading to binder embrittlement and decreases in fatigue resistance. Critical questions to pavement performance prediction are: 1) to what extent might embrittlement and decrease in fatigue resistance lead to a decline in pavement life, and 2) do different mixture designs react differently with regard to this question.

Seven different laboratory-aged (aged at 60 °C, 1 atm air) mixtures were analyzed for fatigue resistance and mixture rheological properties. Also, their recovered binders were analyzed for oxidation and rheological properties. Finally, laboratory-aged (aged at 60 °C, 1 atm) neat binders were analyzed for oxidation and rheological properties for comparison with the recovered mixture-aged binders.

Declines in mixture fatigue life (determined using the calibrated mechanistic fatigue analysis approach with surface energy measurement, CMSE) due to oxidation, coupled with a Miner's hypothesis analysis of cumulative damage, predict very significant decreases in pavement durability. Additionally, different mixtures can provide dramatically different calculated pavement lives when this decline in fatigue with oxidative aging is considered. The differences in expected pavement life arise from the initial fatigue lives but, even more significantly, from differences in the rate of binder stiffening due to oxidation in mixtures and the impact of this stiffening on fatigue life decline.

Introduction

Binder oxidation has a great potential impact on long-term performance of hot-mix asphalt concrete (HMAC) pavement. HMAC is a complex composite material of air, aggregates, and binder that is used in more than 2.3 million miles of asphalt pavement in the United States (FHWA, 2001). Among the materials in the HMAC mixture, it is mainly the binder that changes due to oxidation. Binder oxidation causes both the elastic (G') and loss (G") moduli of binder to increase and the phase angle of binder to decrease (Glover et al., 2005). These detrimental effects increase the susceptibility of HMAC mixtures to fatigue cracking.

The mechanical properties, anisotropic behavior, and fatigue performance of HMAC mixtures depend on traffic loading rate, and environmental conditions (Kim et al., 1997b; Lee, 1996; Lytton et al., 1993). HMAC mixtures also have the potential to heal (closure of fracture surfaces) during traffic loading rest periods (Cheng, 2002; Kim et al., 1997a; Si, 2001). The complicated characteristics of HMAC mixtures are difficult to adequately model.

Previous studies (Doyle, 1958, Kandahl and Koehler, 1984, Kandhal, 1977, Clark, 1958, Halstead, 1963) indicate that pavement long term durability relates well to asphalt binder ductility. Ruan et al. (2003) found a good correlation between a fundamental rheological function, also called DSR function (G'/(η'/G')) and ductility below ductilities of 10 cm. They found that binder long-term durability is not dependent on a single rheological property such as the dynamic elastic shear modulus, G' and the dynamic shear viscosity, η' but rather both G' and η'/G'. Al-Azri et al (2006) showed that the DSR function can represent binder hardening as well as binder durability (represented by ductility) in field asphalt pavements with binder oxidation.

The primary goal of this study was to develop a method of estimating changes in pavement service life due to the decline of HMAC mixture fatigue with binder oxidation. The relation of the fatigue life to oxidative binder hardening, the binder hardening rate, pavement loading rates and estimated initial fatigue lives are investigated

for their impact on the expected pavement service lives.

Objectives

In this study, the effects of binder oxidative aging on HMAC fatigue resistance were investigated using a continuum micromechanics-based calibrated mechanistic fatigue analysis approach with surface energy measurement. The specific objectives of the study were 1) to develop a cumulative damage understanding of fatigue decline that utilizes both mixture and binder characteristics, 2) to estimate pavement service life by considering binder oxidation and pavement loading rate simultaneously, and 3) to determine important criteria for pavement service life.

Methodology

Three different types of binders, seven different types of HMAC mixtures and the recovered binders from the HMAC mixtures were tested at several levels of binder oxidation for this study. Binder tests include: gel permeation chromatography (GPC) using a refractive index (RI) detector to insure complete solvent removal in the binder recovery process; dynamic shear rheometry (DSR) to measure the rheological properties of the binder; and Fourier transform infrared (FTIR) spectroscopy to measure the carbonyl content in the binder. The CMSE laboratory tests for the HMAC mixtures involve the use of Whilhelmy plate (WP), the universal sorption device (USD), and other instruments to determine tensile strength (TS), uniaxial relaxation modulus (RM) and dissipated pseudo strain energy (DPSE). More details and references are given in Chapter III.

Results and Discussion

The results can be divided into two parts of interest: first, the impact of binder oxidative hardening on the HMAC mixture fatigue performance and second, the estimation of expected pavement service life by using a cumulative damage approach. In the first part, neat binder aging is compared with the mixture aging to emphasize that binder oxidation gives a detrimental impact on both binders. Then, the fatigue decline due to binder oxidation is noted. In the second part, a method of estimating pavement service life by simultaneously considering binder oxidative hardening impact and pavement loading rate and the other parameters which can impact pavement service life are studied.

Binder Aging Versus Mixture Aging

The physico-chemical properties of thin film aged neat binders and those of recovered binders from aged mixtures are compared to help assess whether the mixture aging process ages binders with the same aging mechanism as the neat binder aging process. Figure IV-1 shows that the DSR function (G'/(η'/G')) for the recovered binders versus the CA, increases with aging. The DSR function is plotted on a logarithmic scale against the CA which represents the amount of aging, thereby removing aging time as a factor. In the figure, both the mixture aged binders and the neat aged binders have the same linear relations between CA and DSR function after the initial jump (rapid aging) period. The results suggest that neat binder aging and mixture aging have the same aging mechanism even though there is diffusion resistance in the mixture aging, that shows the binder hardening and oxidation rates compared to neat binder aging.

The figure also indicates that the PP2 level aged binders (PP2+0M) are more aged than the SAFT level aged binders (SAFT+0M) but later, after 3 and 6 months additional aging in the 60 ^{o}C room, the neat aged binders are either catching up with or passing by the mixture aged binders because, after SAFT, it is still in the higher aging-

rate initial jump period, but also because binder aging in thin films has more access to oxygen than binder in compacted mixtures. In the case of the Bryan binder, it appears that the same process is occurring but that the neat binder takes longer to catch up to the mixture-aged binder.

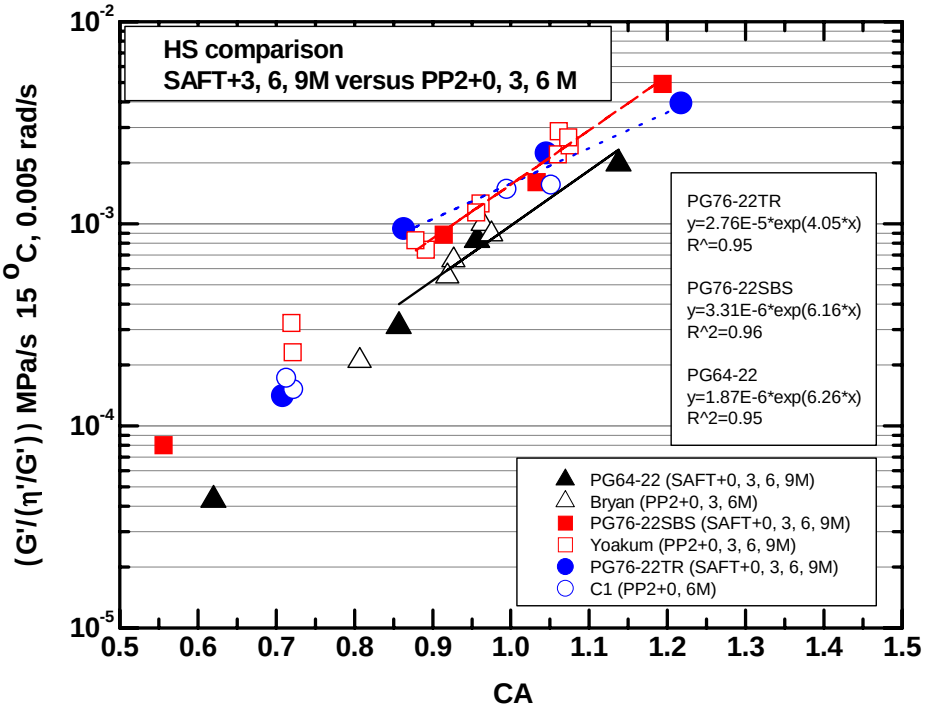

Figure IV-1. DSR Function versus CA for the Binders.

The Impact of Binder Oxidation on Mixture Fatigue Life

In Figure IV-2, the effect of binder oxidative aging on mixture fatigue resistance is presented. The decrease in controlled strain fatigue life with aging is striking, and

significant differences in the rate of decline were noted among the mixtures. The details of the fatigue results are given in Chapter III. The reasons for these differences are as yet unknown. The discussion in next section elaborates on the possible impact of this decline in fatigue resistance on a pavement's service life and its relationship to binder mixture characteristics.

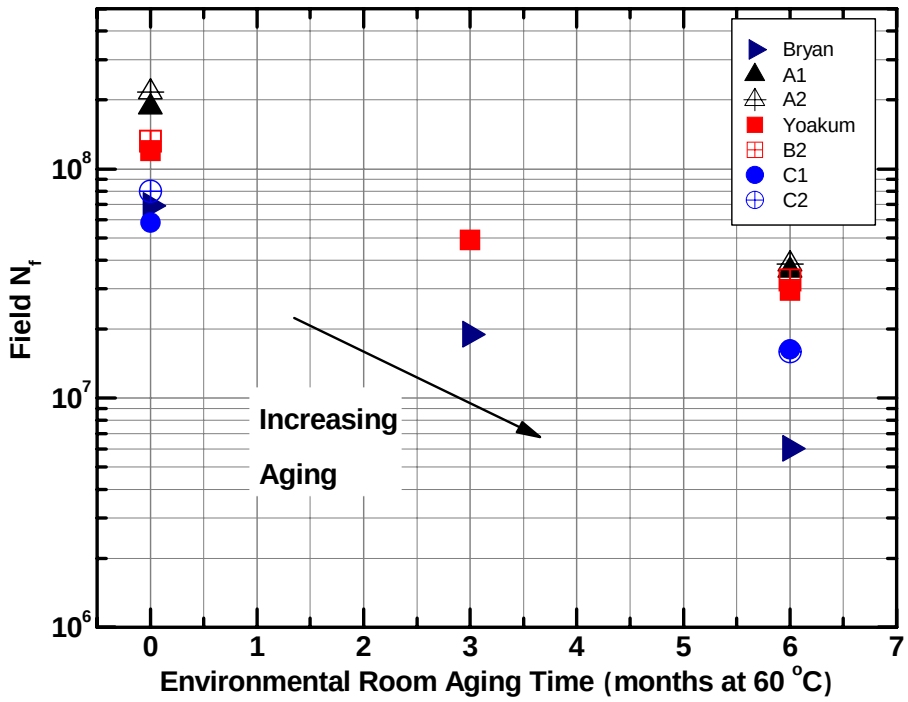

Figure IV-2. Decline of Field N_f due to Binder Oxidation

Cumulative Damage Approach

The approach discussed below utilizes the binder DSR function, attempts to incorporate the significant aspect of traffic loading, and is based on Field N_f. First, the following definitions are made:

N_f = Field fatigue life, in ESALs

R_L = Pavement loading rate, ESALs/yr

Then N_f / R_L = Pavement Fatigue Life Expectancy, in years, assuming that the fatigue is the only factor consuming the pavement life (no decline due to aging, for example). If, however, Field N_f is a function of time due to a decline with binder oxidative aging, for example, then this decline must be taken into account when estimating the pavement fatigue life. This process is typically quantified by calculating cumulative damage by Miner's Hypothesis as:

$$D = \sum \frac{n_i}{N_i} \tag{IV-1}$$

where D is the total damage (as a fraction) and N_i is the fatigue life when n_i loads are applied.

In this work, damage and hardening rates due to oxidation are related by the same approach but expressed in terms of time rather than loads. For a differential time period *dt*, during which the field fatigue life is $N_f(t)$, the fraction of a pavement's total available fatigue life consumed during *dt* is calculated as:

$$\text{Fraction of Life Expended During Time } dt = \frac{dt}{N_f(t) / R_L} \tag{IV-2}$$

Then, Miner's hypothesis is used to sum over the pavement's entire life, defined to be the amount of time to reach an integrated fraction equal to unity:

$$\int_0^{t_{end}} \frac{dt}{N_f(t)/R_L} = 1 \qquad \text{(IV-3)}$$

Now, from the experimental data for the decline of Field N_f with binder oxidative aging, $N_f(t)$ can be represented by an exponential relation:

$$N_f(t) = N_{f0} e^{-K_1 K_2 t} \qquad \text{(IV-4)}$$

where K_1 is the magnitude of the power law slope that relates the decline of N_f to the increase in the DSR function G'/(η'/G') with aging and K_2 is the (exponential) rate of increase of the DSR function with aging time in the pavement. More explanations on K_1 and K_2 are on page 81 to 83. N_{fo} is the initial fatigue life at t = 0. Solving this integral for t_{end} gives:

$$t_{end} = \frac{\ln(K_1 K_2 N_{f0}/R_L + 1)}{K_1 K_2} \qquad \text{(IV-5)}$$

Equation IV-5 also can be solved numerically for t_{end} if an analytical expression is not available.

An aging shift factor can be defined as the ratio of the age-shortened fatigue life to the unaged fatigue life expectancy:

$$SF_{aging} = \frac{\text{Age} - \text{shortened Life}}{\text{Unaged Life Expectancy}} = \frac{\ln(K_1 K_2 N_{f0}/R_L + 1)}{K_1 K_2 N_{f0}/R_L} \qquad \text{(IV-6)}$$

From this relationship, the bigger K_1 and K_2 are, the smaller the aging shift factor, i.e., the shorter the pavement's fatigue life expectancy. Equation IV-6 also shows that K_1 and K_2 have an identical effect on this shift factor. That is, the impact of aging on

the DSR function and the response of the fatigue life to these changes in DSR function produce the same effect on the final aging shift factor.

The decline of mixture fatigue life with increasing DSR function is shown in Figure IV-3. Values of N_{f0} (here equal to the fatigue life of the PP2-aged compacted mixtures) were reported in Table IV-1, and K_2, the ln(DSR function) hardening rate, is taken from a lab-to-field hardening rate conversion factor of 15 field months per one ER month obtained in Project 0-1872 (Glover et al., 2005) and applied to the DSR function hardening rate in Figure IV-4. Hardening rates of course vary from pavement to pavement and depend principally upon the climate but also on air voids and binder content. Consequently, the value used here gives only an approximate indication for any specific pavement.

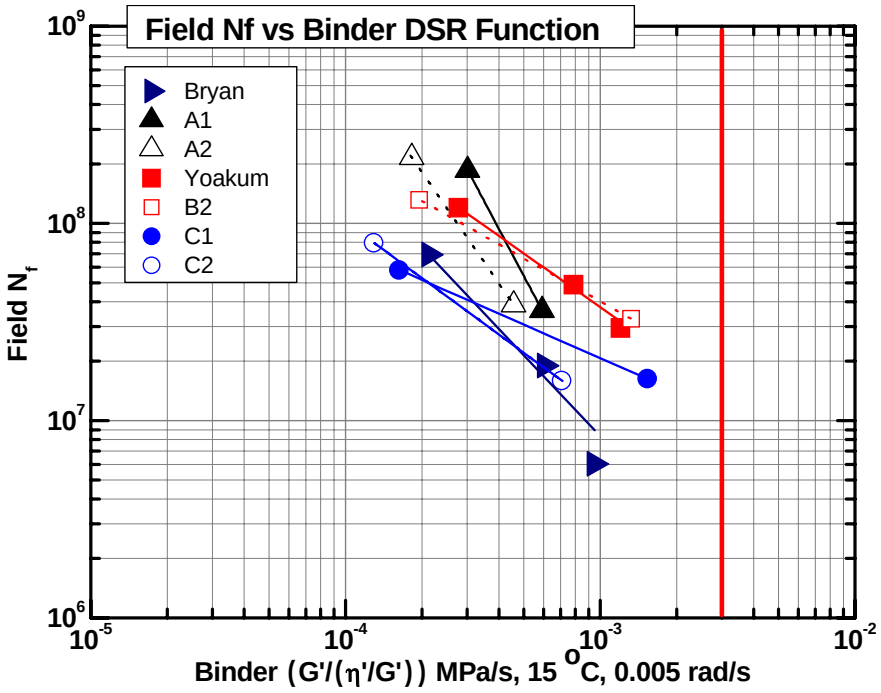

Figure IV-3. Decline of Mixture Field N_f with Binder DSR Function Hardening.

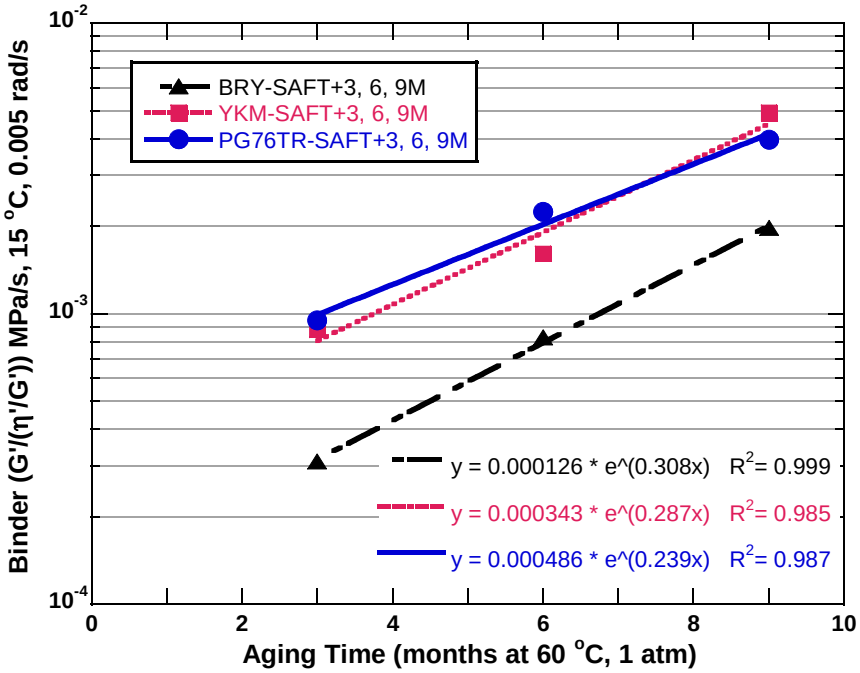

Figure IV-4. DSR Function Hardening Rate of Neat Binder after Initial Jump.

Table IV-1. Summary of Pavement Fatigue Life Parameters

Mixture	N_{fo} 10^6 ESALs	R_L 10^6 ESALs/yr	K_1	K_2	SF_{aging}	Pavement Life (yrs after PP2)
Bryan	69	0.25	1.37	0.25	0.049	13.5
A1	186	0.25	2.44	0.25	0.014	10.2
A2	216	0.25	1.87	0.25	0.015	13.0
Yoakum (B1)	120	0.25	0.91	0.23	0.046	22.1
B2	132	0.25	0.73	0.23	0.051	26.9
C1	58	0.25	0.57	0.19	0.129	30.1
C2	80	0.25	0.95	0.19	0.070	22.5

Table IV-1 summarizes the parameters and calculations for the mixtures. A loading rate of 0.25 million ESALs/year was selected for these calculations, consistent with the hypothetical field condition discussed in the HMAC Mixtures Tests section of

chapter III. These calculations are intended primarily to represent a calculation procedure that shows the differences in fatigue life that might be expected between different mixtures, based upon laboratory measurements that account for binder oxidative aging. More laboratory and field data are needed to verify this approach.

As an additional calculation, a remaining fraction of a pavement service life (*fr*) can be expressed in Equation IV-7 because the fraction of the remaining service life (*fr*) is equal to 1 minus the fraction of the consumed pavement service life (*fc*).

$$fr = 1 - fc = 1 - \frac{R_L}{N_{f0} K_1 K_2} \left(e^{K_1 K_2 t} - 1 \right) \qquad \text{(IV-7)}$$

The difference in the estimated pavement service lives (after PP2 short-term aging) for the mixtures is striking. The results are shown in the figures IV-5 to IV-7, where the curved lines represent the remaining service life change with aging, and the straight lines represent remaining service life change without aging impact. The remaining fraction of estimated service life drastically decreases with aging time in all cases, when aging impact was considered.

The pavement service lives of the Bryan and the A mixtures, for which the PG 64-22 unmodified binder is used, are shown in Figure IV-5. Even though the N_{f0} values for the A mixtures are much greater than the N_{f0} values for the Bryan mixture, the pavement service life of the Bryan mixture is better than the A1 mixtures and about the same as the A2 mixtures, which has 0.5 percentage point more binder than the A1 mixture. These results show that the impact of K_1 is greater than that of N_{f0} because their K_2 and R_L values are the same but N_{f0} and K_1 are not.

While the Yoakum mixture (B1) also has the smaller N_{f0} than the A1 mixtures, it has the much longer pavement service life primarily due to the lower K_1 value. This result is shown in Figure IV-6 where the B2 mixture has a higher calculated service life than the B1 mixture. The B mixtures like the A mixtures, improve service life with more

binder content; however, the impact of binder content increases is not significant, compared to the impact of K_1 and K_2.

The C1 mixture also indicates the importance of the K_1 and K_2 values, Figure IV-7. Even though the C1 mixture has the lowest N_{f0} among the seven different mixtures, it has the highest calculated pavement service life due to its lowest K_1 K_2 product.

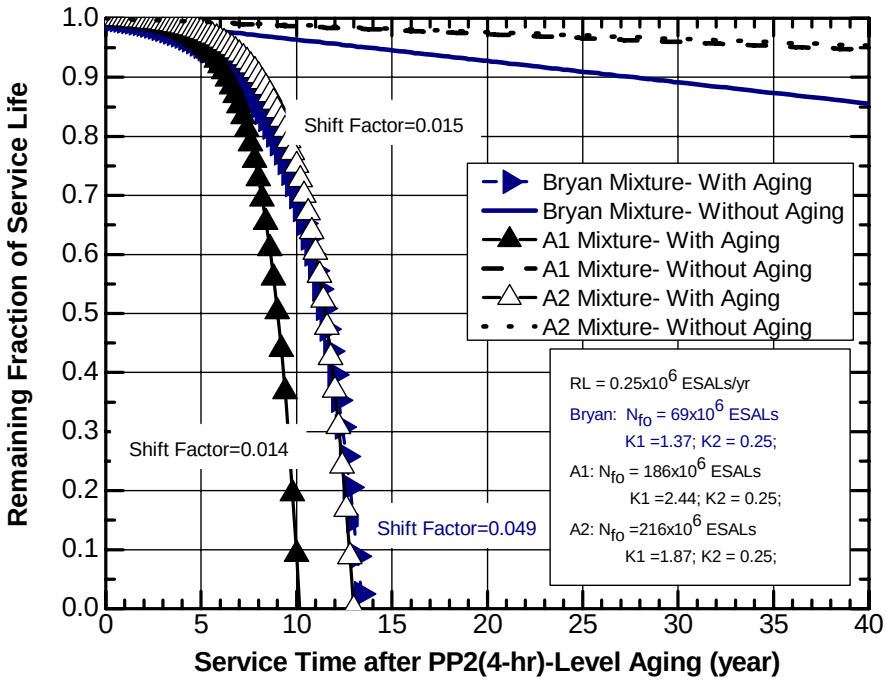

Figure IV-5. Service Life Decline for Bryan, A1, and A2 Mixtures due to Aging

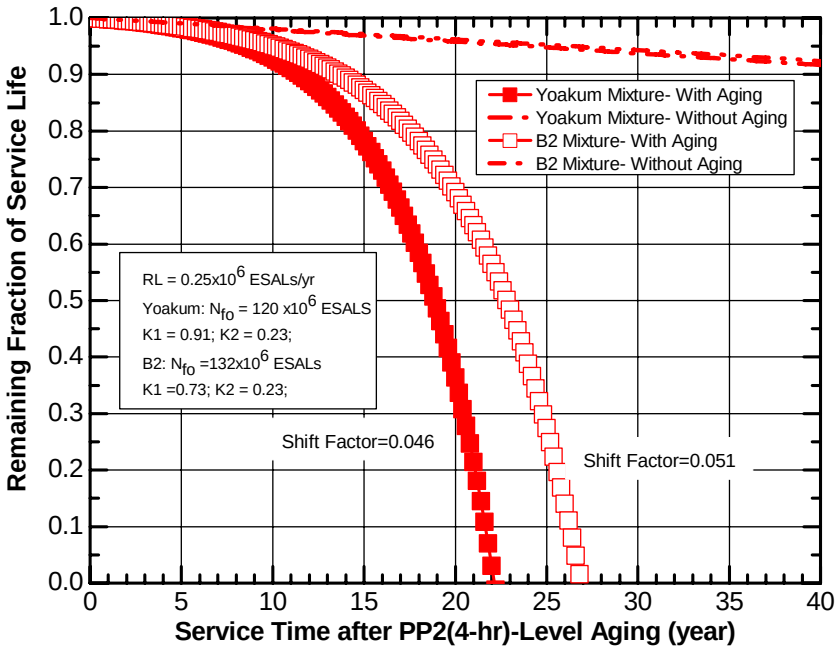

Figure IV-6. Service Life Decline for Yoakum Mixtures due to Aging

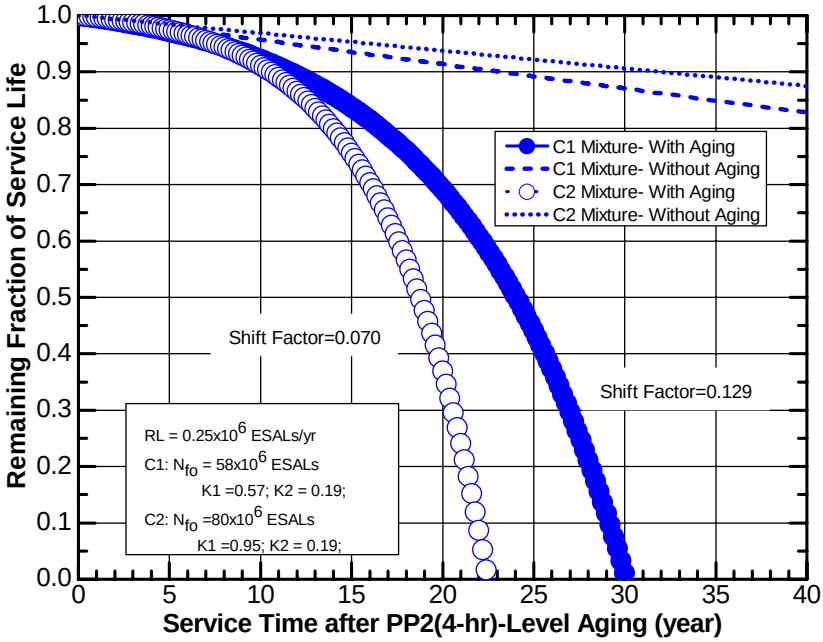

Figure IV-7. Service Life Decline for C1 and C2 Mixtures due to Aging

In summary, the C and the B mixtures have longer estimated service lives than the A mixture even though the A mixture has a higher fatigue life than the other mixtures at PP2 level aging. All the data are shown in Figure IV-8 for comparison.

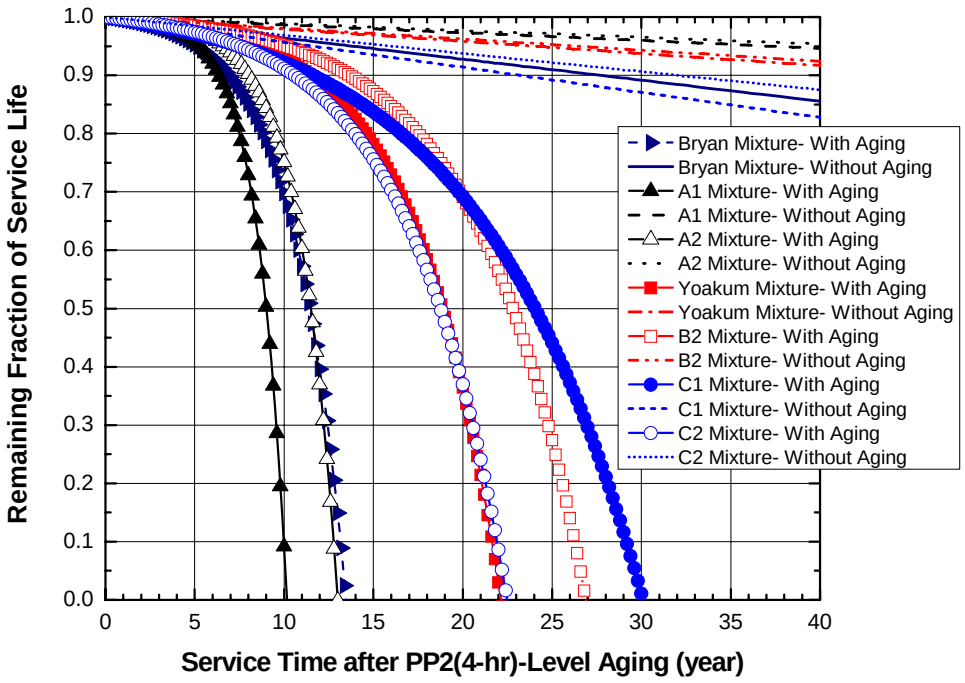

Figure IV-8. The Effect of Oxidative Aging on Estimated Pavement Service Life

It should be noted again that PP2 short-term aging produces a binder in the mixture that is significantly more aged than the SAFT (Rolling Thin Film Oven Test equivalent) aged binder. How PP2 aging compares to the aging of an in-service HMAC pavement is yet unknown. However, based upon the work of Glover et al., the PP2 aging may reflect as much as four years of HMAC pavement in-service life (Glover et al., 2005). If so, the calculated 10 years service life after PP2 aging (A1 mixture) amounts to

14 years of HMAC pavement total service life, the 20 years service life after PP2 (Yoakum mixture) 24 years and the 30 years after PP2 for the C1 mixture would correspond to 34 years of HMAC pavement total service life.

The differences in pavement fatigue lives for the mixtures are the results of K_1, the rate at which the fatigue life declines with binder oxidative hardening and K_2, the binder's hardening rate in the pavement. The hypothetical impacts of K_1, K_2, N_{f0} and R_L on the pavement service lives are compared in Figures IV-9 – IV-12. These comparisons suggest that K_1 and K_2 values have significant roles on the pavement service life.

In Figure IV-9, the impact of the initial fatigue life on the pavement service life while holding other parameters constant is not overwhelming. Note that '*' in the figure represents the measured N_{f0} values for a given mixture, Table IV-1. The N_{f0} increases over those data points do not result in dramatic increases in their service lives. Therefore, N_{f0} (the field fatigue life at PP2 level aging) may not be the most important indicator of fatigue life.

Figure IV-10 shows the impact of K_1 on the pavement service life while holding other parameters constant, which suggests that it has the most significant effect of the four parameters. All the given mixture's service lives are greatly affected by the K_1 values no matter how good their other parameters are. However, a fundamental understanding of how K_1 might be decreased by changes in mixture parameters is unknown and more research is strongly recommended.

The impact of K_2 is shown in Figure IV-11 where the pavement service lives greatly decrease as the binder hardening rate increases. Therefore, more oxidative hardening resistant binders are desirable to expand pavement service lives.

Figure IV-12 shows the impact of R_L (pavement loading rate) which greatly affects the pavement service life below approximately 0.5 million ESALs/year and its detrimental impact is greatly reduced beyond 1.5 million ESALs/year. It also shows again that the mixtures with the better K_1 and K_2 provide better pavement service lives at a constant R_L (C1> Yoakum> Bryan> A1).

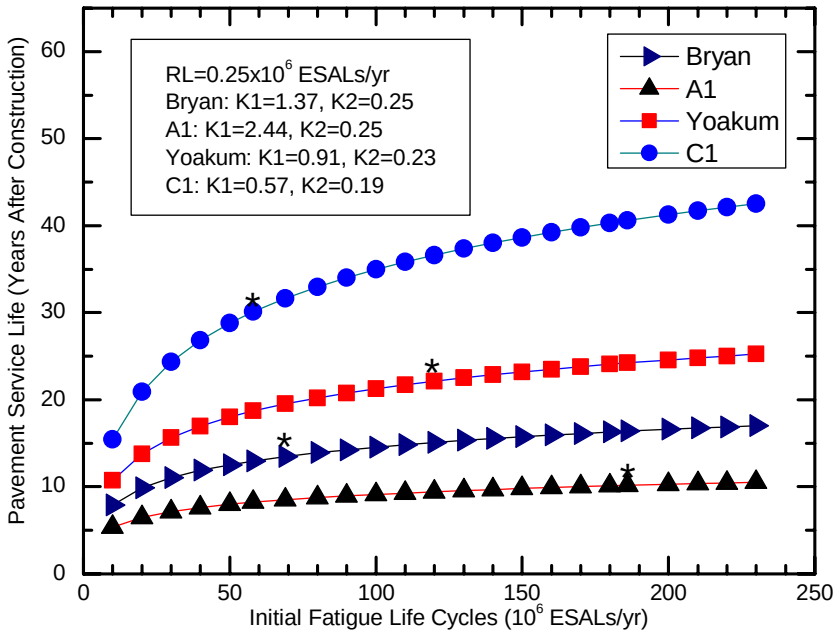

Figure IV-9. The Impact of N_{f0} on Pavement Service Life.

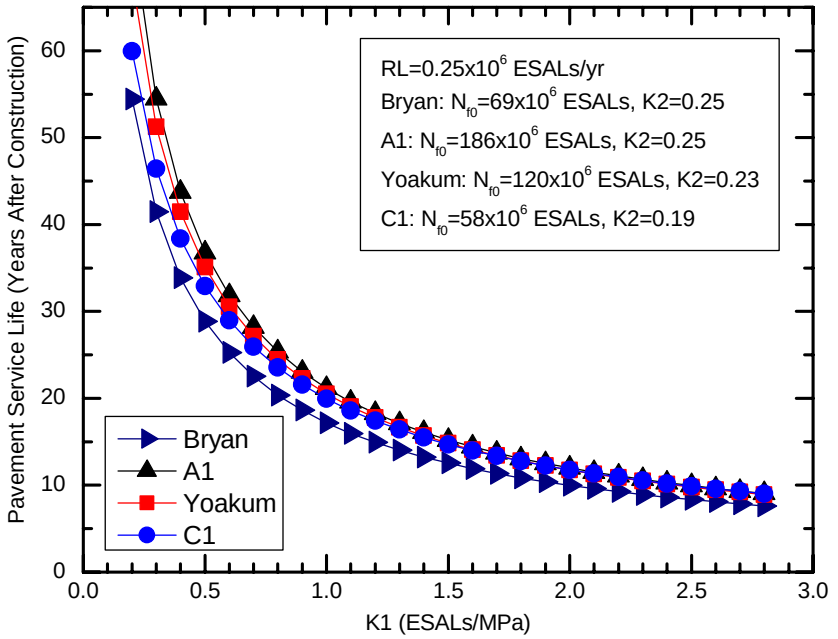

Figure IV-10. The Impact of K_1 on Pavement Service Life.

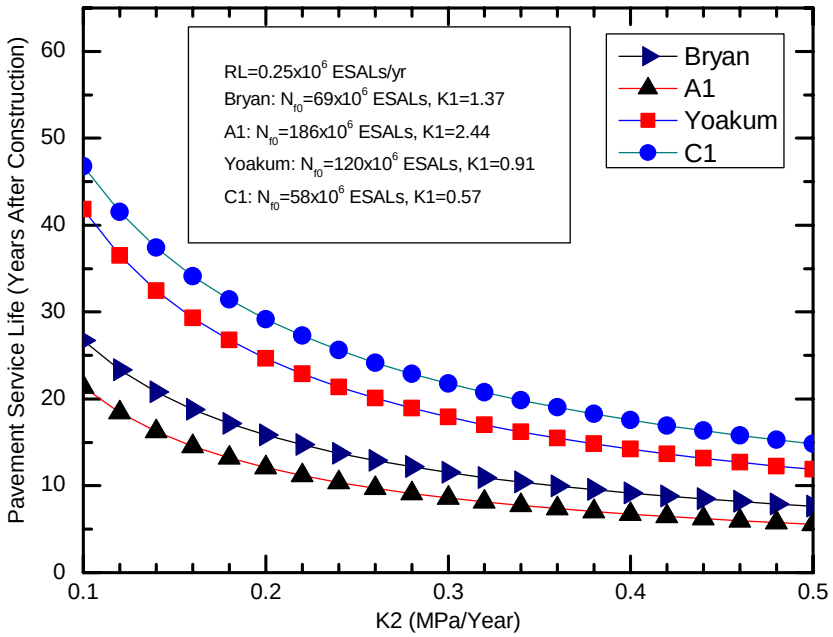

Figure IV-11. The Impact of K_2 on Pavement Service Life

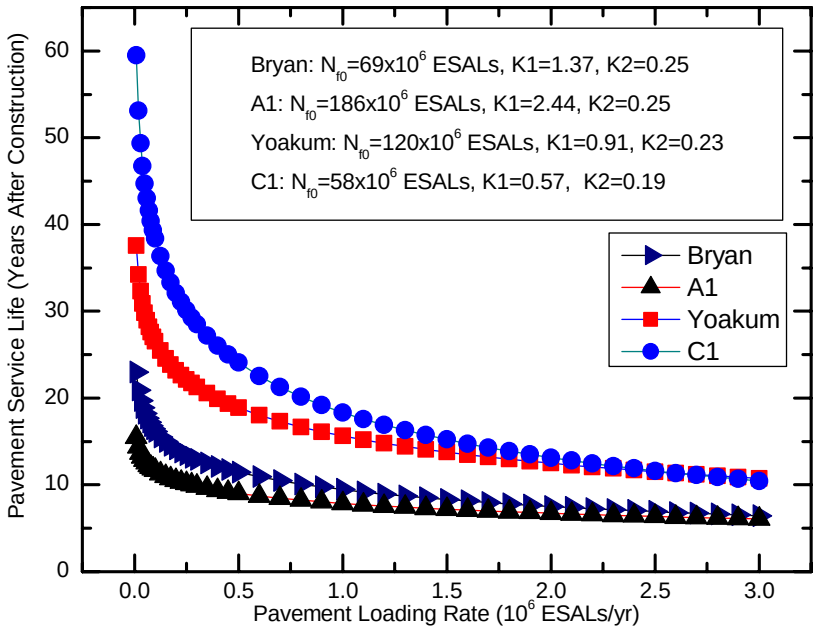

Figure IV-12. The Impact of R_L on Pavement Service Life

As a comparison method for calculating the binder hardening rate (K_2), the global aging model (GAM) of Mirza and Witczak was used to calculate viscosity at 60 °C versus time for the Bryan binder (the unmodified PG 64-22 binder) (Mirza and Witczak, 1995); the GAM is used by the mechanistic empirical pavement design guide (MEPDG) (AASHTO, 2004). For each viscosity over time, a value of the DSR function was determined from the known viscosity versus DSR function relationship for this specific binder shown in Figure III-3 in chapter III. Thus DSR hardening over time was determined from the GAM. Then, using the decline in fatigue life that results from increases in the DSR function, the field N_f as a function of time was determined. Finally, the integral in Equation IV-5 was evaluated numerically to give t_{end}.

The value thus obtained from the GAM (using a mean average annual temperature of 70 °C and a mix/laydown viscosity of 6,500 poise) was 73 years versus 12.9 years from the laboratory and field experimental data. The GAM appears to calculate oxidative hardening rates that would significantly underestimated the impact of oxidation on pavement service life.

Additional comments about pavement aging are appropriate. The above data suggest that when binder aging occurs in the pavement, it can have a significant impact on pavement service life in terms of fatigue performance. However, it does not address whether or not binders in pavements actually age. At least one report in the literature is used to support the idea that pavements age primarily near the surface and little more than an inch below the surface, and the GAM appears to follow this assumption (Coons and Wright, 1968). A separate but related issue is the extent to which binders in pavements harden in service and how quickly they harden. This issue is discussed by Al-Azri et al. (2006).

Summary and Conclusions

Binder oxidative aging in mixtures significantly decreases the controlled-strain fatigue performance. Fatigue life decline with binder oxidation is characteristic of each

mixture type. The cumulative damage approach provides a rational method for quantitatively estimating pavement service life by simultaneously considering both the pavement loading rate and the fatigue life decline due to binder oxidative aging. The differences in expected pavement life arise from differences in their initial fatigue lives and much more significantly from different declines in fatigue life with binder stiffening combined with different binder hardening rates in the mixtures. The cumulative damage controlled-strain calculation shows a rapidly accelerating decline in pavement life as oxidative aging progresses.

CHAPTER V
BINDER-MIXTURE RELATIONS DUE TO BINDER OXIDATION

Synopsis

Binder oxidation and embrittlement has a significant impact on fatigue performance; mixture field fatigue life, measured at controlled-strain conditions, decreases dramatically with oxidative aging. However, the fundamental properties of binders and mixtures that are responsible for this fatigue life decline are unknown. In this work, the fundamental rheological properties of binders and their mixtures were studied to establish binder-mixture relationships and the impact of oxidative binder hardening and temperature on these relationships.

Results indicate that binder oxidative hardening greatly increases mixture stiffness. The mixture G* versus binder G* correlation illustrates 1) that compacted mixtures formed from AASHTO PP2 (4-hr) loose mix aging follow quite well the Hirsch model correlation established by Christensen, but 2) that subsequent binder oxidation stiffens the mixture significantly more than would be indicated by this Hirsch model. Evidently, binder oxidation produces a fundamental change in binder and mixture properties that is not captured by the Hirsch Model. Binder and mixture stiffening with decreases in temperature follow much more closely the Hirsch model. A mixture visco-elastic function correlates well to the binder DSR function and may provide a useful indication of mixture durability in the presence of oxidative binder hardening.

Introduction

Pavements deteriorate over time and eventually fail in service. While the traffic loading is considered to be a major factor leading to pavement failure, binder embrittlement due to oxidative aging almost certainly plays a significant role as well. One objective of this study is to determine the impact of oxidative aging on mixture

failure resistance and on other mixture properties in general. In the previous chapters, the effect of binder oxidation on the mixture fatigue performance was found to be significant.

However, fundamental properties of mixtures related to binder oxidation which affect the mixture fatigue performance are not known. This study addresses binder mixture relationships other than fatigue and the impact of oxidative binder hardening on these relationships.

Objectives

Of particular interest is the impact of binder aging on mixture stiffness, as characterized by the mixture's rheology. In addition to the aging effect, the impact on mixture stiffness and fatigue life due to binder hardening that result from temperature decreases are studied as a possible rapid surrogate for the effects of oxidative aging.

Methodology

Loose mix, aged according to AASHTO PP2 four hour short-term aging (AASHTO, 1996b), was compacted, tested in the nondestructive relaxation modulus procedure, and aged further in a 60 °C environmental room. Two types of mixtures were aged at intervals of 3 months (from 0 to 9 months) and tested after each of these aging intervals. In this way, the same physical specimen was tested at each aging level so that the effect of binder aging could be determined independent of other mixture variables. Replicate compacted mixture specimens were aged for the specified intervals and the binder recovered and tested for DSR properties that could be compared to the mixture properties.

Binders and Tests

To associate oxidative binder hardening with mixture stiffening, two different binders were used in this study: a PG 64-22 from a basic mixture design and a PG 76-22 SBS modified binder from a rut resistance mixture design. The mixtures were conditioned and the binders recovered and tested as shown in Figure V-1.

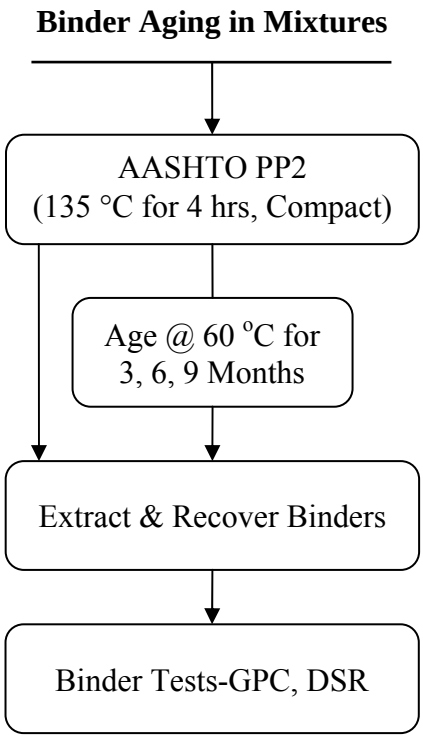

Figure V-1. Binder Oxidative Aging and Testing.

Binders were recovered from laboratory mixtures through the extraction and recovery process. Then, size exclusion chromatography was used to ensure complete solvent removal in the recovered binders and dynamic shear rheometry (DSR) tests were

used to measure the rheological properties of the recovered binders; details are described in Chapter III.

Binder Data Analysis

From DSR measurements, dynamic storage (G') and loss moduli (G") were measured at three different temperatures (20, 40, 60 ^{o}C), with a 2.5 cm composite parallel plate used for 60 ^{o}C measurement and a 1.5 cm metal parallel plate used for 20 and 40 ^{o}C in order to prevent upper assembly compliance problems with the stiffest binder.

Master-curves for the dynamic complex modulus (G*) were constructed using time-temperature superposition (TTSP) at 20 ^{o}C shown in Equation V-1 (Ferry, 1980; Williams, 1971) and compared with the Mixture *G**.

$$\log a_T = \frac{-C_1\left(T - T_{ref}\right)}{\left(C_2 + T - T_{ref}\right)} \tag{V-1}$$

where a_T is the shift factor at temperature T relative to the reference temperature T_{ref} and C_1 and C_2 are empirically determined coefficients. In addition to master-curves, the DSR function (G'/(η'/G')), measured at 44.7 ^{o}C, 10 rad/s but shifted to 15 ^{o}C 0.005 rad/s by TTSP, was used to track changes in binders with oxidative aging (Ruan et al., 2003b).

HMAC Mixtures and Tests

Two different HMAC mixtures were used to assess the binder-mixture (BM) relationships. One was a dense graded TxDOT type C mixture with a PG 64-22 binder and limestone aggregate (defined as the Bryan mixture), and the other was a 12.5 mm Superpave HMAC mixture with a PG 76-22 SBS modified binder and river gravel

aggregate (defined as the Yoakum mixture). The mixture BM test was the same CMSE relaxation modulus (RM) tensile test described in Chapter III. Because the RM test was assumed to be non-destructive, the same HMAC specimen was repeatedly tested at different aging conditions. Thus data were obtained at each test temperature and at each aging level for which the only variable mixture parameter was binder stiffening; other mixture parameters (void in mineral aggregates (VMA), void filled with asphalt (VFA), binder content, aggregate size distribution and configuration, etc.) were identical within

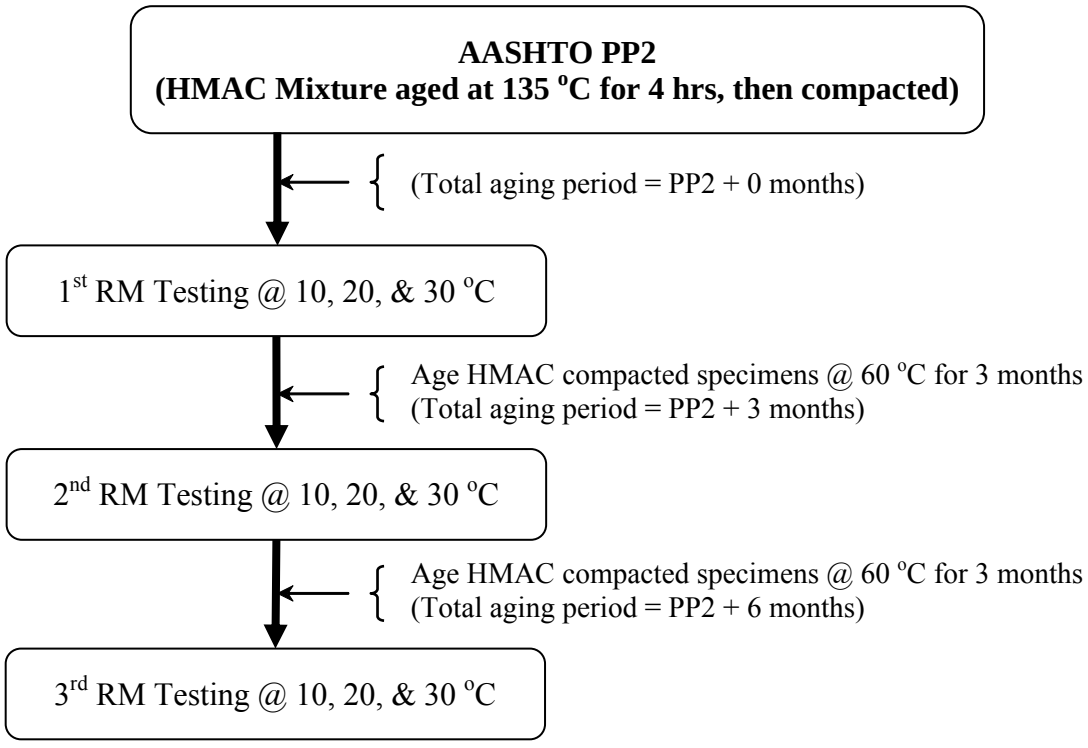

Figure V-2. Binder-Mixture Characterization Test Procedure.

the same specimen. The test was performed with both mixtures (Bryan and Yoakum) at 0, 3 and 6 months beyond PP2, four hour aging conditions (60 °C, 1 atm air) with at least

two replicate specimens for each mixture. Figure V-2 is a schematic illustration of the BM characterization test plan with RM testing.

HMAC Mixture Viscoelastic Characterization

The data obtained from the tensile RM test includes the time-dependent elastic relaxation modulus (E(t)), loading time (t), and test temperature (T). From these data, a master curve for E(t) was constructed at a reference temperature of 20 ^{o}C by using TTSP. Then, a master curve for E(t) and dynamic shear storage (G'(ω)), loss (G"(ω)) and complex (G*(ω)) moduli for a mixture were calculated to be compared with binder G*(ω). A viscoelastic function (VE function) for mixtures was calculated to be compared with binder DSR function in the frequency range where neither the viscous nor the elastic property is dominant.

Elastic Modulus (E(t)) Master Curve

A master curve for $E(t)$ is constructed at a reference temperature of 20 ^{o}C from the data obtained at three different temperatures (10, 20, and 30 ^{o}C) by using the TTSP procedures. $E(t_r)$ is found to be well represented by the model given by Equations V-2 - V-4:

$$E(t_r) = E_\infty + E_1 t_r^{-m} \cong E_1 t_r^{-m} = E_1 \left(\frac{t}{a_T(T)} \right)^{-m} \quad \text{(V-2)}$$

$$m = a \log(t_r) + b \quad \text{(V-3)}$$

$$t_r = \frac{t}{a_T(T)} \quad \text{(V-4)}$$

where $E(t)$,and $E(t_r)$ = time-dependent elastic modulus at time t (MPa); E_1 = initial (t_r = 1 sec) elastic modulus (MPa); t_r = reduced time (second); T = Temperature (^oC); $a_T(T)$ = shift factor at temperature T relative to the reference temperature T_{ref}; a and b = empirically determined coefficients.

The elastic modulus obtained by the RM test is a function of time because of the viscoelastic nature of the HMAC mixture. Under deformation, the stress builds because of the mixture's elastic nature but then relaxes at fixed strain because of its ability to undergo viscous flow. This relaxation is reflected in the decrease of $E(t_r)$ over time in the RM test. Therefore, storage (elastic) and loss (viscous) moduli can be calculated from the $E(t_r)$ master curve.

The m value in Equation V-3 is assumed to be a function of time and temperature according to Equation V-4. Once the temperature shift factors are determined through TTSP alignment of the data, and the model parameters E_1, a, and b are estimated, $E(t_r)$ can be calculated.

Dynamic Mixture Storage and Loss Moduli

The elastic modulus is converted to a shear modulus according to Equation V-5

$$G(t_r) = \frac{E(t_r)}{2(1+\nu)},\ G_1 = \frac{E_1}{2(1+\nu)} \tag{V-5}$$

Converting to frequency by Equation V-6

$$\omega \cong \frac{1}{2t_r} \tag{V-6}$$

dynamic shear storage (G') and loss (G") moduli are calculated by Equations V-7and V-8 (Lytton et al., 1993; Schapery, 1973)

$$G'(\omega) = G_1 \frac{\Gamma(1-m)}{\omega^{-m}} cos\left(\frac{m\pi}{2}\right) \quad \text{(V-7)}$$

$$G''(\omega) = G_1 \frac{\Gamma(1-m)}{\omega^{-m}} sin\left(\frac{m\pi}{2}\right) \quad \text{(V-8)}$$

and the magnitude of the complex dynamic shear modulus (G*) is given by Equation V-9

$$G^*(\omega) = \left(\left(G'(\omega)\right)^2 + \left(G''(\omega)\right)^2\right)^{\frac{1}{2}} \quad \text{(V-9)}$$

where t_r = reduced time (second); m = exponential stress relaxation rate ($0 \leq m < 1$); ν = Poisson's ratio ($\cong 0.33$); $G(t)$ and $G(t_r)$ = time-dependent shear modulus at time t (MPa); G_1 = initial shear modulus (MPa); $G'(\omega)$ = elastic (storage) dynamic shear modulus (MPa); $G''(\omega)$ = viscous (loss) dynamic shear modulus (MPa); $G^*(\omega)$= Complex dynamic shear modulus (MPa); Γ = gamma function.

For ν, a value of 0.33 was used for the HMAC mixture consistent with the work done by Huang and Lytton et al (Huang, 1993, Lytton et al., 1993). Γ is the Laplace (or Euler) Gamma transformation function.

Results and Discussion

The test results are presented in five sections that address 1) binder rheology, 2) mixture rheology, 3) binder-mixture relationships (including the impact of temperature compared to that of oxidation), 4) the impact of temperature versus oxidation on DSR map, and 5) the impact of temperature on mixture fatigue resistance.

As discussed at the beginning of this chapter, aged mixture samples were prepared using the PP2 four hour short-term procedure. This aged mixture was then used to make replicate compacted mixtures. One of these replicates was tested as is (PP2 plus 0 months), then aged and tested, according to Figure V-2.

Binder was recovered from other replicate compacted and aged mixture samples and tested to provide binder properties to compare to the tested mixtures. From the binder properties and their corresponding mixture properties, the effect of binder hardening on mixtures was evaluated directly and without the variability created by mixture parameters other than binder rheology.

Effect of Mixture Oxidation on Binder Rheology

Binder master curves at 20 ^{o}C for the complex dynamic shear modulus $G^*(\omega)$ were used to track changes in binder properties with aging. Figures V-3 and V-4 show the results for binders recovered from Bryan and Yoakum mixtures respectively. Note that the Yoakum mixture has one more level of aging (PP2+ 9 months in 60 ^{o}C room).

The figures show that $G^*(\omega)$ increases with aging for both unmodified (Bryan) and modified (Yoakum) binders. Continued binder hardening is evident through the higher aging level. These increases at low frequency reflect the well-documented, and seemingly without-limit, increases in the low shear rate viscosity (η^*_0) that accompany binder aging because $\eta^* = G^*/\omega$.

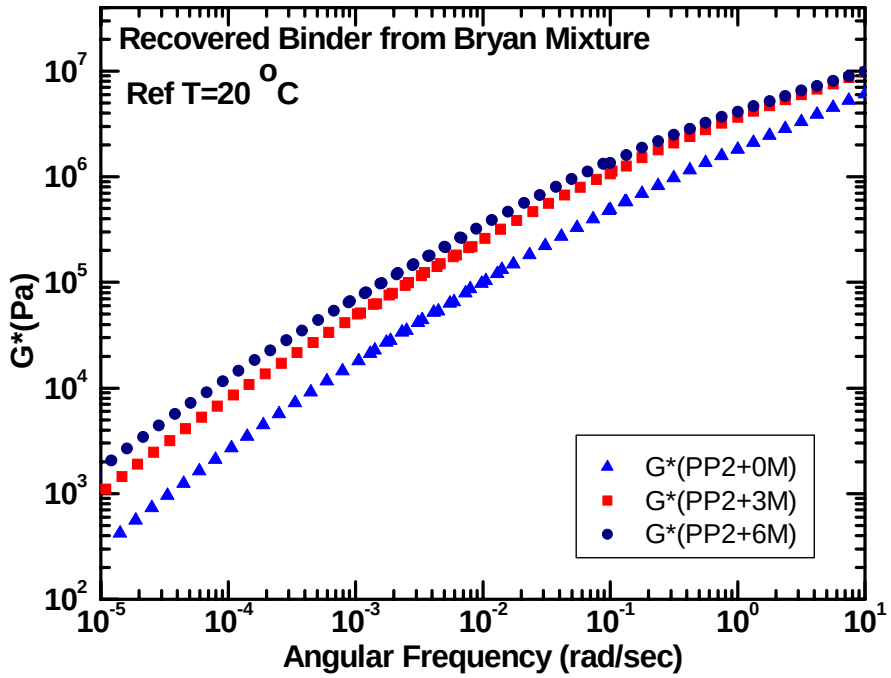

Figure V-3. Recovered Binder Master Curves for G*(ω) (Bryan Mixture).

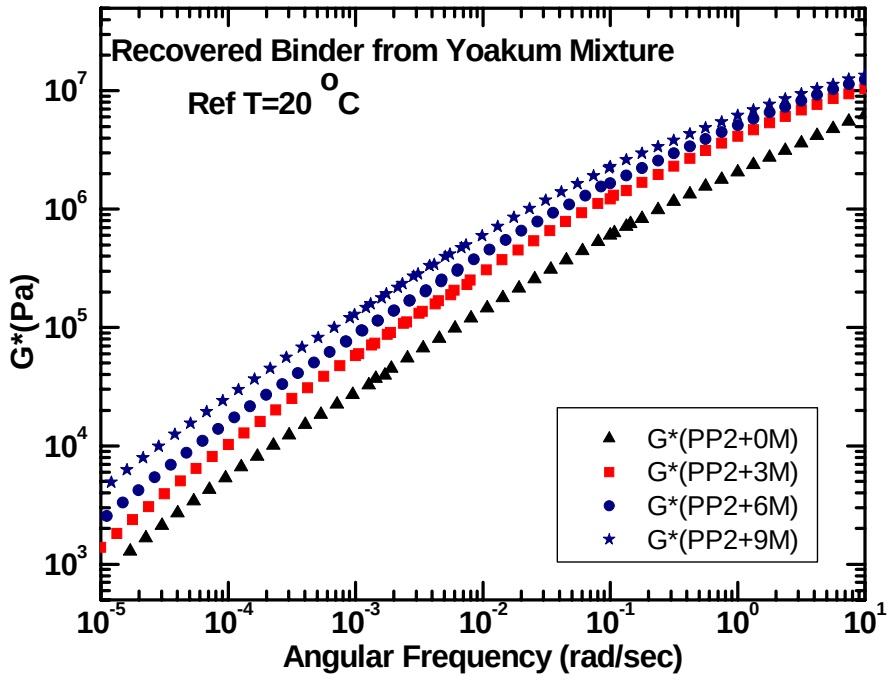

Figure V-4. Recovered Binder Master Curves for G*(ω) (Yoakum Mixture).

Effect of Mixture Oxidation on Mixture Rheology

Binder oxidation affects mixture properties as well as binder. Figures V-5 and V-6 show mixture stiffness increases due to binder oxidation. Elastic modulus (E(t)) in a controlled tensile strain mode was measured at each aging level (PP2 + 0, 3 and 6 months) with three different temperatures (10, 20 and 30 ^{o}C). Tensile RM master curves were determined for both the Bryan and Yoakum mixtures at a reference temperature of 20 °C by using TTSP.

Clearly, there are inconsistencies in the data, most notably toward the end of each relaxation test, that make the master curve determination somewhat problematic. The value of *m* in Equation V-3 is assumed to be a function of time to allow the master curves to be non-linear on the log-log plot to explain mixture's non linear behavior.

Additional experience with this method and independent verification with other experiments (dynamic modulus, for example) is necessary in order to achieve more confidence in the mixture viscoelastic properties. The objective of obtaining a set of data at different aging levels from the same mixture specimen is to study the effect of binder aging alone on mixture stiffness and viscoelastic behavior. If different specimens are studied, then the whole host of mixture variables (aggregate gradation, VMA, VFA, binder content, and aggregate alignment configuration) is brought to play, and greater variability in the aging data will result.

From these figures, it is clear that oxidative aging stiffens the tensile RM of the mixture significantly, consistent with stiffening of the neat binder with aging. Also noted is that the Bryan mixture is stiffer than the Yoakum mixture at comparable levels of aging and test conditions even though, as noted above, the Bryan binder is less stiff than the Yoakum binder at comparable aging conditions, probably because the Yoakum mixture has a higher binder content and these thicker binder films than the Bryan mixture. A more fundamental study is recommended to better understand these relationships.

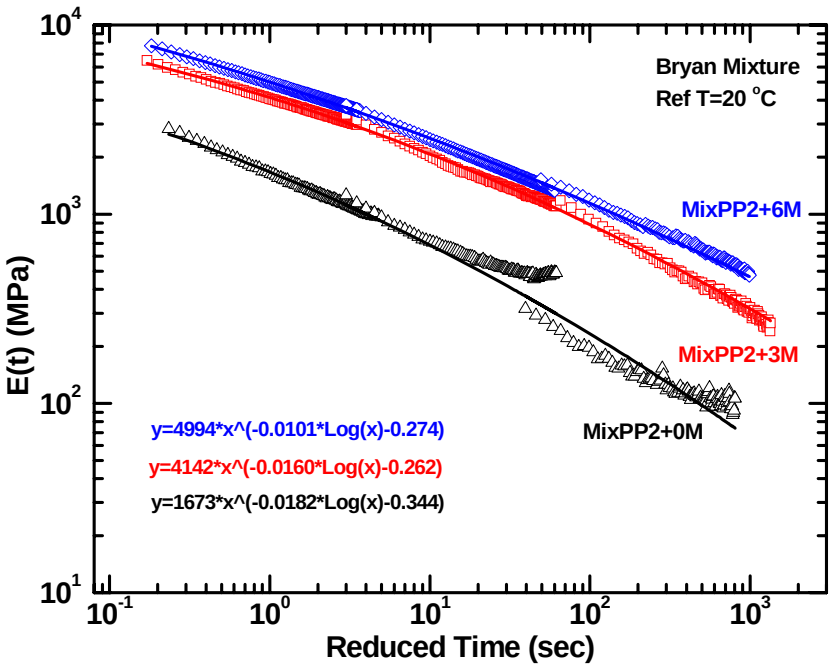

Figure V-5. Master Curves of Bryan Mixture for E(t).

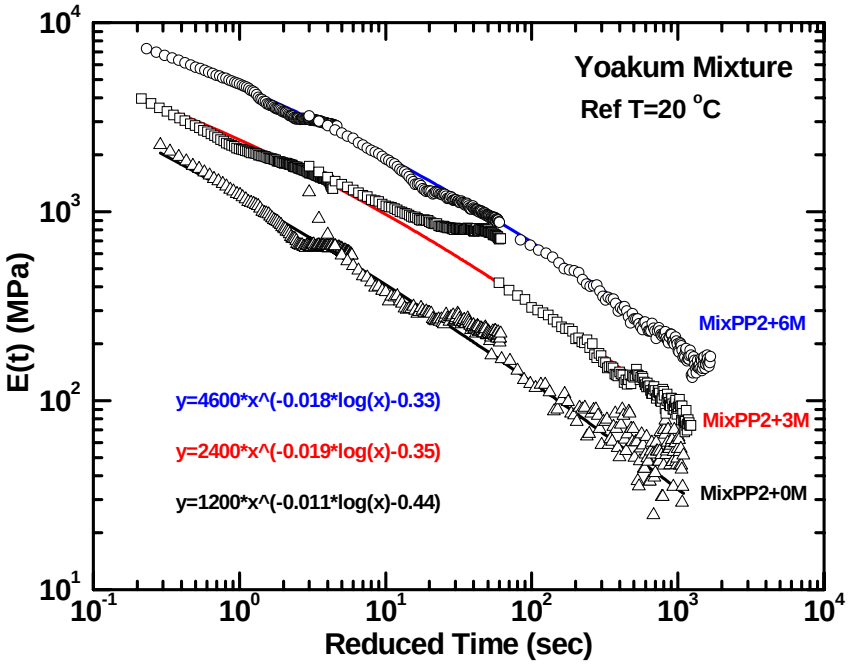

Figure V-6. Master Curves of Bryan Mixture for E(t).

From these tensile RM master curves, dynamic shear moduli master curves, also at a reference temperature of 20 °C, were calculated as defined by Equations V-5 through V-9. The results are given in Figure V-7 (G', G'') for the Bryan mixtures and in Figure V-8 (G', G'') for the Yoakum mixtures. In addition, Figure V-9 compares the complex dynamic shear moduli (G^*) of the Bryan and Yoakum mixtures. Note that G^* increases with aging for both mixtures and that the Bryan mixture is stiffer than the Yoakum mixture, most evident at the lower frequencies.

Again, stiffening of the mixture with oxidative aging is evident as G', G'', and G^* all increase, and the crossover frequency (frequency at which $G' = G''$) moves to a lower frequency. The effects of 60 °C aging for 0, 3, and 6 months beyond PP2 conditioning are evident in the Figures V-5 and V-6.

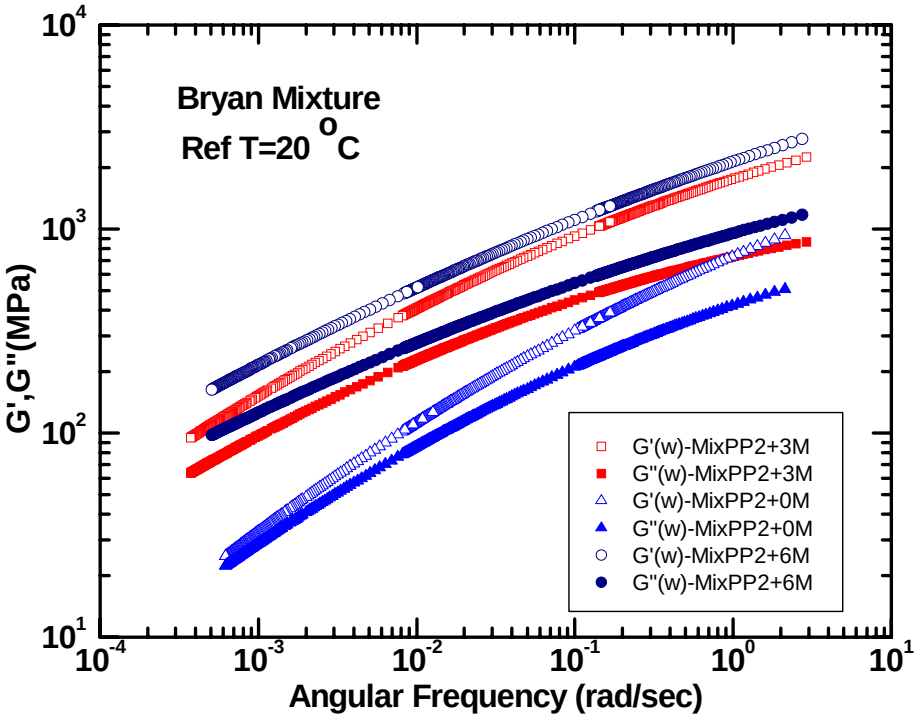

Figure V-7. Master Curves of Bryan Mixture for G'(ω), G"(ω).

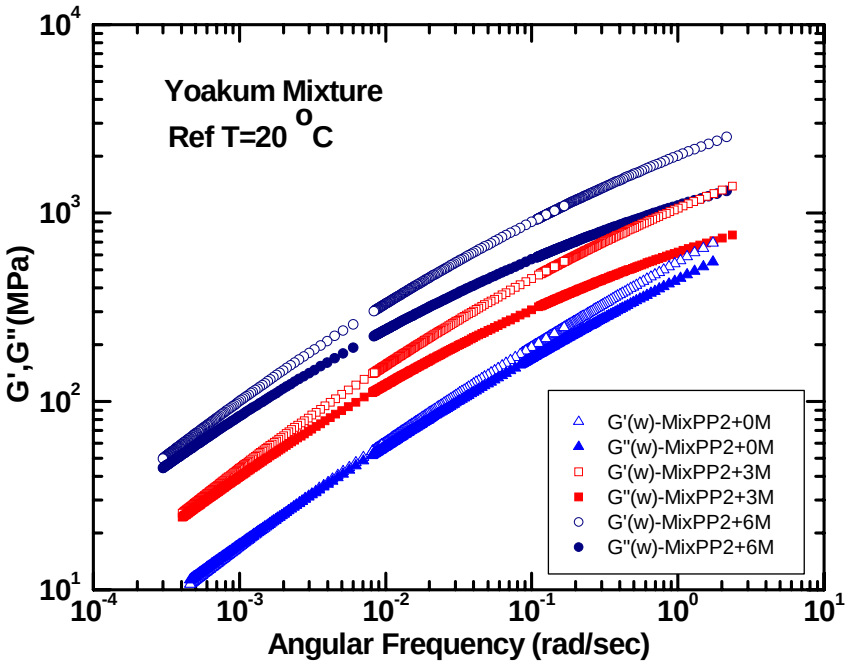

Figure V-8. Master Curves of Yoakum Mixture for G'(ω), G"(ω).

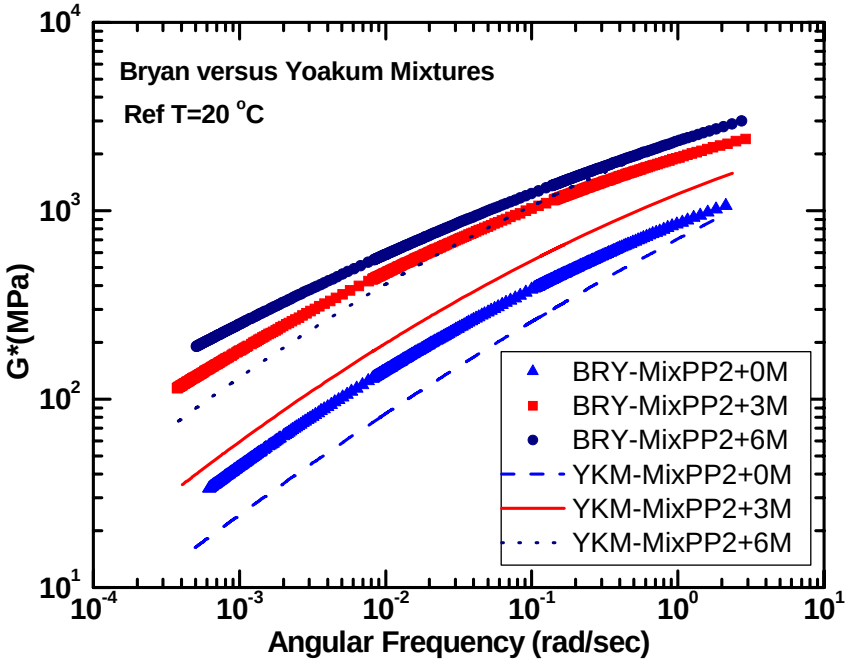

Figure V-9. Master Curves Comparison between the Mixtures for G*(ω).

Similar to the DSR map for the recovered binders (shown in chapter III), a viscoelastic property aging map can be constructed from the mixture viscoelastic master curves. Goodrich (1991) mentioned that the mid-temperature mixture rheological properties (0.1 rad/sec, from 10 ^{o}C to 50 ^{o}C) are influenced by both the binder and the aggregate. As a first trial in this study, an angular frequency, 0.002 rad/sec was arbitrarily selected where G"/G' is close to unity at 20 ^{o}C, as it is for an aged binder at 15 ^{o}C, 0.005 rad/sec. In this way it was hoped that aging of the mixture would be readily observed from the viscoelastic properties. If the frequency is too high or the temperature too is low, then the mixture would reflect elastic limit properties and not be sensitive to aging. So the VE function was calculate as follows:

$$\text{VE function} = G'/\left(G''/\left(G'\omega\right)\right) \text{ at } 20\ ^{\circ}\text{C, } 0.002 \text{ rad/sec} \qquad \text{(V-10)}$$

Values from the 20 °C reference master curves at 0.002 rad/sec are used to plot G' versus η'/G', and the results are shown in Figures V-10 (Bryan) and V-11 (Yoakum). In both figures, one six month aged mixture (star symbol) is a different compacted mixture specimen than the others; nevertheless, the VE values for the two 6 month aged mixtures are quite close.

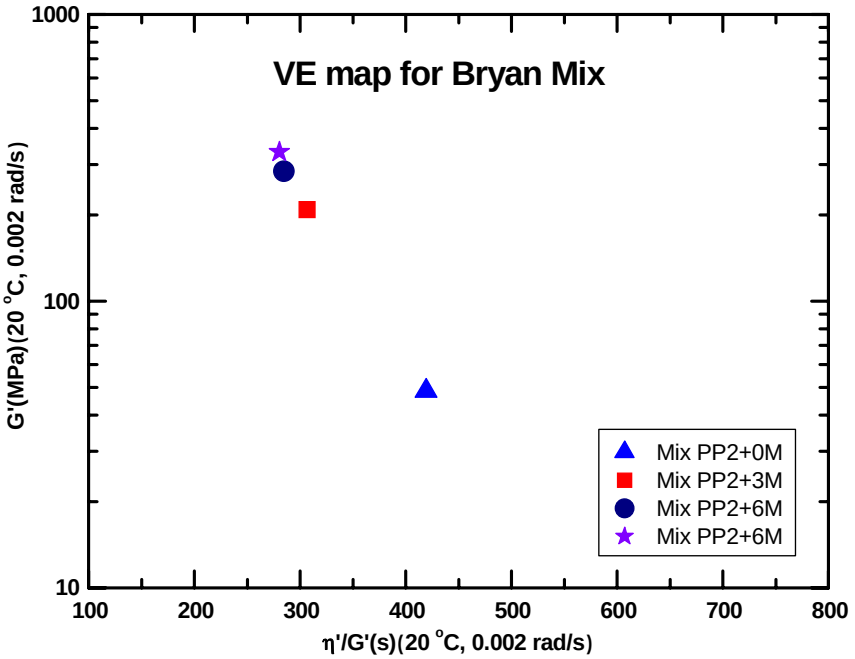

Figure V-10. VE Function Map of Bryan Mixtures

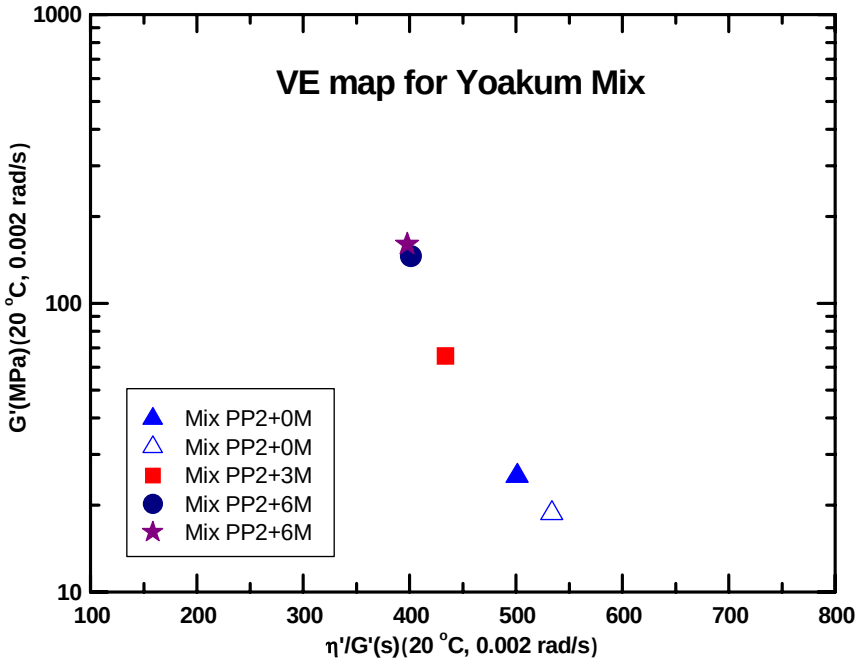

Figure V-11. VE Function Map of Yoakum Mixtures

Binder-Mixture Relationships

The previous sections considered binder and mixture rheology, as affected by mixture oxidation, separately. Binder master curves, binder movement across the DSR map with aging, mixture master curves and the mixture movement across a mixture VE function map were presented.

In this section, the mixture properties are related to their corresponding analogous binder properties. For example, a mixture G* is related to binder G* (at the same reference temperature and frequency) or a mixture VE function is related to its binder DSR function. Working from the mixture and binder master curves, these relationships are obtained over a range of mixture and binder properties.

Determining the impact of binder oxidation on mixture rheology, separate from other mixture variables and parameters is of particular interest in this effort. Key to achieving this objective is observing changes in mixture rheology that occur due to oxidative aging of the same mixture specimen, as was outlined in Figure V-2.

As noted previously, the DSR function relates well to the binder ductility at 15 ^{o}C, 1 cm/min. This ductility has been reported to relate to road failure, with 3 cm being a performance limit. The objective in developing a mixture VE function is to assess whether a mixture property might be used in lieu of a binder property as an indicator of durability as well as to better understand the relation between mixture and binder properties.

Relating mixture G* to binder G* is of interest because of correlations previously reported in the literature, correlations that were developed through model parameter estimates using a large number of different mixtures (Christensen et al., 2003). The work reported in this section provides a detailed experimental analysis of one such correlation through measurements of changes in mixture G* caused by binder oxidation and by changes in temperatures, while mixture parameters and variables remain constant.

VE Function Related to the Binder DSR Function

The VE function mixture trends of the previous section are obvious and very similar to those of the recovered binder DSR map. With aging, the VE function moves to the left and upward due to binder stiffening. The correlation between the mixture VE function and binder DSR function is shown in Figure V-12. Interestingly, the slopes of the Bryan and Yoakum plots are very close and differences are manifested primarily in an offset (magnitude) of the two sets of data. For each aging level, the Yoakum binder is stiffer than Bryan binder whereas the Bryan mixture is stiffer than the Yoakum mixture.

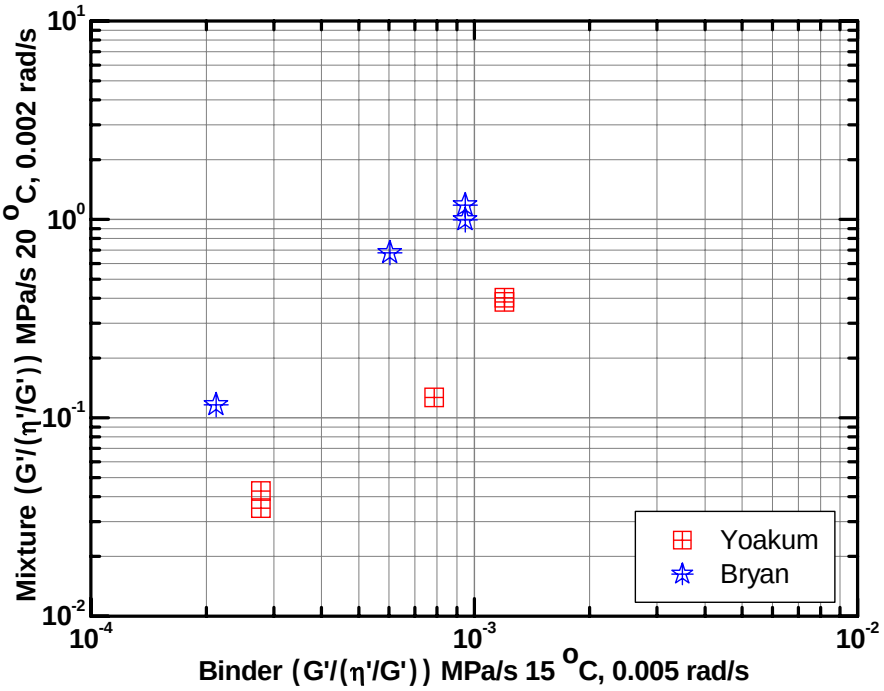

Figure V-12. VE Function versus DSR Function

Mixture G versus Binder G**

Hirsch Model. According to Christensen et al, G* for a mixture is a function of aggregate contact volume, voids in mineral aggregate (VMA), voids filled with asphalt (VFA), and G* of the binder according to the Hirsch model, which is expressed in Equations V-11 and V-12 (Christensen et al., 2003).

$$\left|G^*\right|_{mix} = Pc\left[601{,}000(1-VMA/100)+\left|G^*\right|_{binder}\left(\frac{VFA\times VMA}{10{,}000}\right)\right] + (1-Pc)\left[\frac{1-VMA/100}{601{,}000}+\frac{VMA}{VFA\left|G^*\right|_{binder}}\right]^{-1} \quad \text{(V-11)}$$

$$Pc = \frac{\left(3+\frac{VFA\times\left|G^*\right|_{binder}}{VMA}\right)^{0.678}}{396+\left(\frac{VFA\times\left|G^*\right|_{binder}}{VMA}\right)^{0.678}} \quad \text{(V-12)}$$

where Pc = aggregate contact volume; VFA = voids filled with asphalt; VMA = voids in the mineral aggregate.

Figure V-13 shows the mixture G* as a function of binder G* according to the Hirsch model for Bryan mixture design which has a VMA of 17 and a VFA of 58.8. According to this model, the mixture G* varies by less than two orders of magnitude as the binder G* varies by three orders of magnitude.

A reasonable assumption is that mixture stiffness depends upon binder stiffness and not upon the manner in which it reaches this stiffness. Thus, original binder composition, oxidative aging, and temperature might all be presumed equal with respect to mixture stiffness when they provide binder of equal stiffness (G* for example). This assumption is implicit in the Hirsch model. HM-0M in Figure V-13 is the mixture G*

calculated from the Hirsch model by using Equations V-11and V-12 where G* of the binder is that of the binder recovered from the PP2-aged Bryan mixture. Similarly, the binder G* from PP2+3M and PP2+6M are used for HM-3M and HM-6M. These calculations show how mixture stiffening due to binder oxidation is assumed by the Hirsch model to follow the same relationship as less-aged binder.

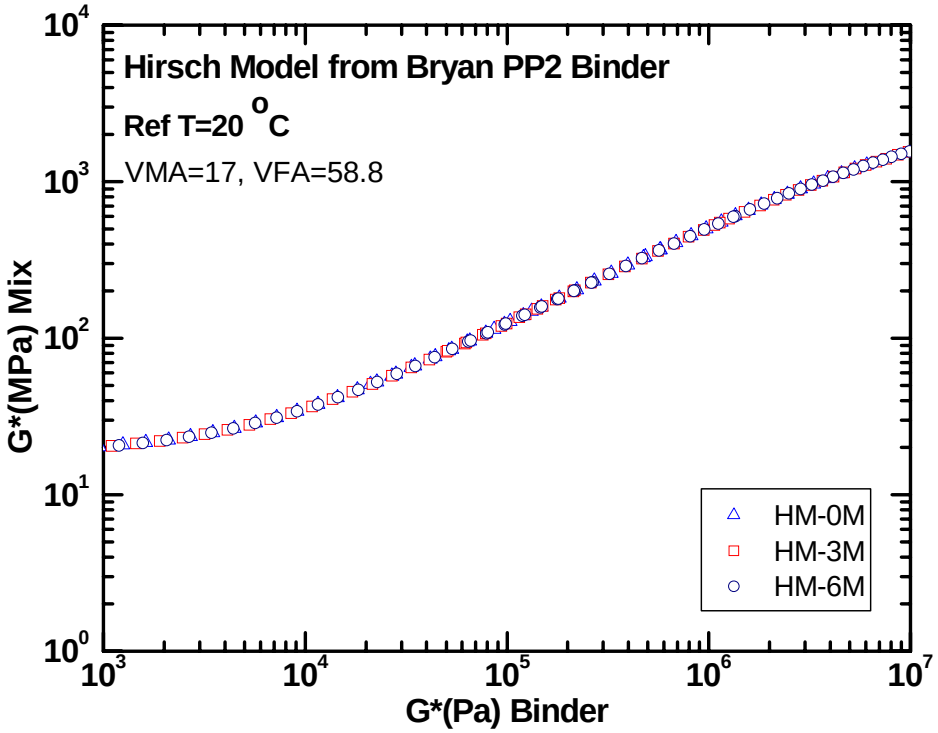

Figure V-13. Hirsch Model from Bryan PP2 Binder.

Experimental Binder-Mixture G* Relationships Compared to the Hirsch Model. Figures V-14 and V-15 show experimentally measured PP2-aged mixture G* versus recovered binder G* compared to the Hirsch model calculations. At PP2 level aging (PP2+0M) the Bryan mixture (Figure V-14) follows the Hirsch model quite well above a binder G* of 10 kPa, while the Yoakum mixture at PP2 level aging (PP2+0M, Figure V-15), does not agree with the Hirsch model well.

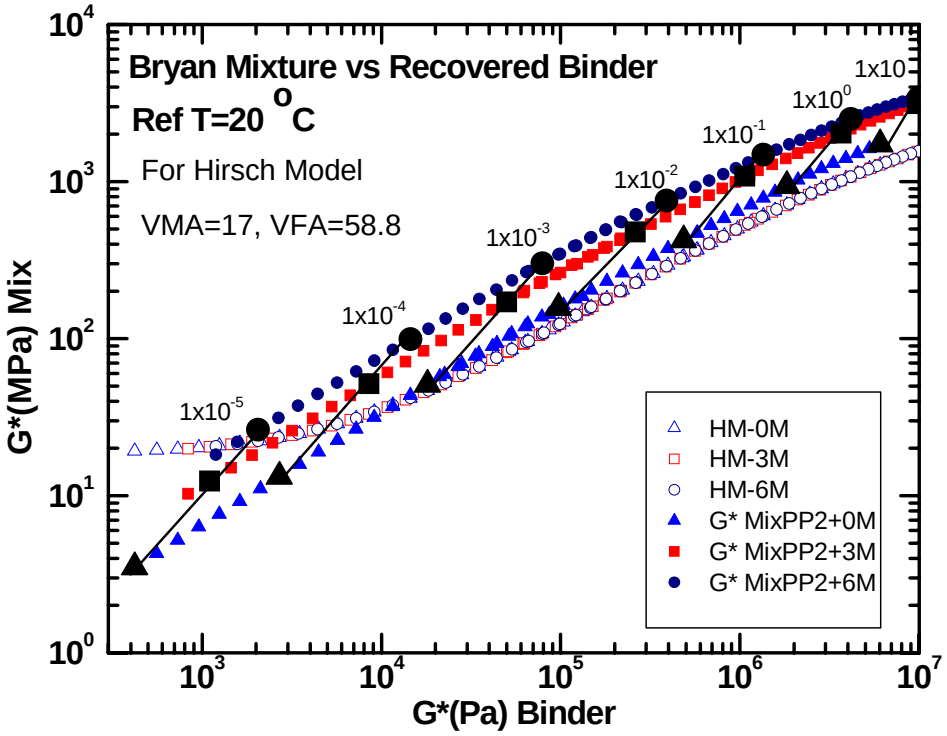

Figure V-14. Comparison between Bryan Mixture PP2 and Hirsch Model.

Subsequent aging of both the Bryan and Yoakum compacted mixtures, to PP2+3M and PP2+6M levels shifted the mixture-binder curves further away from the PP2-0M data. These shifts are contrary to the Hirsch model which assumes a shift along the same curve rather than away from it, as noted above.

These shifts with aging are indicated by the lines that connect points at the some test frequency at each level of aging. These lines represent the path followed at a constant test temperature (20 ^{o}C) and test frequency while the binder stiffens due to oxidation. According to the Hirsch model, such lines would be tangent to the PP2-0M curve. The fact that they are not indicates that the changes in binder composition that occur with oxidation play a more fundamental role in establishing mixture G* than just changing binder G*.

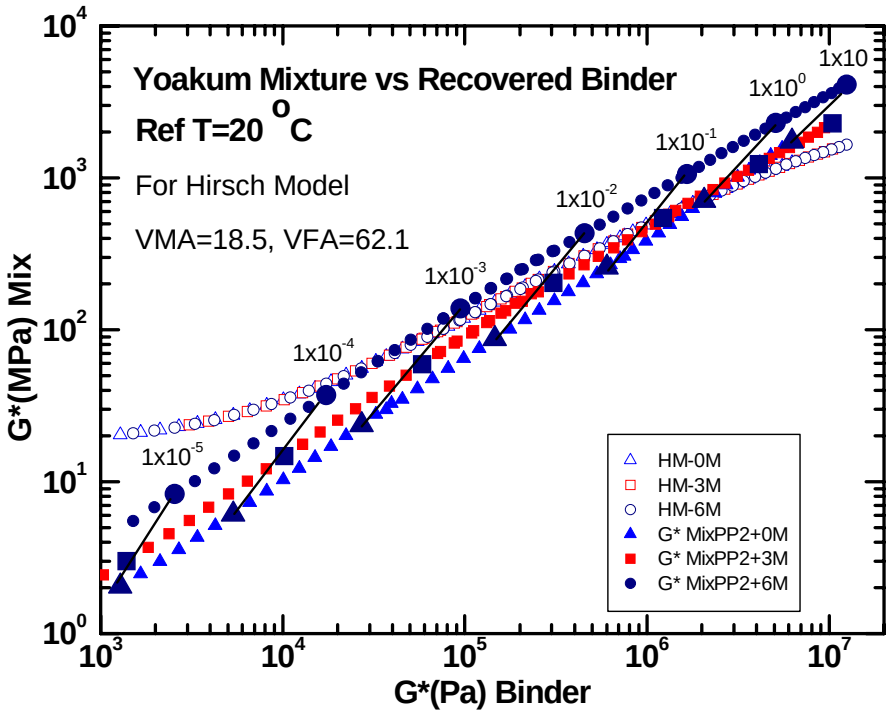

Figure V-15. Comparison between Yoakum Mixture PP2 and Hirsch Model.

Mixture Stiffening from Binder Hardening: Oxidation versus Temperature.

In the paragraphs above, the effect of oxidative aging on the mixture G* versus binder G* relationships was presented, with the conclusion that binder stiffening due to oxidation has a different effect than that assumed by the Hirsch model. In this section, the effect of stiffening due to a decreasing temperature is considered and compared to the oxidation results.

For the PP2 level of aging (PP2+0M), mixture and binder master curves were determined at several different reference temperatures: 10, 20, 30 and 40 ^{o}C. Then the mixture and binder G* values at 0.01 rad/s were added to Figures V-14 and V-15 to give Figures V-16 and V-17. These new data produce a path that would be followed if the PP2 aged mixture were tested first at 40 ^{o}C, then 30 ^{o}C, then 20 ^{o}C, and finally 10 ^{o}C, all at 0.01 rad/s.

Interestingly, this temperature-stiffening path much more nearly follows the PP2+0M aging state curve than the oxidative aging path. For example, starting at the 20 ^{o}C point and moving toward the 10 ^{o}C point (while holding the frequency at 0.01 rad/s), the path is nearly tangent to the PP2+0M curve and much more in agreement with the Hirsch model calculations. Starting at that same point and increasing aging (while holding the temperature at 20 ^{o}C and the test frequency at 0.01 rad/s), the path (shown by the solid line) is much steeper and moves away from the PP2+0M curve.

These results again suggest a fundamental difference between changes in mixture-binder relations brought on by decreasing temperature versus those caused by oxidation. This is an important observation and bears further study.

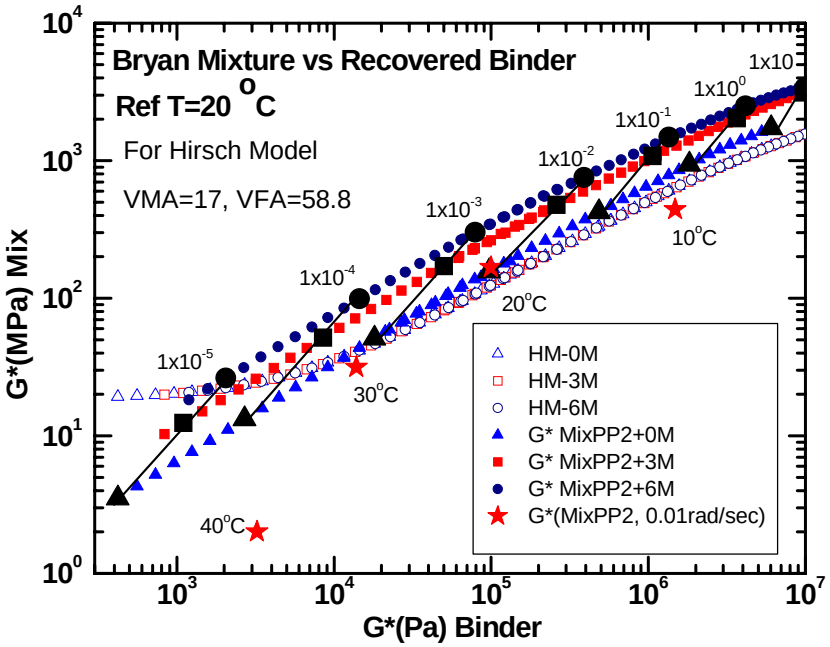

Figure V-16. Mixture Stiffening for Bryan Mixture: Oxidation versus Temperature

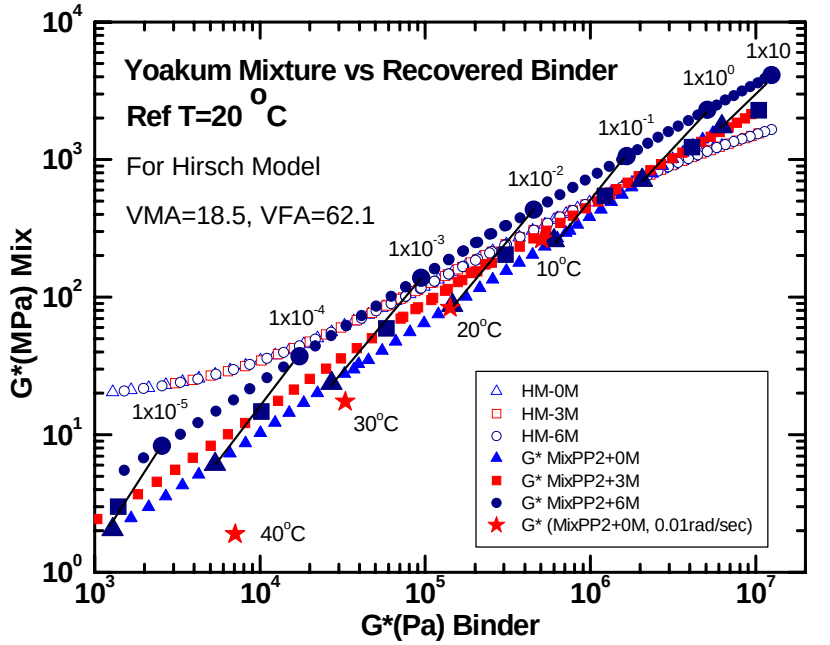

Figure V-17. Mixture Stiffening for Yoakum Mixture: Oxidation versus Temperature.

Binder Stiffening: Oxidation versus Temperature. The impact of temperature change on binder movement across the DSR map was evaluated to further explain binder characteristics. Of interest is how the impact of binder stiffening due to decreases in temperature compared to stiffening due to oxidation (both oxidation as neat binders and in compacted mixtures).

Recovered binders at PP2 level aging (PP2+0M) were used to understand temperature hardening effects. G' and G" at 10 rad/s were measured at several temperatures and converted by TTSP to DSR function values at a frequency of 0.005 rad/s. The measurement temperatures were 50, 45, 40, 35 and 30 ^{o}C and the corresponding reference temperatures were 20, 15, 10, 5 and 0 ^{o}C.

The results are shown in Figures V-18 and V-19, together with the data in Figures III-13 and III-14 for comparison. Both the measurement and reference temperatures are shown for convenience. The path across the DSR map followed by these measurements at different temperatures tracks the aged-binder path for the Bryan binder well. The agreement is somewhat less for the Yoakum binder, especially for the measurements at higher temperatures (softer binder).

The stiffer binder regions are particularly relevant to pavement failure and in this region the agreement provides significant hope that temperature may be used to establish an aging path as a more rapid surrogate method for aging tests. Data on more binders are needed to assess the universality of this approach. Also, it should be noted that even though the aging path across the DSR map might be determined by measurements at different temperature, the rate across the map due to oxidation cannot be determined by a surrogate temperature test protocol.

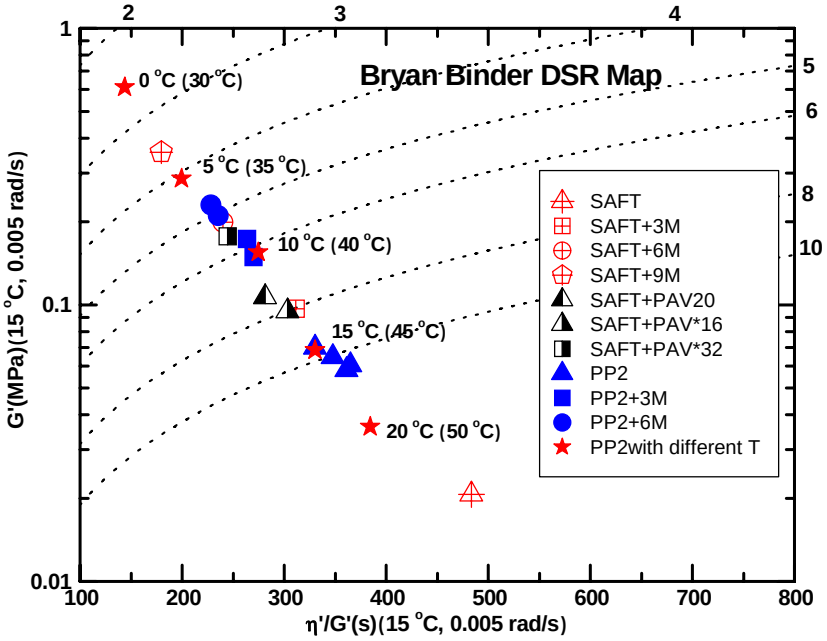

Figure V-18. Binder Stiffening for Bryan Mixture: Oxidation versus Temperature.

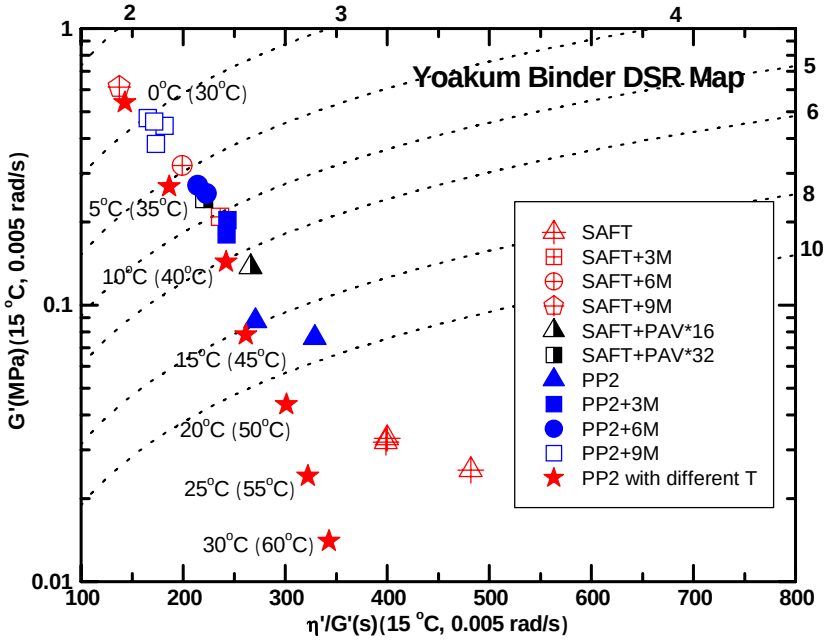

Figure V-19. Binder Stiffening for Yoakum Mixture: Oxidation versus Temperature.

Impact of Temperature on Mixture Fatigue. Previous sections have addressed the question of whether binder stiffening due to decreasing temperature might be used as a surrogate to predict the impact of oxidation. The results were inconclusive because the mixture G* versus binder G* relations were shifted differently by temperature than by oxidation; yet the binder path across the DSR map (after a certain level of stiffness was reached) was essentially the same, whether determined by decreasing temperature or by oxidation. This section addresses a third comparison of temperature versus oxidation, i.e. their impact on mixture fatigue life.

In Figure IV-3, the mixture field N_f (CMSE calculation at 20 ^{o}C) decline with oxidation was presented as a function of the binder DSR function (at 15 ^{o}C, 0.005 rad/s) for both the Bryan and Yoakum mixtures. Using mixture and binder PP2+0M master curves, calculations were also done for the mixture N_f at 30 and 10 ^{o}C and for the binder DSR function at 25 and 5 ^{o}C. These calculations shift both the mixture and binder PP2+0M data to 10 degrees higher and 10 degrees lower than the data reported previously. These additional data are compared to the oxidative aging results in Figure V-20.

As would be expected, decreasing the temperature results in a decline in fatigue life, most certainly because of the stiffening of the binder. Furthermore, the decline in mixture N_f relates to the increase in binder DSR function quite well, in a quantitative sense. For the Bryan mixture, the agreement with the aging decline is excellent; for the Yoakum mixture, the agreement is not as good, with significantly less decline due to temperature than to aging. The differences in the comparison may be related to the fact that the Yoakum binder is SBS polymer modified whereas the Bryan binder is unmodified. More data are needed on a variety of mixtures and binders to better determine whether temperature can be used as a surrogate for the effects of oxidative aging.

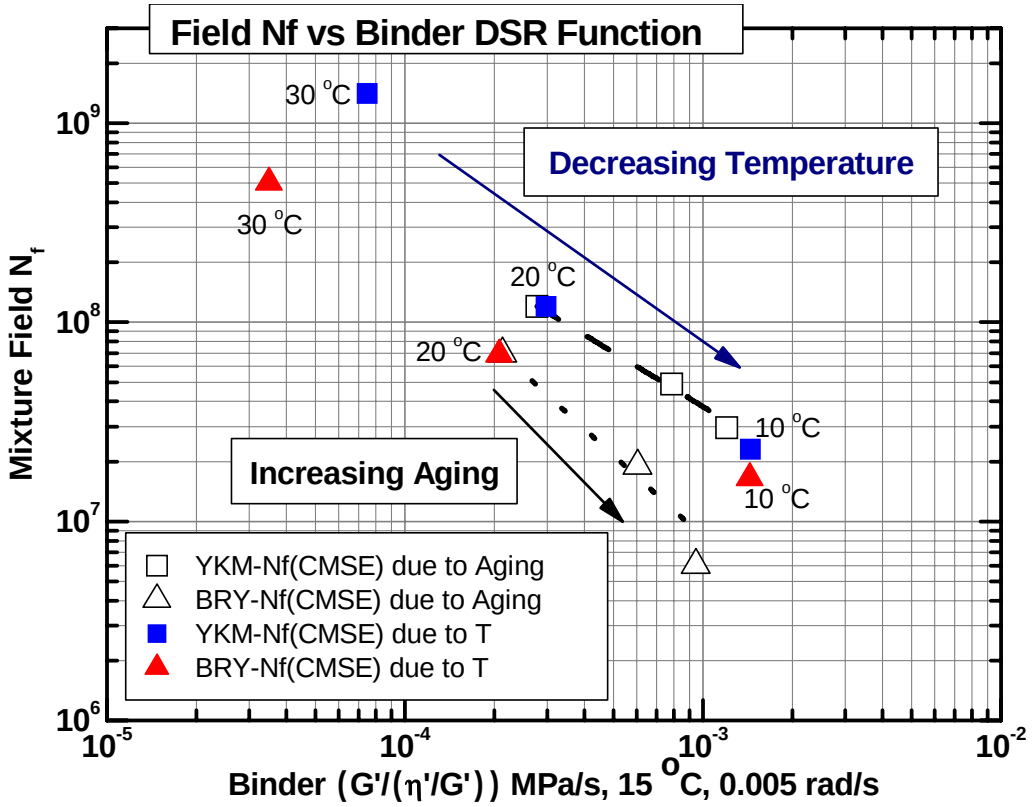

Figure V-20. Fatigue Life Decline with Binder Hardening.

Summary and Conclusions

In this chapter, two HMAC mixtures were tested to obtain mixture viscoelastic properties at three conditions (0, 3, and 6 months) of binder aging. Nondestructive tensile RM tests were used to produce mixture dynamic shear complex moduli master curves. Binders recovered from aged mixtures were used to determine corresponding master curves for the binder. From these binder-mixture aging experiments, the following results were obtained:

- Mixtures stiffened significantly in response to binder oxidative aging. Mixture stiffening was reflected in both the tensile relaxation modulus and the dynamic shear moduli.
- A mixture viscoelastic property map of G' versus η'/G' at the three levels of mixture aging (PP2, PP2+3 months, PP2+6 months) provided a useful means of tracking mixture stiffening with binder oxidative aging. This mixture VE map is analogous to the binder DSR map.
- A mixture VE function, defined as G'/(η'/G') at 20 °C, 0.002 rad/s correlated linearly with the binder DSR function G'/(η'/G') at 15 °C, 0.005 rad/s.
- The Bryan (PG 64-22) binder was softer than the Yoakum (PG 76-22) binder. Conversely, the Bryan mixture was stiffer than the Yoakum mixture at comparable angular frequency or binder stiffness.
- The Hirsch model provided a reasonable correlation between binder and mixture G* at PP2 level aging, especially for the Bryan mixture.
- Changes in mixture stiffness with temperature at PP2 level aging followed the Hirsch Model reasonably well.
- Changes in mixture stiffness with aging deviated significantly from Hirsch model (stiffened the mixture more).

- Binder stiffening with decreasing temperature followed much the same path on the DSR map as aging.
- The effect of temperature on mixture fatigue life may provide a means of estimating the effect of aging. Data on additional mixtures are required to establish the accuracy of such estimates.

CHAPTER VI
SUMMARY AND CONCLUSIONS

Summary and Conclusions

Binder Oxidative Aging in Texas Pavements

The study of binder oxidation in 15 different Texas highway pavements indicates that binder oxidation is not only a surface reaction. Instead, oxidation has a detrimental impact throughout the entire depth of asphalt pavements. Binders in the pavements become stiffer and more brittle, like laboratory-aged neat binders, even 6 inches below the surface. Binders in pavements can oxidize at rates that are fairly uniform with depth once early oxidation occurs, even for dense-graded mixtures, and these rates may continue for an extended period of time.

The DSR function map serves as an excellent method of tracking pavement aging over time. The Superpave RTFOT plus PAV procedure may not be an appropriate long-term binder aging test for Texas pavement due to the high ductility value of the binder, (greater than 10 cm) which does not represent a very severe level of aging compared to the recovered binder data from the ten LTPP sites and Texas SH 21 pavement.

The level of hardening reached in pavement binders significantly exceeds estimated values calculated by the Global Aging Model, both at the pavement surface and at 5 inch below the surface.

Impact of Binder Oxidation on Mixture Aging and Fatigue Performance

Binder oxidation significantly affects the decline of strain-controlled fatigue due to the detrimental impact on the binder durability of the mixture. The HMAC mixture fatigue performance is also determined to be a function of mixture design. Binder oxidation in mixtures follows a path similar to neat binders (DSR function hardening

rate, hardening susceptibility, DSR map) even though hardening rates in mixtures are slower than in thin-film neat binders due to diffusion resistance.

DSR function hardening rate is used to track the binder stiffness changes and is found to be a very good rheological property that tracks binder durability due to oxidative hardening for both conventional binders and the polymer modified binders in thin film aging and mixture aging. This conclusion is based on one conventional binder and two polymer modified binders; however more samples should be studied.

The PP2 level aging process ages binders more severely than SAFT level aging. However, the PP2 level aged binders for this study do not completely pass the initial jump period. Standard PAV after SAFT aging is less than PP2 plus 3 months aging in 60 ^{o}C room, which indicates that this may not be appropriate for measuring the long-term aging binder properties for Texas asphalt pavement.

Estimating the Effect of Binder Oxidation on Pavement Service Life

The cumulative damage approach provides a rational method for quantitatively measuring pavement service life that considers both binder oxidation and pavement loading rate. Binder hardening rate, as well as the ratio of fatigue life decline rate to binder hardening rate has a great impact on the pavement service life estimation. Pavement service life can be estimated by the following equation:

$$t_{end} = \frac{\ln(K_1 K_2 N_{f0} / R_L + 1)}{K_1 K_2} \qquad \text{(VI-1)}$$

where: t_{end} is pavement service life, K_1 is the magnitude of the power law slope that relates the decline of fatigue life to the increase in the DSR function with aging; K_2 is the (exponential) rate of increase of the DSR function with aging time in the pavement; N_{f0} is the initial fatigue life at t = 0.

N_{f0}, which is commonly used for pavement fatigue performance, has much less of an impact than K_1 and K_2. Therefore, the impact of binder oxidation must be included for a long-term pavement performance test.

Impact of Binder Oxidation on Binder and Mixture Rheology

The tensile relaxation modulus and the dynamic shear modulus of mixtures are greatly affected by binder oxidation. The mixture G* of oxidative binder hardening has a different stiffening mechanism from the mixture G* of temperature binder hardening. Even though the Hirsch model provides a reasonable correlation between binder and mixture G* at PP2 level aging, changes in mixture stiffness with aging deviate significantly from the Hirsch model. Actual mixture aging stiffened the mixture more than the model predicted due to binder hardening. Mixture stiffness may not be dependent only on binder hardening but both binder hardening and binder aggregate bond strength with binder oxidation.

The mixture viscoelastic function, defined as G'/(η'/G') at 20 ^{o}C and 0.002 rad/sec, provides a useful means of tracking mixture stiffening with binder oxidative aging and is correlated linearly with the binder DSR function at 15 ^{o}C and 0.005 rad/sec. Binder stiffening with decreasing temperature follows much the same path on the DSR map as aging. The effect of temperature on mixture fatigue life shows a possible means of estimating the effect of aging.

Recommendations

Field and Laboratory Aging Comparison

Two pavements out of the 15 Texas pavements in this study had several different aging levels and only one original neat binder used for the highway was available. More field data from different years with the same neat binders used for the pavements should

be studied to provide an accurate relation between the lab aging and field aging. Further, kinetic parameters for laboratory aged binders and more accurate pavement temperature profile data would improve the comparison of lab aging with field aging. Therefore, it is desirable for each TxDOT district to retain a sample of the original neat binders from pavements and begin regular sampling of the field cores and pavement failure data. This will lead to a more accurate pavement service life prediction and a better pavement maintenance method.

Binder Oxidation on Mixture Rheological Properties and Fatigue Performance

Mixture fabrication is very expensive and aging mixtures is very time consuming work. Five out of 7 different mixtures had only one aging level besides PP2 level aging. The PP2 level aged binder was not aged past the initial jump period even though it is more heavily aged than the SAFT aged binder. Therefore, mixtures with more aging levels above PP2 level aging are recommended in order to obtain more accurate fatigue results and analysis.

This research shows that binder oxidation greatly affects mixture fatigue performance and mixture rheological properties. However, the reasons are not yet fully understood. More fundamental studies are required to understand why the decline of fatigue life is a function of mixture design and why a certain binder has better fatigue performance with the same aggregates after aging. In addition, more accurate extraction and recovery processes for the polymer modified binder are needed for binder-mixture characterization and aging comparison among neat binder aging, mixture aging and field aging.

More study of the effects of temperature on mixture stiffness and fatigue performance is also recommended to create a substitute binder and mixture aging process. Development of a faster mixture aging method is also needed to accelerate the mixture fatigue test.

LITERATURE CITED

AASHTO, "Designation PP1-98, Standard Practice for Accelerated Aging of Asphalt Binder Using a Pressurized Aging Vessel (PAV)," *AASHTO provisional standards*. 3rd ed. AASHTO, Washington, DC (1996a).

AASHTO, "Designation PP2-00, Standard Practice for Mixture Conditioning of Hot-Mix Asphalt (HMA)," *AASHTO provisional standards*. 3rd ed. AASHTO, Washington, DC (1996b).

AASHTO, "Designation TP4-00, Standard Method for Preparing and Determining the Density of Hot-Mix Asphalt (HMA) Specimens by Means of the Superpave Gyratory Compactor," *AASHTO provisional standards*. 3rd ed. AASHTO, Washington, DC (1996c).

AASHTO, AASHTO 2002 Pavement Design Guide (NCHRP 1-37A Report), (2004). http://www.trb.org/mepdg/guide.htm, Accessed June 2006.

Al-Azri, N.A., S.H. Jung, K.M. Lunsford, A. Ferry, J.A. Bullin, R.R. Davison, and C.J. Glover, "Binder Oxidative Aging in Texas Pavements: Hardening Rates, Hardening Susceptibilities, and the Impact of Pavement Depth," *Trans. Res. Rec.*, (2006).

Barth, E.J., *Asphalt : Science and Technology*. Gordon and Breach Science Publishers, New York (1962).

Burr, B.L., R.R. Davison, C.J. Glover, and J.A. Bullin, "Solvent Removal from Asphalt," *Trans. Res. Rec.*, **1269**, 1 (1990).

Burr, B.L., R.R. Davison, C.J. Glover, and J.A. Bullin, "Softening of Asphalts in Dilute Solutions at Primary Distillation Conditions," *Trans. Res. Rec.*, **1436**, 47 (1994).

Burr, B.L., R.R. Davison, H.B. Jemison, C.J. Glover, and J.A. Bullin, "Asphalt Hardening in Extraction Solvents," *Trans. Res. Rec.*, **1323**, 70 (1991).

Burr, B.L., C.J. Glover, R.R. Davison, and J.A. Bullin, "New Apparatus and Procedure for the Extraction and Recovery of Asphalt Binder from Pavement Mixtures," *Trans. Res. Rec.*, **1391**, 20 (1993).

Cheng, D., "Surface Free Energy of Asphalt-Aggregate System and Performance Analysis of Asphalt Concrete Based on Surface Free Energy," Ph.D. Dissertation, Texas A&M University, College Station, (2002).

Christensen, D.W., Jr., T. Pellinen, and R.F. Bonaquist, "Hirsch Model for Estimating the Modulus of Asphalt Concrete," *J. AAPT*, **72**, 97 (2003).

Cipione, C.A., R.R. Davison, B.L. Burr, C.J. Glover, and J.A. Bullin, "Evaluation of Solvents for Extraction of Residual Asphalt from Aggregates," *Trans. Res. Rec.*, **1323**, 47 (1991).

Clark, R.C., "Practical Results of Asphalt Hardening on Pavement Life," *J. AAPT*, **27**, 196 (1958).

Coons, R.F., and P.H. Wright, "An Investigation of the Hardening of Asphalt Recovered from Pavements of Various Ages," *J. AAPT*, **37**, 510 (1968).

Domke, C.H., R.R. Davison, and C.J. Glover, "Effect of Oxidation Pressure on Asphalt Hardening Susceptibility," *Trans. Res. Rec.*, **1661**, 114 (1999).

Domke, C.H., R.R. Davison, and C.J. Glover, "Effect of Oxygen Pressure on Asphalt Oxidation Kinetics," *Ind. Eng. Chem. Res*, **39**(3), 592 (2000).

Doyle, P.C., "Cracking Characteristic of Asphalt Cement," *J. AAPT*, **27**, 581 (1958).

Ferry, J.D., *Viscoelastic Properties of Polymers*, 3rd ed., Wiley, New York (1980).

FHWA, " Highway Statistics 2000." Office of Highway Policy Information, Federal Highway Administration, Washington, D.C. (2001).

Gillespie, H.M., and C. Crawford, *A Century of Progress: the History of Hot Mix Asphalt*, 1st ed., National Asphalt Pavement Association, Lanham, MD (1992).

Glover, C.J., R.R. Davison, C.H. Domke, Y. Ruan, P. Juristyarini, D.B. Knorr, and S.H. Jung, "Development of New Method For Assessing Asphalt Binder Durability with Field Validation." Texas Dept. of Transportation, Austin (2005).

Glover, C.J., and H.L. Jones, *Conservation Principles for Continuous Media*, 4th ed., McGraw-Hill, New York (1996).

Halstead, W.J., "The Relation of Asphalt Ductility to Pavement Performance," *J. AAPT*, **32**, 247 (1963).

Hardin, J.C., *Physical Properties of Asphalt Cement Binders*, American Society for Testing and Materials, Philadelphia, PA,1241 (1995).

Huang, Y.H., *Pavement Analysis and Design*, Prentice Hall, Englewood Cliffs, NJ. (1993).

Huber, G.A., and D.S. Decker, *Engineering Properties of Asphalt Mixtures and the Relationship to Performance*, American Society for Testing and Materials, Philadelphia, PA, 1265 (1995).

Jemison, H.B., B.L. Burr, R.R. Davison, J.A. Bullin, and C.J. Glover, "Application and Use of the ATR, FT-IR Method to Asphalt Aging Studies," *Preprints - American Chemical Society, Division of Petroleum Chemistry*, **35**(3), 490 (1990).

Jemison, H.B., B.L. Burr, R.R. Davison, J.A. Bullin, and C.J. Glover, "Application and Use of the ATR, FT-IR Method to Asphalt Aging Studies. In: American Chemical Society Symposium on Chemistry and Characterization of Asphalts, August 1990, Washington, D.C," *Fuel Science & Technology International*, **10**(4), 795 (1992).

Juristyarini, P., "Asphalt Modification and Testing of Performance-Related Cracking Failure Properties," Ph.D. Dissertation, Texas A&M University, College Station (2003).

Kandhal, P.S., "Low-Temperature Ductility in Relation to Pavement Performance. In ASTM STP 628: Low-Temperature Properties of Bituminous Materials and Compacted Bituminous Paving Mixtures." American Society for Testing and Materials, Philadelphia, PA, 95 (1977).

Kandhal, P.S., and W.C. Koehler, "Significant Studies on Asphalt Durability: Pennsylvania Experience," *Trans. Res. Rec.*, **999**, 41 (1984).

Kandhal, P.S., and M.E. Wenger, "Asphalt Properties in Relation to Pavement Performance," *Trans. Res. Rec.*, **544**, 1 (1975).

Kim, Y.R., H.J. Lee, Y. Kim, and D.N. Little, "Mechanistic Evaluation of Fatigue Damage Growth and Healing of Asphalt Concrete: Laboratory and Field Experiments," *Proceedings Eighth International Conference on Asphalt Pavements*, University of Washington, Seattle, 1089 (1997a).

Kim, Y.R., H.J. Lee, and D.N. Little, "Fatigue Characterization of Asphalt Concrete Using Viscoelasticity and Continuum Damage Theory (with Discussion)," *J. AAPT*, **66**, 520 (1997b).

Lau, C., K. Lunsford, C. Glover, R. Davison, and J. Bullin, "Reaction Rates and Hardening Susceptibilities as determined from Pressure Oxygen Vessel aging of asphlats," *Trans. Res. Rec.*, **1342**, 50 (1992).

Lee, H.J., "Uniaxial Constitutive Modeling of Asphalt Concrete Using Viscoelasicity and Continuum Damage Theory," Ph.D. Dissertation, North Carolina State University, Raleigh, (1996).

Leicht, S.E., P. Juristyarini, R.R. Davison, and C.J. Glover, "An Investigation of Oxidative Curing on the Properties of High Cure Asphalt Rubber," *Pet. Sci. & Tech.*, **19**(3-4), 317 (2001).

Lin, M.S., J.M. Chaffin, M. Liu, C.J. Glover, R.R. Davison, and J.A. Bullin, "The Effect of Asphalt Composition on the Formation of Asphaltenes and their Contribution to Asphalt Viscosity," *Fuel Sci. & Tech. Int.*, **14**(1-2), 139 (1996).

Lin, M.S., K.M. Lunsford, C.J. Glover, R.R. Davison, and J.A. Bullin, "The Effects of Asphaltenes on the Chemical and Physical Characteristics of Asphalt," *Asphaltenes*, 155 (1995).

Liu, M., M.A. Ferry, R.R. Davison, C.J. Glover, and J.A. Bullin, "Oxygen Uptake as Correlated to Carbonyl Growth in Aged Asphalts and Asphalt Corbett Fractions," *Ind. & Eng. Chem. Res.*, **37**(12), 4669 (1998a).

Liu, M., K.M. Lunsford, R.R. Davison, C.J. Glover, and J.A. Bullin, "The Kinetics of Carbonyl Formation in Asphalt," *AIChE J*, **42**(4), 1069 (1996).

Liu, M.M., M.S. Lin, J.M. Chaffin, R.R. Davison, C.J. Glover, and J.A. Bullin, "Oxidation Kinetics of Asphalt Corbett Fractions and Compositional Dependence of Asphalt Oxidation," *Pet. Sci. & Tech.*, **16**(7-8), 827 (1998b).

Lu, X., and U. Isacsson, "Chemical and Rheological Evaluation of Ageing Properties of SBS Polymer Modified Bitumens," *Fuel*, **77**(9/10), 961 (1998).

Lu, X., and U. Isacsson, "Chemical and Rheological Characteristics of Styrene-Butadiene-Styrene Polymer-Modified Bitumens," *Trans. Res. Rec.*, **1661**, 83 (1999).

Lytton, R.L., J. Uzan, E.G. Fernando, R. Roque, D. Hiltunen, and S.M. Stoffels, "Development and Validation of Performance Prediction Models and Specifications for Asphalt Binders and Paving Mixes." Strategic Highway Research Program, 518 (1993).

Marek, C.R., and M. Herrin, "Tensile Behavior and Failure Characteristics of Asphalt Cements in Thin Films," *J. AAPT*, **37**, 386 (1968).

Martin, K.L., R.R. Davison, C.J. Glover, and J.A. Bullin, "Asphalt Aging in Texas Roads and Test Sections," *Trans. Res. Rec.*, **1269**, 9 (1990).

Mirza, M.W., and M.W. Witczak, "Development of a Global Aging System for Short and Long Term Aging of Asphalt Cements (with Discussion)," *J. AAPT*, **64**, 393 (1995).

Monismith, C.L., J.A. Epps, and F.N. Finn, "Improved Asphalt Mix Design (with Discussion)," *J. AAPT*, **54**, 340 (1985).

Monismith, C.L., J.A. Epps, D.A. Kasianchuk, and D.B. McLean, "Asphalt Mixture Behavior in Repeated Flexure," University of California, Berkeley (1970).

Palade, L.I., P. Attane, and S. Camaro, "Linear Viscoelastic Behavior of Asphalt and Asphalt based Mastic," *Rheol. Acta*, **39**(2), 180 (2000).

Park, D.W., "Characterization of Permanent Deformation in Asphalt Concrete Using a Laboratory Prediction Method and an Elastic-Viscoplastic Model," Ph.D. Dissertation, Texas A&M University, College Station, (2004).

Petersen, J.C., J.F. Branthaver, R.E. Robertson, P.M. Harnsberger, J.J. Duvall, and E.K. Ensley, "Effects of Physicochemical Factors on Asphalt Oxidation Kinetics," *Trans. Res. Rec.*, **1391**, 1 (1993).

Roberts, F.I., P.S. Kandhal, E.R. Brown, D.-Y. Lee, and T.W. Kennedy, *Hot Mix Asphalt Materials, Mixture Design, And Construction*, 2nd ed., NAPA Educaton Foundation, Lanham, Maryland (1996).

Roque, R., D.R. Hiltunen, W.G. Buttlar, and T. Farwanna, "*Development of the SHRP SUPERPAVE^{TM} Mixture Specification Test Method to Control Thermal Cracking Performance of Pavements*," Symposium on Engineering Properties of Asphalt Mixture and Relation to Performance, G. A. Huber and D. S. Decker E, editors. ASTM STP 1265, Philadelphia, PA (1994).

Rosen, S.L., *Fundamental Principles of Polymeric Materials*, 2nd ed., Wiley, New York (1993).

Ruan, Y., "Dynamic Linear Viscoelastic Properties and Extensional Failure of Asphalt Binders," Texas A&M University, College Station (2002).

Ruan, Y., R.R. Davison, and C.J. Glover, "The effect of long-term oxidation on the rheological properties of polymer modified asphalts," *Fuel*, **82**(14), 1763 (2003a).

Ruan, Y., R.R. Davison, and C.J. Glover, "An Investigation of Asphalt Durability: Relationships between Ductility and Rheological Properties for Unmodified Asphalts," *Pet. Sci. & Tech.*, **21**(1-2), 231 (2003b).

Schapery, R.A., "A Theory of Crack Growth in Viscoelastic Media." Mechanics & Materials Research Center, Texas A&M University (1973).

Schapery, R.A., "Correspondence Principles and a Generalized J Integral for Large Deformation and Fracture-Analysis of Viscoelastic Media," *Int. J. Fracture*, **25**(3), 195 (1984).

Si, Z., "Characterization of Microdamage and Healing of Asphalt Concrete Mixtures," Ph.D. Dissertation, Texas A&M University, College Station, (2001).

TxDOT, "Condition of Texas Pavements. Pavement Management Information System (PMIS) Annual Report, FY 2001-2003." Texas Dept. of Transportation, Construction Division, Materials and Pavement Section, Austin (2003).

Walubita, L.F., A. Epps Martin, S.H. Jung, C.J. Glover, E.S. Park, and A. Chowdhury, "Comparison of Fatigue Analysis Approaches for Two Hot Mix Asphalt Concrete (HMAC) Mixtures." Texas Dept. of Transportation, Austin (2005).

Williams, D.J., *Polymer Science and Engineering*. Prentice-Hall, Englewood Cliffs, N.J. (1971).

Williams, M.L., R.F. Landel, and J.D. Ferry, "Temperature Dependence of Relaxation Mechanisms in Amorphous Polymers and Other Glass-Forming Liquids," *J. American Chemical Society*, **77**(14), 3701 (1955).

APPENDICES

APPENDIX A
DATA TABLES

Table A-1. Locations and Coring Dates for the Sixteen Texas LTPP Sites

LTTP site	Lat/Long, Route, county	Year Constructed	89-90 Date Taken	2002 Cores Date Taken
48-1046	32.5/101.34, IH 40, Carson	1995	8/3/1989	Aug-02
48-1049	31.65/94.67, US 59, Nacogdoches	1984	3/28/1990	NA
48-1050	30.35/95.92, SH105, Grimes	1984	6/7/1989	NA
48-1056	36.19/100.71, US 83, Ochiltree	1969	8/2/1989	Sep-02
48-1060	28.5/97.05, US 77, Refugio	1986	3/5/1990	NA
48-1068	33.50/95.58, SH 19, Lamar	1985	NA	7/24/2002
48-1109	30.75/95.52, SH 19, Walker	1984	3/21/1990	NA
48-1168	32.67/95.46, FM 564, Wood	1985	NA	7/8/2002
48-2108	29.34/94.92, Spur 37, Galveston	1985	6/6/1989	6/26/2002
48-2133	31.07/97.31, SH 36, Bell	1984	5/12/1989	7/9/2002
48-3679	31.37/94.50, SH 103, Angelina	1988	3/27/1990	NA
48-3689	30.7/94.85, US 190, Polk	1987	3/20/1990	NA
48-3769	31.79/106.25, US 62, EL Paso	1976	7/11/1989	7/9/2002
48-3835	30.73/96.43, SH 6, Brazos	1991	NA	Sep-02
48-6086	28.17/97.86, IH 37, Live Oak	1971	8/3/1990	Jul-02
48-9005	29.51/98.72 FM 1560, Bexar	1986	2/6/1990	7/10/2002

Table A-2. Details of the Pavement Layers for the LTPP Sites

LTPP Site	Route/County	TOP	2ND LAYER	3RD LAYER	4TH LAYER	5TH LAYER	Total
48-1049	US 59	OSL HMA	HMA	S/C			
	Nacogdoches	(1")1984	(3.6")	(0.5")			5.1
48-1050	SH105	OSL HMA	S/C				
	Grimes	(1")1984	(0.8")				1.8
48-1056	US 83	S/C	S/S	OSL HMA			
	Ochiltree	(0.4")7/00	10/88	(1.8")1969			2.2/1.8
48-1060	US 77	OSL HMA	HMA				
	Refugio	(1.7")1986	(5.8")				7.5
48-1068	SH 19	O/L HMA	S/C	S/F	OSL HMA	HMA	
	Lamar	(1.5")11/00	7/28/99	10/92	(3.1")1985	(7.8")	12.4
48-1109	SH 19	OSL HMA	HMA				
	Walker	(0.9")1984	(5.4")				6.3
48-1168	FM 564	S/C	S/E	OSL HMA	S/C		
	Wood	(0.4")2001	1991	(0.8")1985	(0.4")		1.6
48-2108	Loop 197	OSL HMA					
	Galveston	(3")1985					3
48-2133	Loop 363	S/C	OSL HMA	S/C			
	Bell	(0.4")8/00	(1.6")1984	(0.6")			2.6/2.2
48-3679	SH 103	OSL HMA					
	Angelina	(1.6")1988					1.6
48-3689	US 190	OSL HMA	HMA	S/C			
	Polk	(1.1")1987	(1.6")	(0.4")			3.1
48-3769	US 62	S/C rubber	OSL HMA				
	El Paso	(0.4")1986	(2")1976				2.4
48-3835	SH 6	O/L	O/L	CR/S	OSL HMA		
	Brazos	(1.8")6/00	S1.5/N5.5" 6/00	(0.4")9/92	(1.8")1991		S5.5/N9.5
48-6086	IH 37	O/L HMA	S/C	OSL HMA	HMA	HMA	
	Live Oak	(1.5")1985	(0.2")1985	(1.2")1971	(1.2")	(6.1")	10.2
48-9005	FM 1560	O/L HMA	S/C	OSL HMA	S/C		
	Bexar	(1.1")9/98	(0.4")9/98	(1.1")1986	(0.4")		3/1.5
48-1046*	IH 40	HMA	O/L HMA	I/L Geotextile	HMA	HMA	
	Carson	(0.4")1971	(1.7")1971	(0.1")1971	(1.9")1971	(6.4")1971	
	6TH LAYER*	7TH LAYER*					
	OSL HMA	HMA					
	(1.1")5/55	(1.3")					12.9

CR/S- Crack Seal; HMA- Hot Mixed Asphalt; I/L- Inner Layer; O/L- Over Layer

OSL- Original Surface Layer; S/C-Seal Coat; S/E-Sealed Edge; S/S-Seal Strip

*48-1046 has seven layers.

Table A-3. Binder Properties of the LTPP Cores in 1989 or 1990

LTTP site		Const date	Location	1989 or 1990					
				η_0*(poise) @60℃ 0.1 rad/s	DSR Func[a] @15℃ 0.005 rad/s	η'(MPa*s)[a] @15℃ 0.005 rad/s	G'(MPa)[a] @15℃ 0.005 rad/s	η'/G'(s)[a] @15℃ 0.005 rad/s	Calc Duct (cm)
48-1046	A	9-1-55	IH 40	813,087	0.006268	79.14	0.70434	112.4	2.14
	B		Carson	516,476	0.004556	73.43	0.5784	127	2.47
48-1049	A	6-1-84	US 59	36,820	0.000345	34.72	0.1095	317.1	7.67
	B		Nacogdoches	41,970	0.000378	35.68	0.11618	307.1	7.37
48-1050	A	3-1-84	SH105	95,710	0.002185	92.75	0.45016	206.0	3.41
	B		Grimes	89,280	0.002021	85.92	0.41668	206.2	3.53
48-1056	A	6-1-69	US 83	56,790	0.000377	23.12	0.09331	247.8	7.38
	B		Ochiltree	65,420	0.000413	22.95	0.09733	235.8	7.09
48-1060	A	3-1-86	US 77	83,730	0.001036	57.17	0.2434	234.9	4.73
	B		Refugio	97,620	0.001412	73.65	0.32246	228.4	4.13
48-1109	A	2-1-84	SH 19	78,760	0.000927	56.83	0.2295	247.6	4.97
	B		Walker	91,870	0.001029	57.96	0.24424	237.3	4.75
48-2108	A	8-1-85	Loop 197	68,820	0.001113	77.84	0.29428	264.5	4.59
	B		Galveston	64,850	0.000886	65.51	0.24098	271.8	5.07
48-2133	A	5-1-84	Loop 363	52,810	0.000611	54.54	0.18262	298.7	5.97
	B		Bell	60,040	0.000723	59.1	0.20676	285.8	5.54
48-3679	A	6-1-88	SH 103	34,030	0.000363	40.97	0.12188	336.2	7.51
	B		Angelina	28,720	0.000279	36.48	0.10092	361.5	8.42
48-3689	A	4-1-87	US 190	20,810	0.000142	25.81	0.06049	426.7	11.35
	B		Polk	19,990	0.000125	24.44	0.05519	442.8	12.01
48-3769	A	6-1-76	US 62	50,410	0.000751	45.21	0.18428	245.3	5.45
	B		El Paso	67,130	0.001033	50.97	0.22948	222.1	4.74
48-6086	A	6-1-71	IH 37	21,230	0.000176	38.06	0.08192	424.0	10.31
	B		Live Oak	24,800	0.000230	41.37	0.09758	464.6	9.17
48-9005	A	7-1-86	FM 1560	50,060	0.000835	76.3	0.25248	302.2	5.2
	B		Bexar	55,780	0.001043	84.41	0.29678	284.4	4.72

[a] η', G' measured at 44.7 °C, 10 rad/s and converted to 15°C, 0.005 rad/s by TTSP.

[a] DSR Function is G'/(η'/G')

Table A-4. Binder Properties of the LTPP Cores in 2002

LTTP site		Const date	Location	2002					
				η_0*(poise) @60℃ 0.1 rad/s	DSR Func[a] @15℃ 0.005 rad/s	η'(MPa*s)[a] @15℃ 0.005 rad/s	G'(MPa)[a] @15℃ 0.005 rad/s	η'/G'(s)[a] @15℃ 0.005 rad/s	Calc Duct (cm)
48-1046	A	9-1-55	IH 40	55,580	0.000540	38.38	0.14396	266.6	6.3
	B		Carson	40,180	0.000357	30.17	0.10378	290.7	7.56
48-1056	A	6-1-69	US 83	18,070	0.000125	11.57	0.03806	304.0	11.99
	B		Ochiltree	15,960	0.000088	11.17	0.03135	356.3	14
48-1068	A	11-1-85	SH 19	39,990	0.000337	30.68	0.10172	301.6	7.75
	B		Lamar	38,680	0.000277	25.42	0.08387	303.1	8.46
48-1168	A	9-1-85	FM 564	30,760	0.000227	39.34	0.09441	416.7	9.23
	B		Wood	41,990	0.000499	59.36	0.1721	344.9	6.53
48-2108	A	8-1-85	Loop 197	173,860	0.003316	101.68	0.58064	175.1	2.84
	B		Galveston	160,283	0.003266	103.7	0.58198	178.2	2.85
48-2133	A	5-1-84	Loop 363	55,810	0.000674	54.73	0.1921	284.9	5.72
	B		Bell	50,630	0.000577	53.48	0.17566	304.5	6.12
48-3769	A	6-1-76	US 62	49,380	0.000743	47.94	0.18874	254.0	5.48
	B		El Paso	76,330	0.001380	61	0.29018	210.2	4.17
48-3835	A	10-1-91	SH 6	40,270	0.000581	77.57	0.21238	365.2	6.1
	B		Brazos	35,590	0.000411	66.85	0.16582	403.1	7.1
48-6086	A	6-1-71	IH 37	56,980	0.000504	41.44	0.1445	286.8	6.5
	B		Live Oak	55,240	0.000474	39.55	0.13692	288.9	6.67
48-9005	A	7-1-86	FM 1560	33,090	0.000398	46.95	0.13674	343.4	7.21
	B		Bexar	27,760	0.000231	33.5	0.08791	381.1	9.16

[a] η', G' measured at 44.7 °C, 10 rad/s and converted to 15°C, 0.005 rad/s by TTSP.

[a] DSR Function is G'/(η'/G')

Table A-5. Binder Properties of the IH 10 Frontage Road Binders.

Site		η_0*(poise) @60℃ 0.1 rad/s	DSR Func[a] @15℃ 0.005 rad/s	η'(MPa*s)[a] @15℃ 0.005 rad/s	G'(MPa)[a] @15℃ 0.005 rad/s	η'/G'(s)[a] @15℃ 0.005 rad/s	Calc Duct (cm)
IH 10 N	A	929,880	0.019059	77.97	1.219	64.0	1.31
Notrth Bound	B	1,668,514	0.020956	56.32	1.0864	51.8	1.26
IH 10 S	A	196,999	0.004622	114.31	0.7269	157.3	2.45
South Bound	B	172,873	0.003265	94.64	0.5559	170.2	2.86

[a] η', G' measured at 44.7 °C, 10 rad/s and converted to 15°C, 0.005 rad/s by TTSP, [a] DSR Function is G'/(η'/G')

Table A-6. Binder Properties of LTPP Site 48-2108 Top Layer (1.5 inch thickness) with 60 °C Room Aging

Aging Time (months, 60 °C)		η_0*(poise) @60℃ 0.1 rad/s	DSR Func[a] @15℃ 0.005 rad/s	η'/G'(s)[a] @15℃ 0.005 rad/s	G'(MPa)[a] @15℃ 0.005 rad/s	Calc Duct (cm)	Carbonyl Area (CA)
0	A	81,720	0.000888	245.3	0.21792	5.1	1.2276
0	B	80,080	0.000982	249.4	0.24484	4.8	1.2045
3	A	119,800	0.001562	208.4	0.32556	4.0	1.3718
3	B	148,200	0.002041	193.4	0.39468	3.5	1.3612
6.23	A	347,000	0.003361	157.6	0.52964	2.8	1.5215
6.23	B	305,190	0.003068	160.3	0.49184	2.9	1.4961
9	A	510,000	0.005625	129.0	0.72554	2.3	1.6240
9	B	470,000	0.004913	135.8	0.66746	2.4	1.6343

[a] η', G' measured at 44.7 °C, 10 rad/s and converted to 15°C, 0.005 rad/s by TTSP, [a] DSR Function is G'/(η'/G')

* LTPP 48-2108 Site's Oginal Surface Layer has 3 inch thickness

Table A-7. Binder Properties of LTPP Site 48-2108 Bottom Layer (1.5 inch thickness) with 60 °C Room Aging

Aging Time (months, 60 °C)		η_0*(poise) @60℃ 0.1 rad/s	DSR Func[a] @15℃ 0.005 rad/s	η'/G'(s)[a] @15℃ 0.005 rad/s	G'(MPa)[a] @15℃ 0.005 rad/s	Calc Duct (cm)	Carbonyl Area (CA)
0	A	56,720	0.001057	281.9	0.29790	4.7	1.4525
0	B	50,140	0.000768	299.5	0.23012	5.4	1.4545
3	A	87,070	0.002062	214.9	0.44310	3.9	1.5603
3	B	78,490	0.001810	233.2	0.42212	3.6	1.5579
6.23	A	98,760	0.002544	199.0	0.50624	3.2	1.6573
6.23	B	106,000	0.002820	197.1	0.55568	3.1	1.6824
9	A	150,500	0.004027	162.6	0.65468	2.6	1.7329
9	B	154,300	0.004286	163.3	0.70002	2.5	1.6980

[a] η', G' measured at 44.7 °C, 10 rad/s and converted to 15°C, 0.005 rad/s by TTSP, [a] DSR Function is G'/(η'/G')

* LTPP 48-2108 Site's Oginal Surface Layer has 3 inch thickness

Table A-8. Binder Properites of LTPP 48-1046 Site in 1989 with Different Layers

Layer		η_0*(poise) @60℃ 0.1 rad/s	DSR Func[a] @15℃ 0.005 rad/s	η'/G'(s)[a] @15℃ 0.005 rad/s	G'(MPa)[a] @15℃ 0.005 rad/s	Calc Duct (cm)
1st	A	118132	0.000957	248.2	0.23758	4.9
(0.4 inch)	B	86346	0.000502	279.8	0.14044	6.5
2nd	A	6130	0.000022	570.9	0.0127	25.6
(1.7 inch)	B	10520	0.000059	421.0	0.02487	16.7
3rd		Geotestile Innter Layer (0.1 inch)				
4th	A	316522	0.004383	126.3	0.5535	2.51
(1.9 inch)	B	305664	0.003289	146.9	0.48294	2.85
6th	A	516476	0.006266	112.4	0.70434	2.47
(1.1 inch)	B	444396	0.004554	127.0	0.5784	2.86

[a] η', G' measured at 44.7 °C, 10 rad/s and converted to 15°C, 0.005 rad/s by TTSP, [a] DSR Function is G'/(η'/G'

* 5th layer data is not available

Table A-9. Binder Properties of LTPP 48-1046 Site in 2002 with Different Layers

Layer		η_0*(poise) @60℃ 0.1 rad/s	DSR Func[a] @15℃ 0.005 rad/s	η'/G'(s)[a] @15℃ 0.005 rad/s	G'(MPa)[a] @15℃ 0.005 rad/s	Calc Duct (cm)
1st	A	37,090	0.000379	327.2	0.12396	7.4
(0.4 inch)	B	37,400	0.000381	315.3	0.12018	7.3
2nd	A	23,070	0.000205	388.9	0.07965	9.7
(1.7 inch)	B	24,910	0.000195	397.2	0.07726	9.9
3rd			Geotestile Innter Layer (0.1 inch)			
4th	A	49,440	0.000750	290.9	0.21806	5.5
(1.9 inch)	B	42,130	0.000533	314.9	0.16798	6.3
5th	A	23,710	0.000268	365.6	0.09789	8.6
(6.4 inch)	B	31,310	0.000371	383.2	0.142	7.4
6th	A	55,580	0.000540	266.6	0.144	6.3
(1.1 inch)	B	40,180	0.000357	290.7	0.1038	6.3

[a] η', G' measured at 44.7 °C, 10 rad/s and converted to 15°C, 0.005 rad/s by TTSP, [a] DSR Function is G'/(η'/G'

Table A-10. Extra Maintenance Information for LTPP Site 48-1046 from Datapave

MNT_ASPHALT_CRACK_SEAL

SHRP_ID	STATE_CODE	CONSTRUCTION_NO	DATE_COMPLETE	SHRP_CASE_NO	DATE_BEGAN
1046	48	2	12/22/1988	1	12/22/1988
1046	48	3	1/29/1998	1	1/29/1998

SHRP_ID	CRACK_SEVERITY	CRACK_TYPE	CRACK_SEAL_MATL	CRACK_SEAL_MATL_SOURCE	MANUFACTURER_NAME
1046	1	6	6	3	Crafco
1046	1	4	6	1	CRACKFILLER MANUF. CO.

SHRP_ID	MANUFACTURER_MATERIAL	AIR_TEMP_LOW	AIR_TEMP_HIGH	SURFACE_MOISTURE	CONDITION_SOURCE
1046	Rubber Crack Sealer		50	1	3
1046	CRACKFILLER	50	60	1	1

SHRP_ID	TOTAL_LENGTH_SEALED	CLEAN_METHOD	CLEAN_METHOD_SOURCE	RECORD_STATUS
1046	1054	1	1	E
1046	1655	1	1	E

Table A-11. Binder Properties of Bryan Mixture

Name	η* (poise) 60 °C (0.1 rad/s)	η'(Mpa*s) @0.005rad/s	G'(MPa)	η'/G'	G'/(η'/G')	Calculated Ductility(cm)	Carbonyl Area
PG64S	10500	9.97	0.0206	483.4	4.265E-05	19.26	0.6201
PG64-3M	45760	30.18	0.0970	311.3	3.114E-04	8.03	0.8571
PG64-6M	106400	47.84	0.1991	240.3	8.287E-04	5.22	0.9572
PG64-9M	-	63.94	0.3557	179.7	1.979E-03	3.56	1.1382
PG64S+PAV*16	46730	28.75	0.0948	303.4	3.123E-04	8.02	0.8949
PG64S+PAV	60670	30.03	0.1068	281.3	3.796E-04	7.36	0.9191
PG64S+PAV*32	94400	43.28	0.1768	244.8	7.222E-04	5.55	1.0331
Bryan-A	38200	23.21	0.0702	330.5	2.125E-04	9.50	0.7981
Bryan-B	31640	22.48	0.0647	347.5	1.861E-04	10.07	0.7602
Bryan-C	28910	20.99	0.0581	361.3	1.608E-04	10.74	0.7615
Bryan-D	28320	22.11	0.0606	364.9	1.661E-04	10.59	0.7577
Bryan-0MA	36900	23.33	0.0705	330.8	2.132E-04	9.49	0.8071
Bryan-0MB	38200	22.93	0.0696	329.3	2.114E-04	9.52	0.8071
Bryan-3MA	81000	45.66	0.1731	263.8	6.560E-04	5.78	0.9266
Bryan-3MB	75000	40.20	0.1489	270.0	5.516E-04	6.24	0.9186
Bryan-6MA	122600	52.47	0.2297	228.5	0.001005	4.79	0.9642
Bryan-6MB	115500	49.5	0.2102	235.5	0.000892	5.05	0.9753

PG64S Original PG64-22 binder after SAFT

PG64-3, 6, 9M Original PG64-22 binder 3, 6, 9 months aged in 60 °C room after SAFT

Bryan A, B, C, D are recovered from the shell after coring the mixture for reference

0, 3, 6M- 0, 3, 6 months aged in 60 °C room

Table A-12. Calculated Ductility versus Measured Ductility for Bryan Neat Binder

Name	Calculated Ductility(cm)	Measured Ducility (cm)	Error (%)
PG64S[a]	19.3	30.2	36.2
PG64-3M	8.0	7.0	14.7
PG64-6M	5.2	5.4	3.3
PG64S+PAV*16	8.0	7.4	8.4
PG64S+PAV	7.4	6.9	6.7
PG64S+PAV*32	5.5	5.7	2.7

[a] Only for reference, PG64-22 SAFT is too soft to apply the calculated ductility values.

Table A-13. Binder Properties of Yoakum Mixture

Layer	DSR Func[a] @15℃ 0.005 rad/s	η'/G'(s)[a] @15℃ 0.005 rad/s	G'(MPa)[a] @15℃ 0.005 rad/s	Calculated Ductility (cm)	Carbonyl Area (CA)
PG76-22 SAFT A	0.000053	482.1	0.02535	17.6	-
PG76-22 SAFT B	0.000083	400.0	0.03307	14.4	0.556
PG76-22 SAFT C	0.000080	398.9	0.03201	14.6	-
PG76-22 SAFT+3M	0.000883	236.2	0.20848	5.1	0.914
PG76-22 SAFT+6M	0.001609	199.1	0.32018	3.9	1.033
PG76-22 SAFT+9M	0.004925	133.9	0.65934	2.4	1.194
PG76-22 SAFT+PAV*16	0.000515	266.3	0.1372	6.4	0.902
PG76-22 SAFT+PAV*32	0.001093	220.8	0.24144	4.6	1.035
Recovered Binder from Yoakum Mixture					
PP2+0MA	0.000231	329.1	0.0761	9.2	0.72109
PP2+0MB	0.000324	270.8	0.0877	7.9	0.71962
PP2+3MA	0.000743	242.8	0.1803	5.5	0.89119
PP2+3MB	0.000830	243.7	0.2023	5.2	0.87767
PP2+6MA	0.001263	214.5	0.2710	4.3	0.96137
PP2+6MB	0.001138	222.8	0.2535	4.5	0.95541
PP2+9MA	0.002870	165.5	0.4749	3.0	1.060542
PP2+9MB	0.002210	173.3	0.3829	3.4	1.059736
PP2+9MC	0.002440	181.9	0.4439	3.2	1.074944
PP2+9MD	0.002681	171.9	0.4608	3.1	1.073394

[a] η', G' measured at 44.7 °C, 10 rad/s and converted to 15°C, 0.005 rad/s by TTSP, [a] DSR Function is G'/(η'/G')

PG76-22SAFT- Oringial PG76-22 binder after SAFT

PG76-22SAFT+ 0, 3, 6, 9M- Orignal neat binder aged for 0, 3, 6 and 9 months in 60 °C room after SAFT aging.

PP2+0, 3, 6, 9 M- Binders recovered from mixtures aged for 0, 3, 6, 9 months in 60 °C room)

A, B, C, D- Different Replicates

Table A-14. Calculated Ducility versus Measure Ducility for Yoakum Neat Binder

Name	Calculated Ductility (cm)	Measured Ductility (cm)	Error (%)
PG76-22 SAFT+3M	5.1	6.0	15.4
PG76-22 SAFT+6M	3.9	4.4	11.4

APPENDIX B
FIGURES

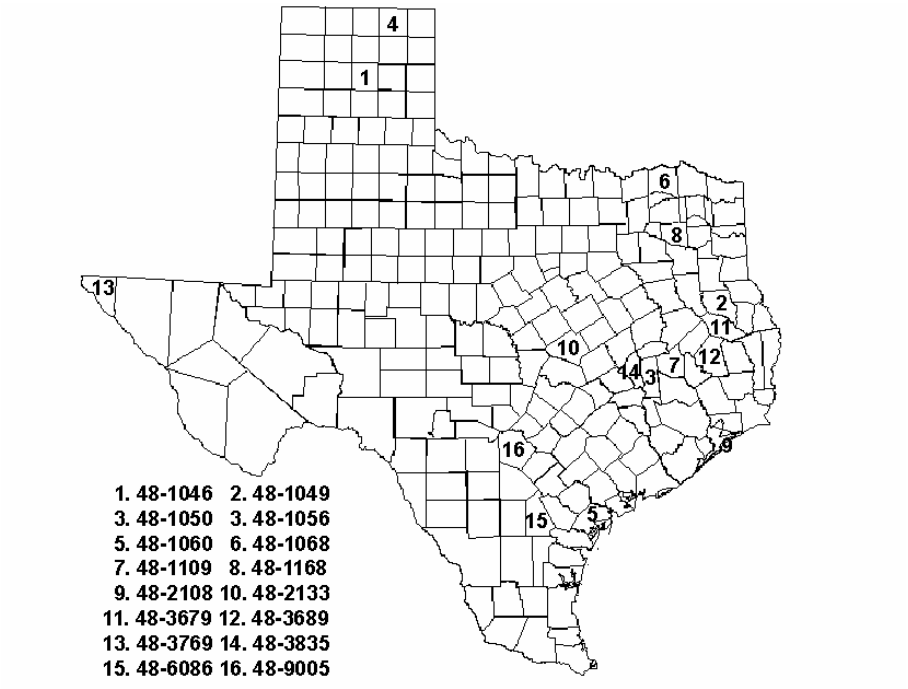

Figure B-1. Locations of the Sixteen LTPP Sites in Texas

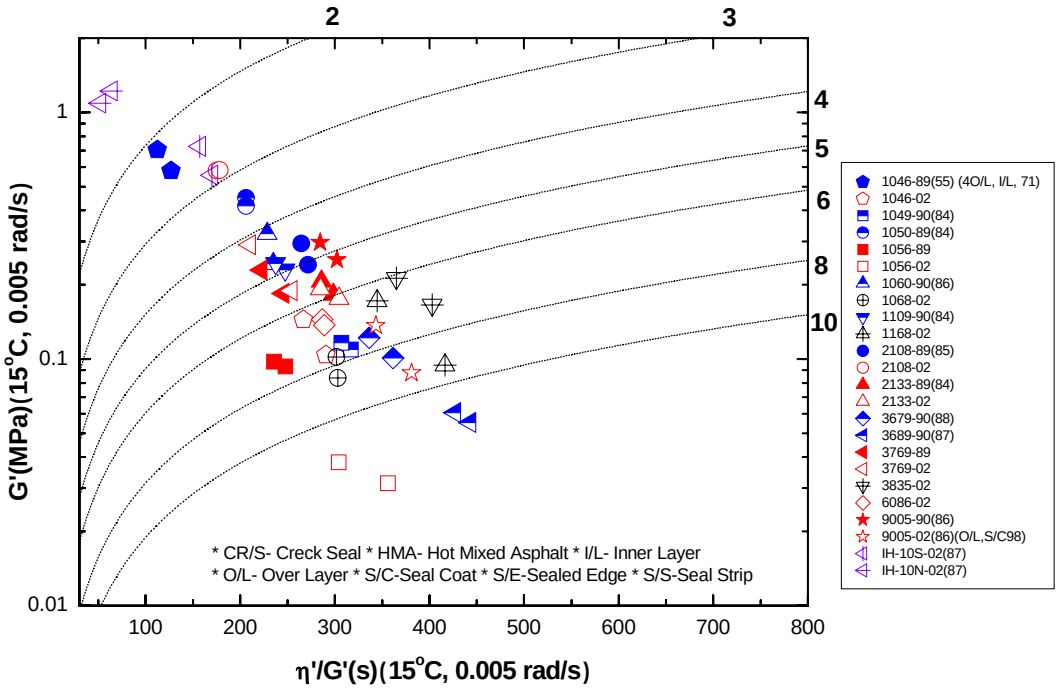

Figure B-2. DSR Map for LTPP Sites in Texas

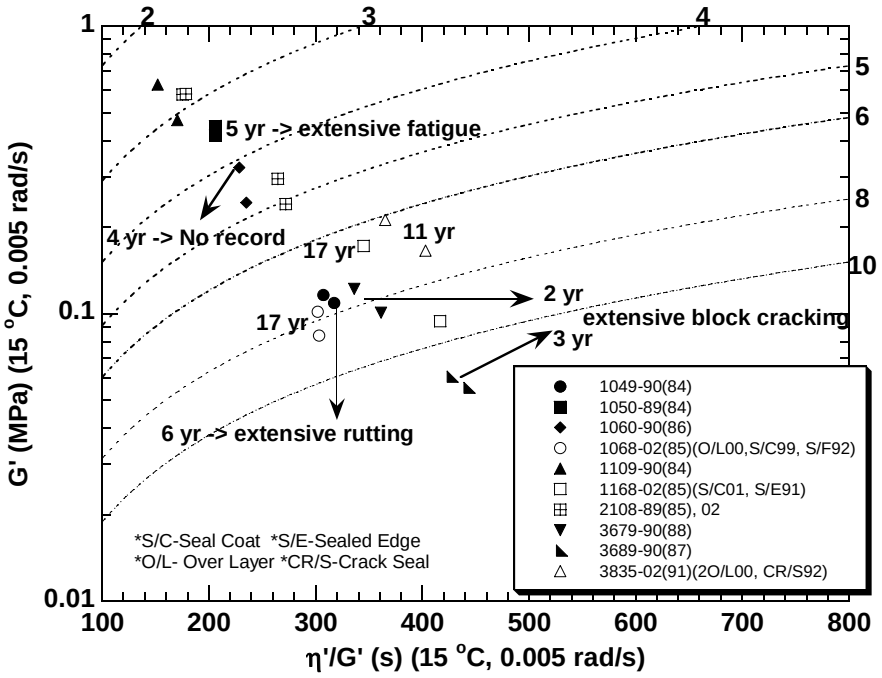

Figure B-3. DSR Function Map with Field Data.

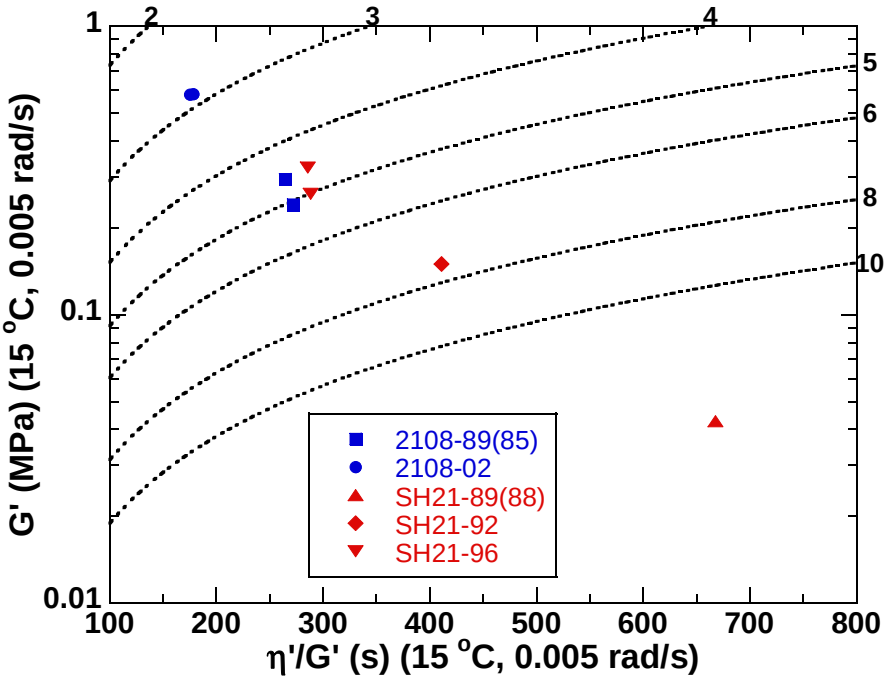

Figure B-4. DSR Map for LTPP 48-2108 and SH 21 with Different Years

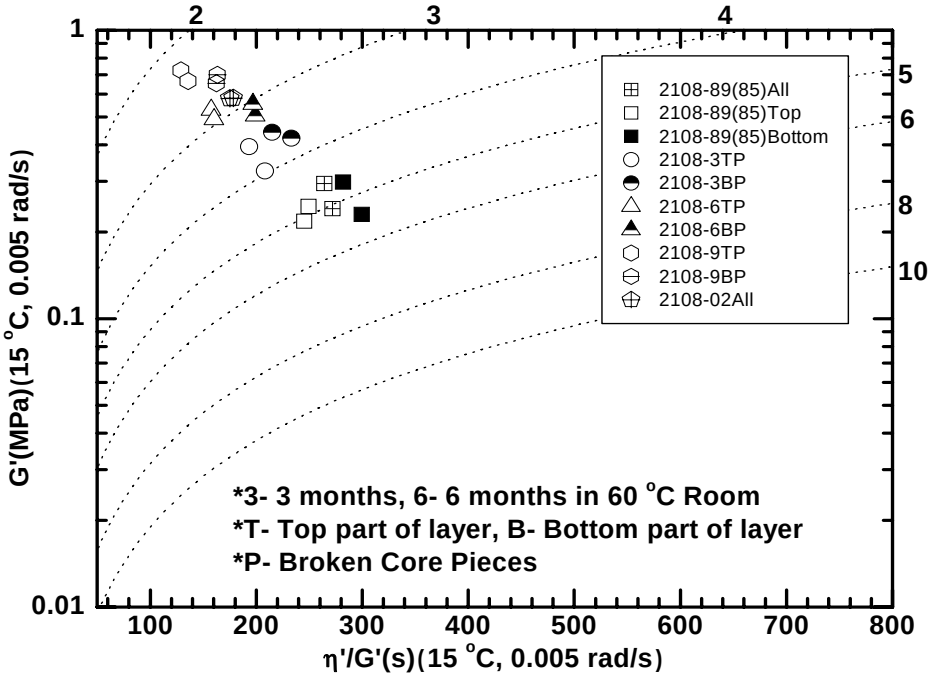

Figure B-5. Field Aging versus Laboratory Aging for LTPP Site 48-2108.

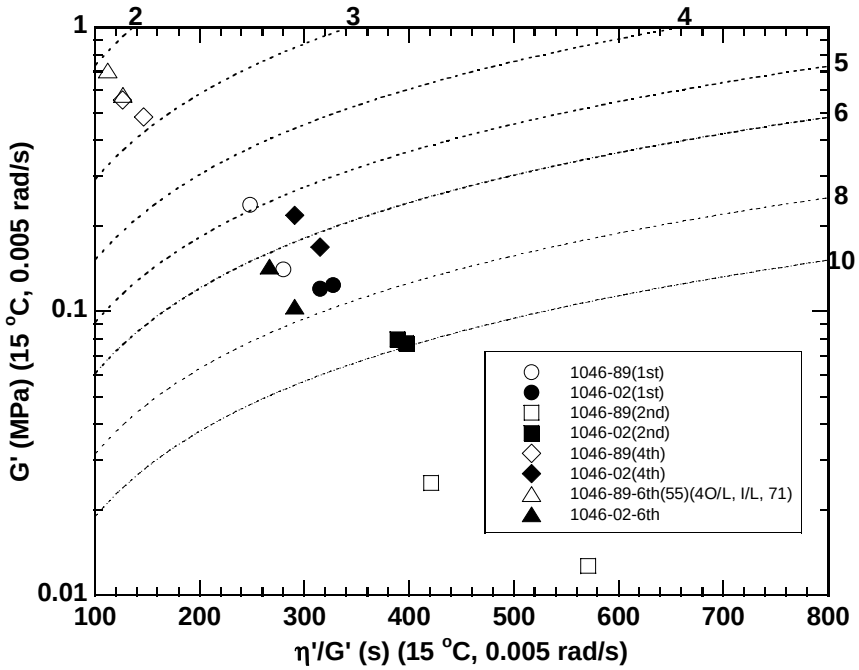

Figure B-6. DSR Map for LTPP 48-1046 with Different Layers: 1989 versus 2002.

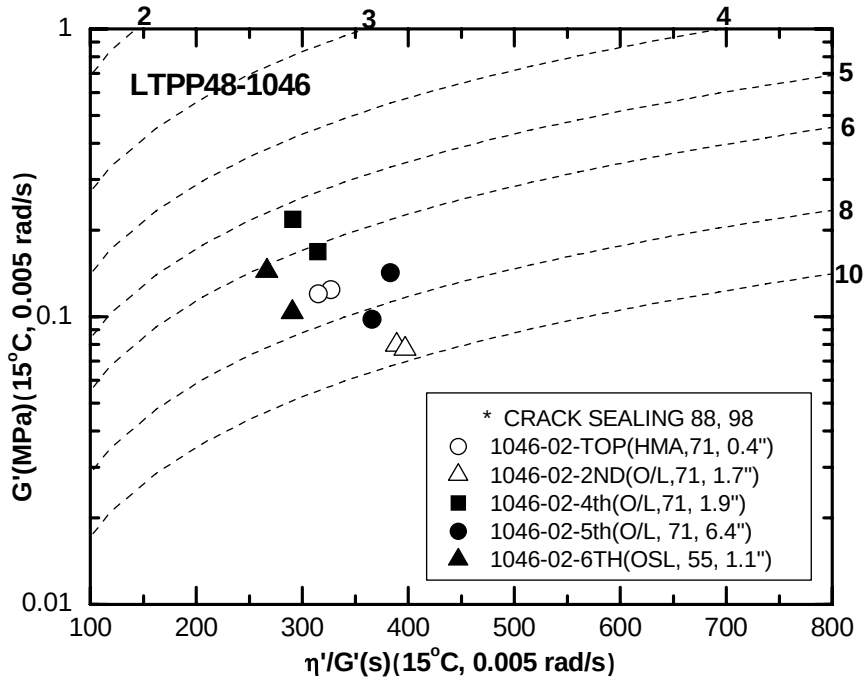

Figure B-7. DSR Map for LTPP 48-1046 With Different Layers in 2002.

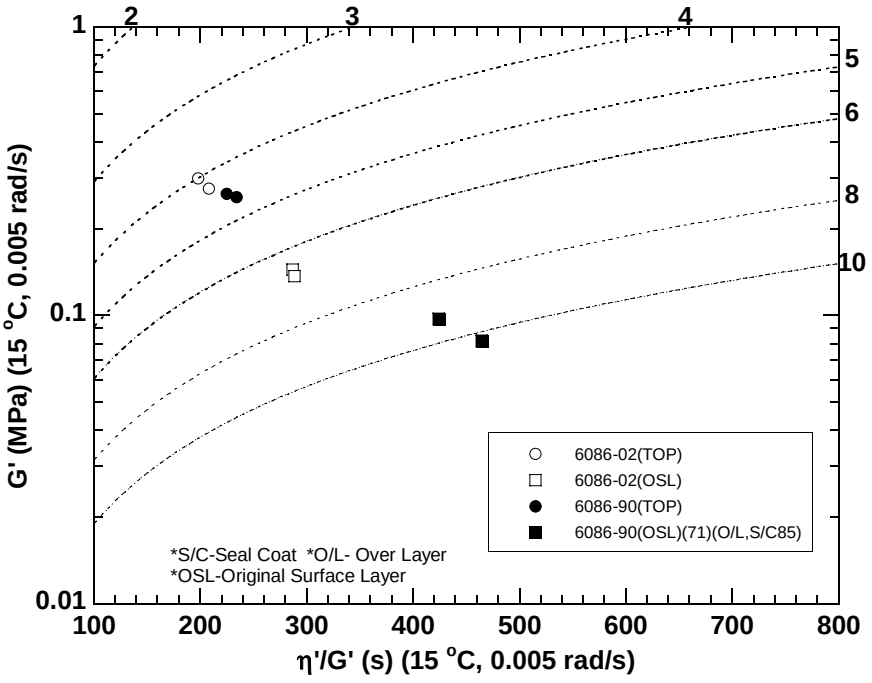

Figure B-8. DSR Map for LTPP 48-6086 with Different Layers

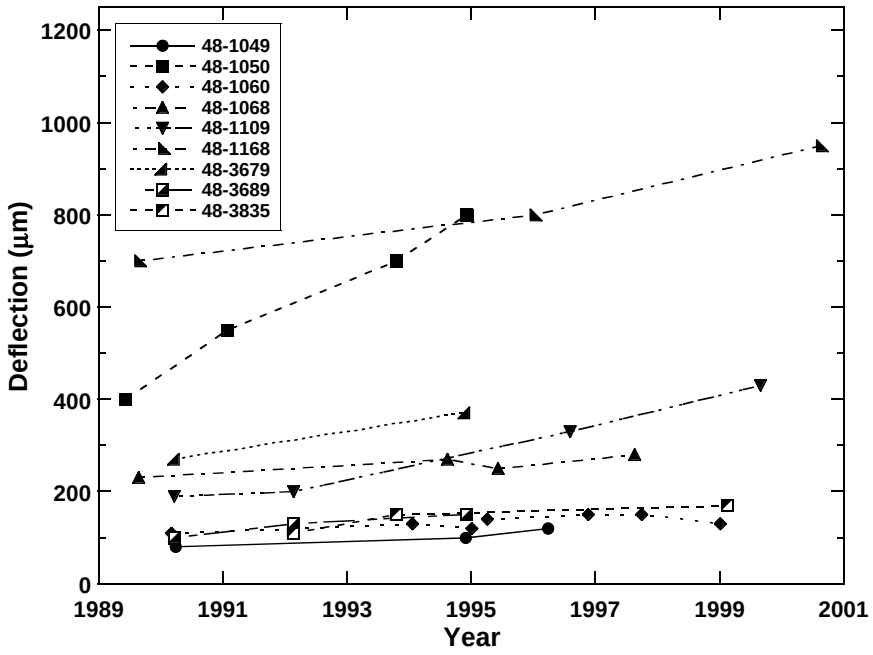

Figure B-9. FWD Data for LTPP Sites of One Aging Level.

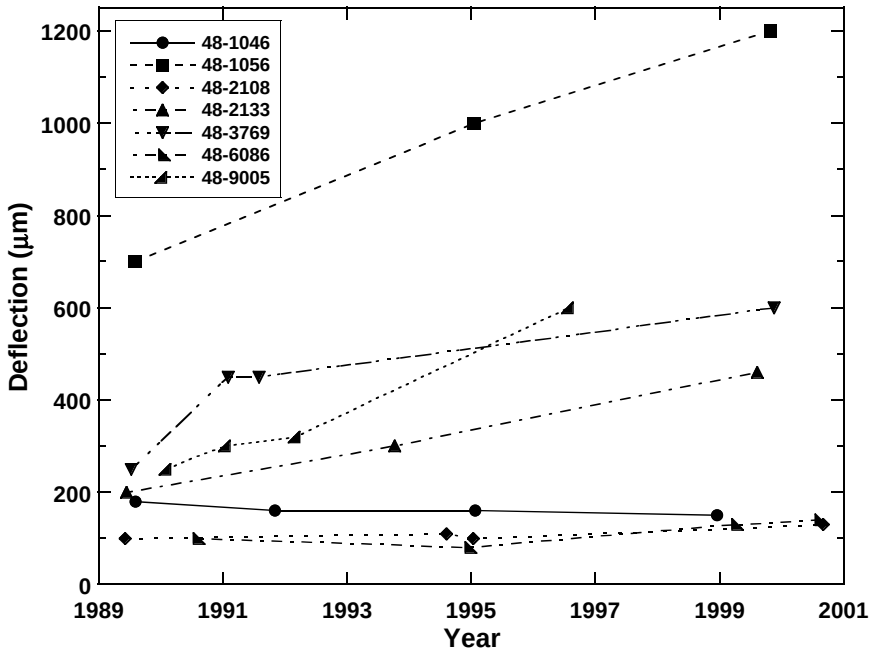

Figure B-10. FWD Data for LTPP Sites of Two Aging Levels.

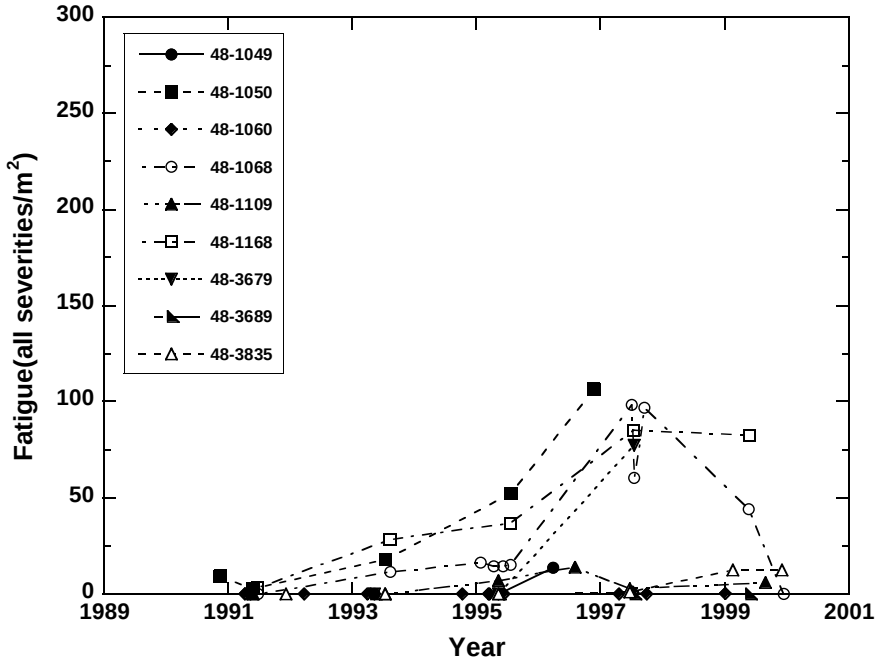

Figure B-11. Fatigue Cracking for LTPP Sites of One Aging Level.

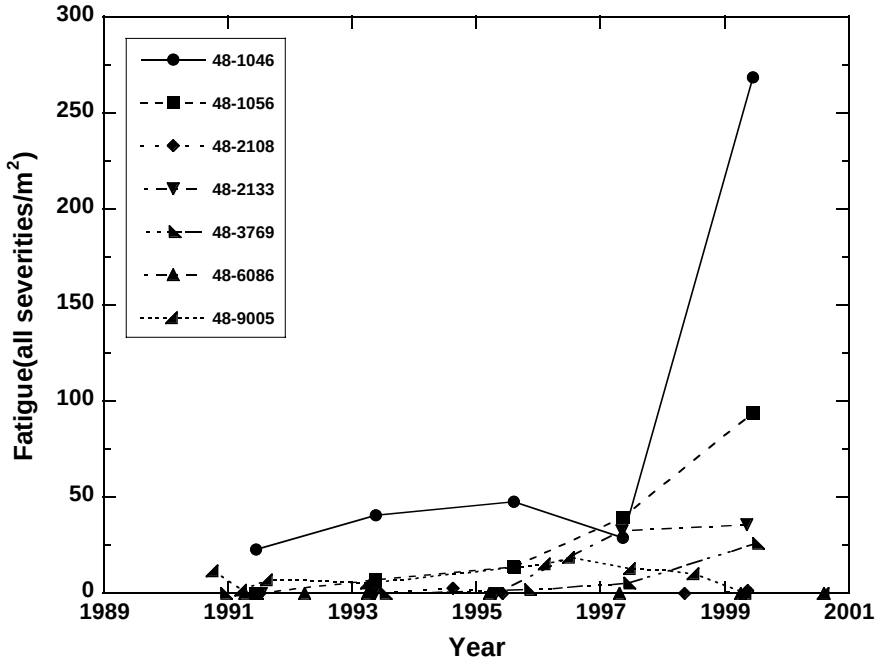

Figure B-12. Fatigue Cracking for LTPP Sites of Two Aging Levels.

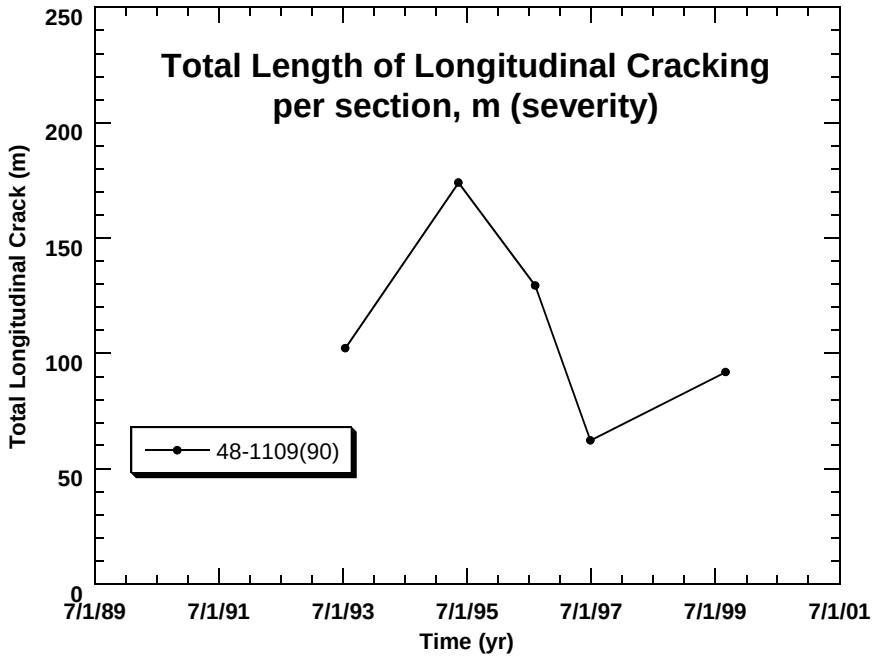

Figure B-13. Longitudinal Cracking for LTPP 48-1109.

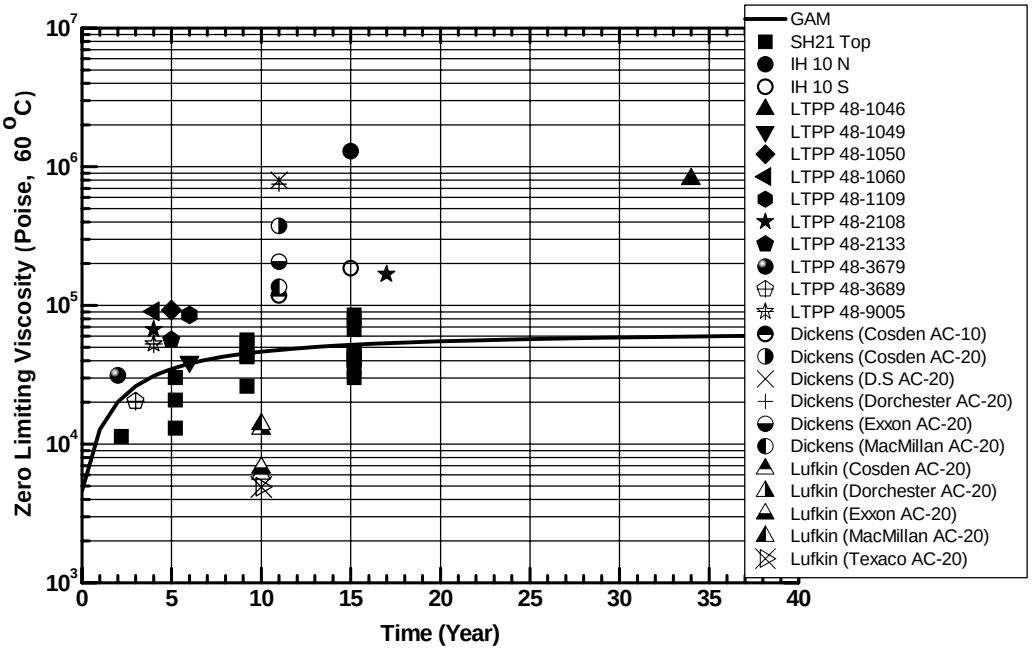

Figure B-14. Binder Aging in the Original Surface Layer versus Global Aging Model.

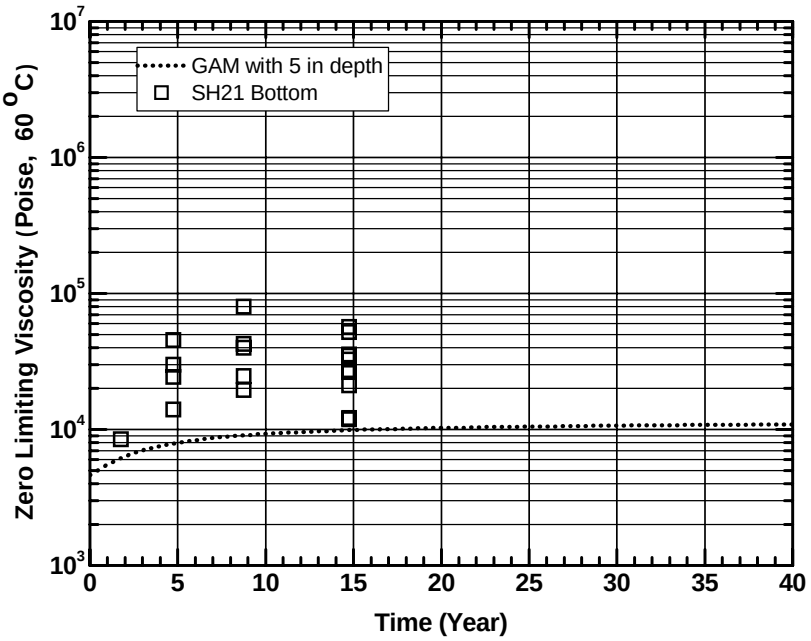

Figure B-15. Binder Aging in the Bottom Layer versus Global Aging Model

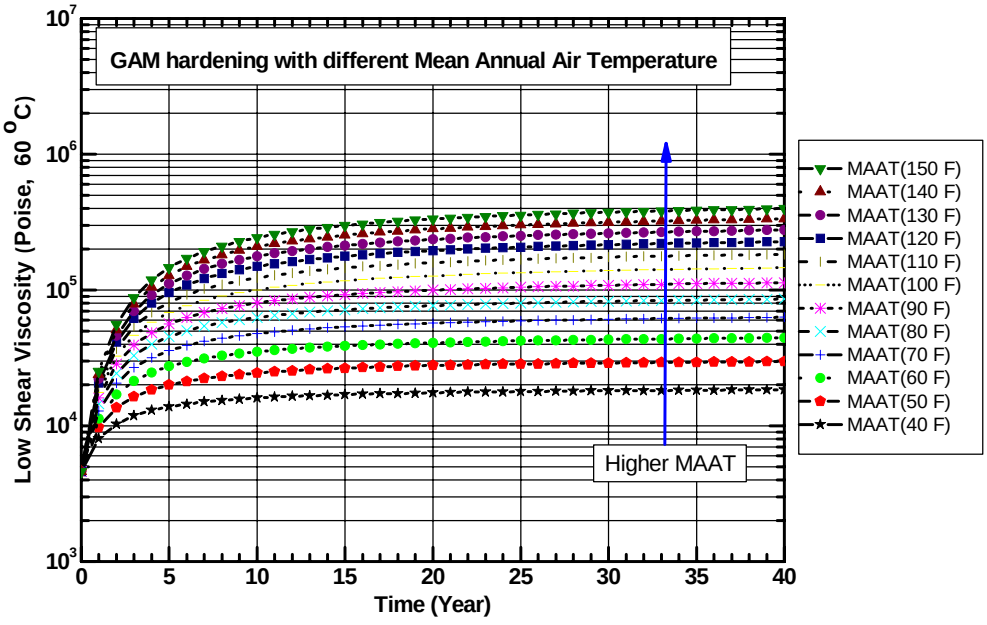

Figure B-16. Global Aging Hardening with Different Mean Annual Air Temperature.

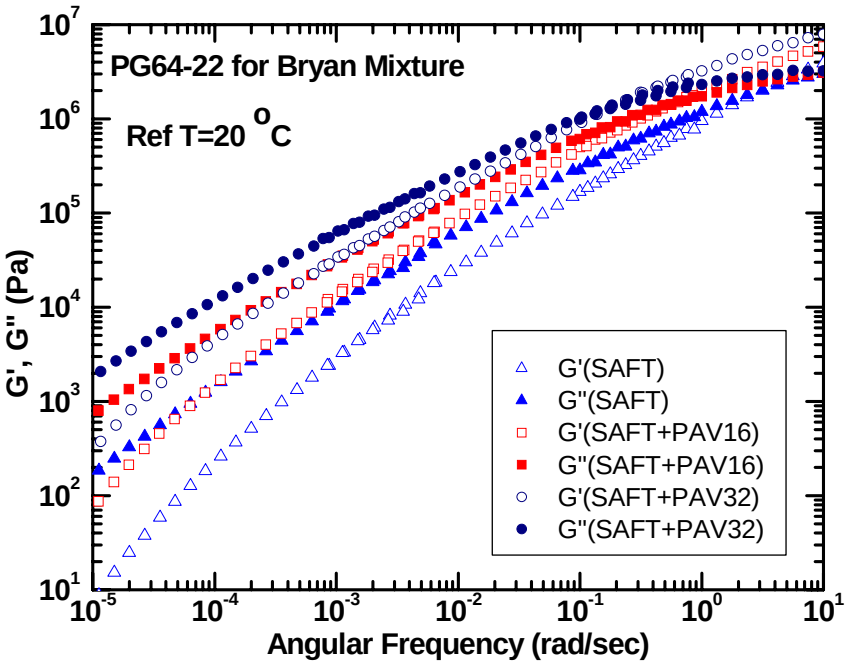

Figure B-17. Master Curves of Curves of Bryan Neat Binder for G'(ω) and G"(ω).

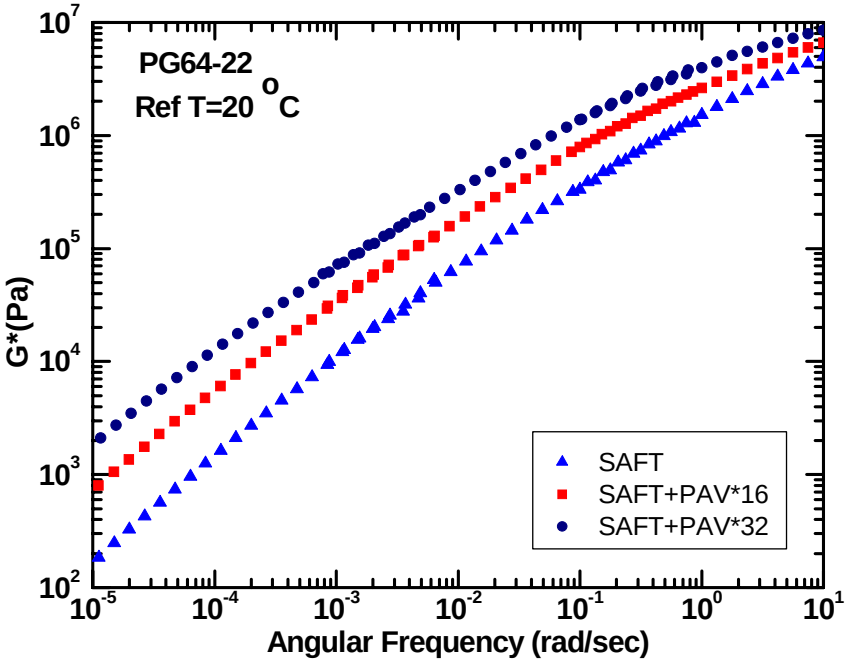

Figure B-18. Master Curves of Bryan Neat Binder for G*(ω).

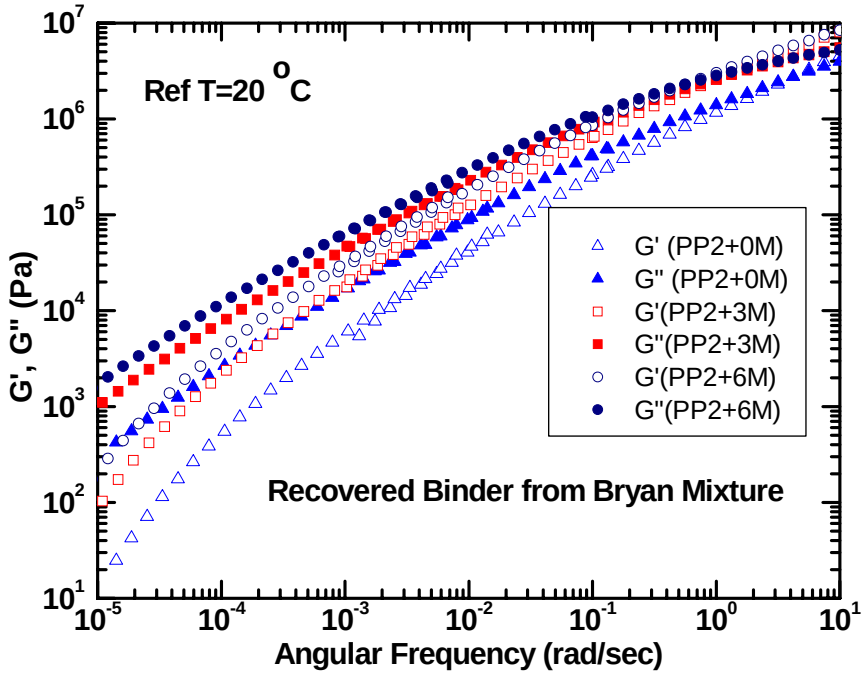

Figure B-19. Master Curves of Bryan Binder for G'(ω) and G"(ω).

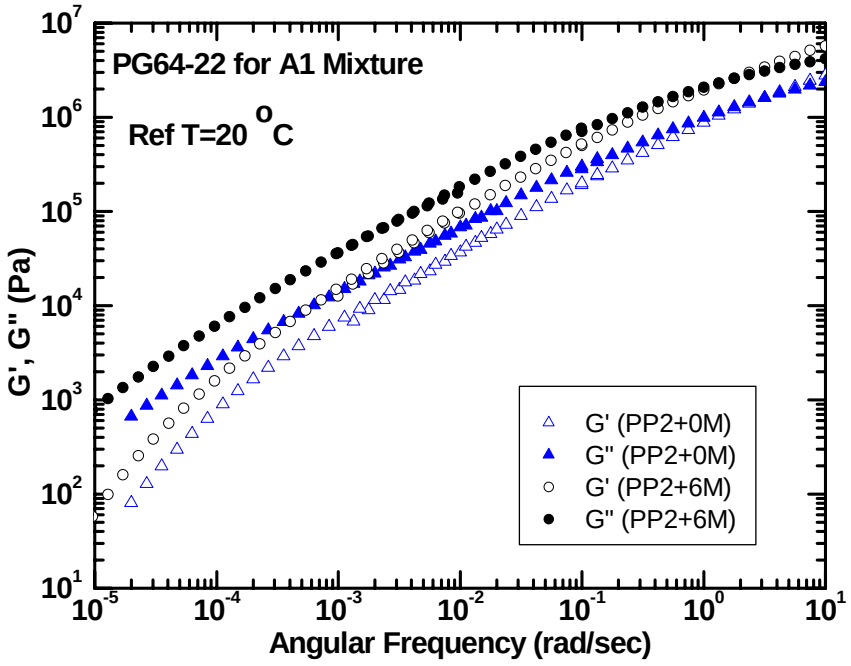

Figure B-20. Master Curves of A1 Mixture Binder for G'(ω) and G"(ω).

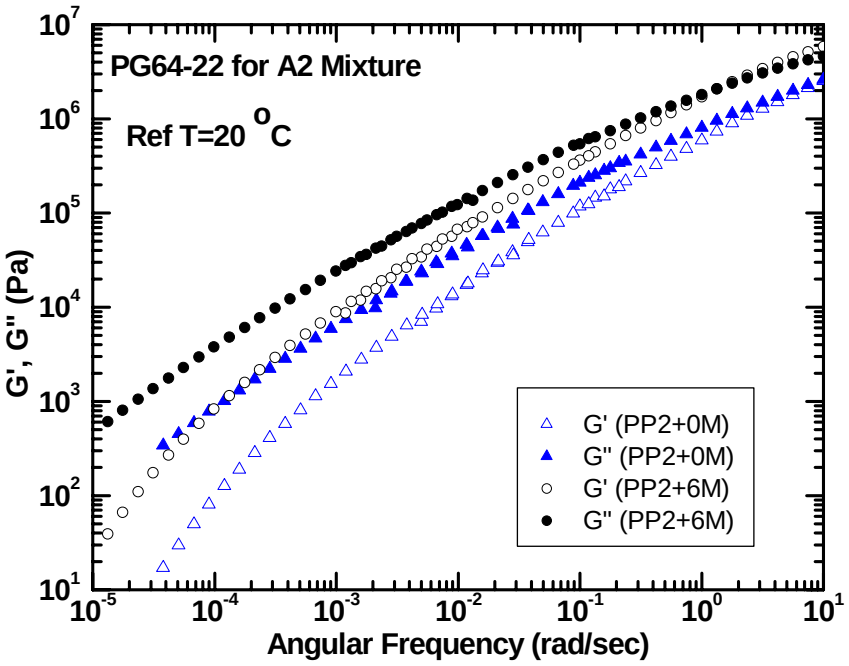

Figure B-21. Master Curves of A2 Mixture Binder for G'(ω) and G"(ω).

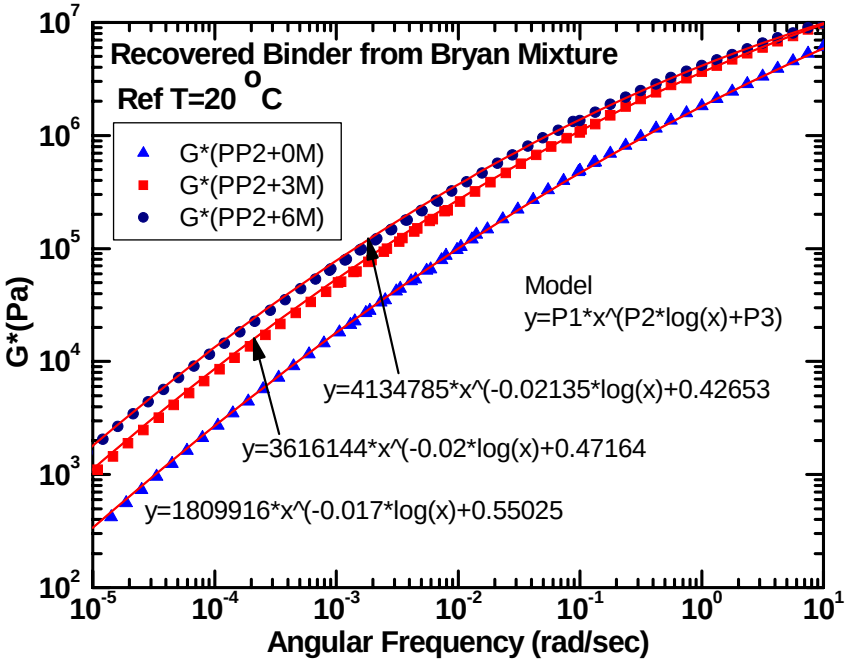

Figure B-22. Master Curves of Bryan Binder for G*(ω).

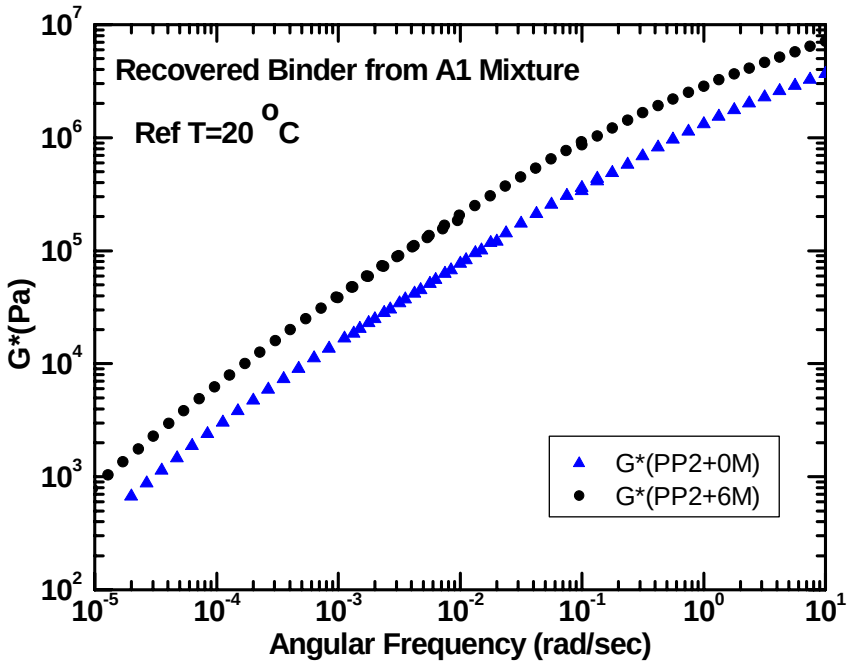

Figure B-23. Master Curves of A1 Mixture Binder for G*(ω).

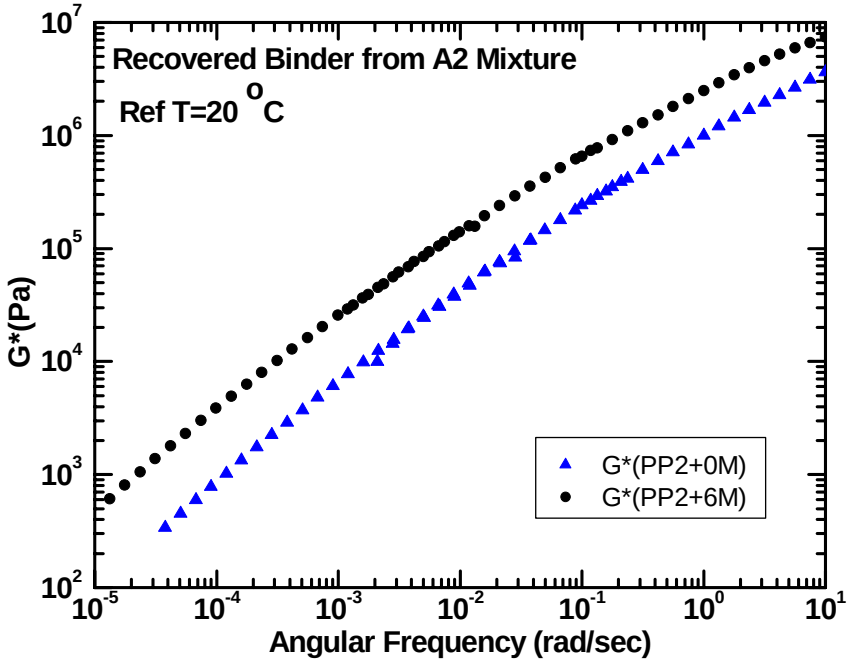

Figure B-24. Master Curves of A2 Mixture Binder for G*(ω).

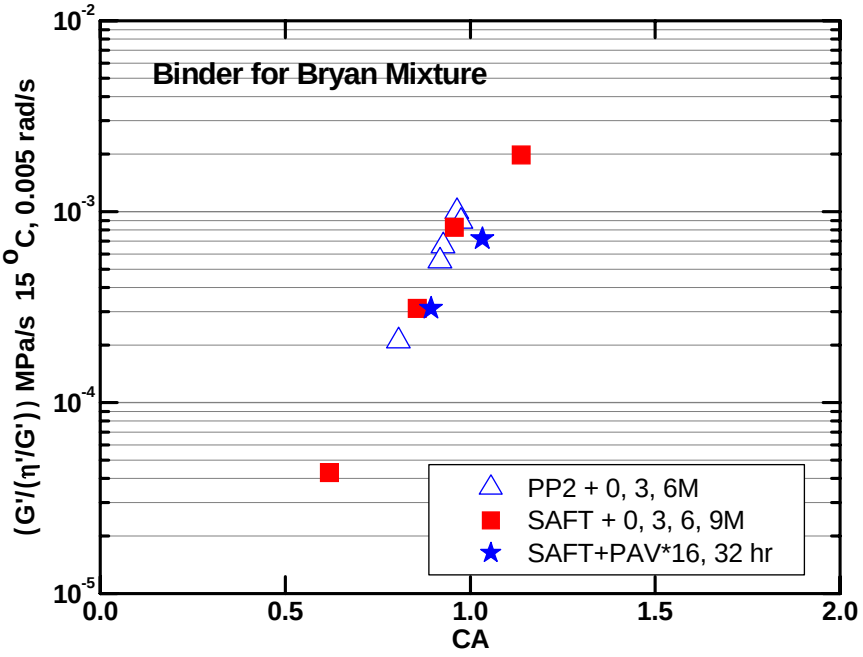

Figure B-25. DSR Function Hardening Susceptibility for Bryan Binder.

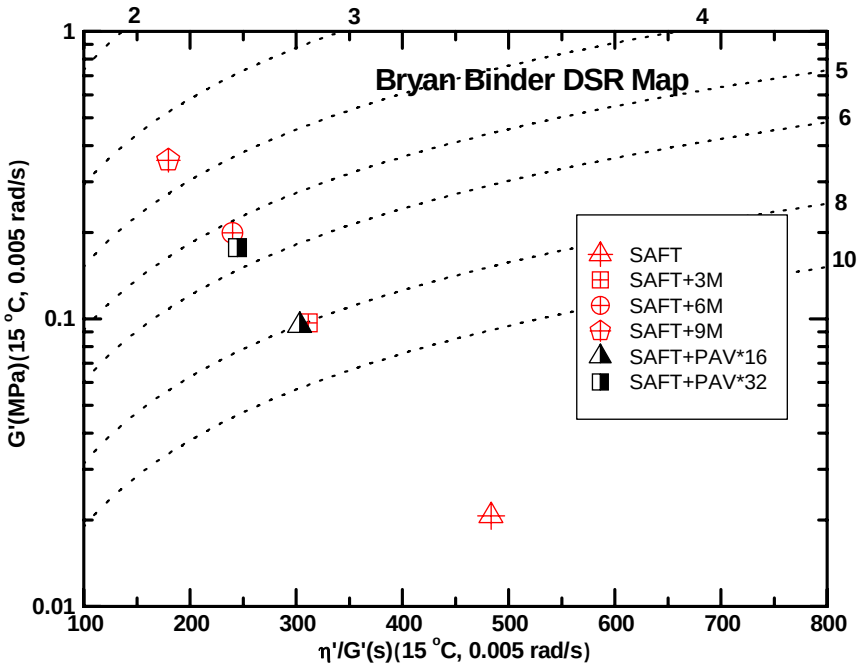

Figure B-26. DSR Map for Bryan Binder (Thin Film Aging).

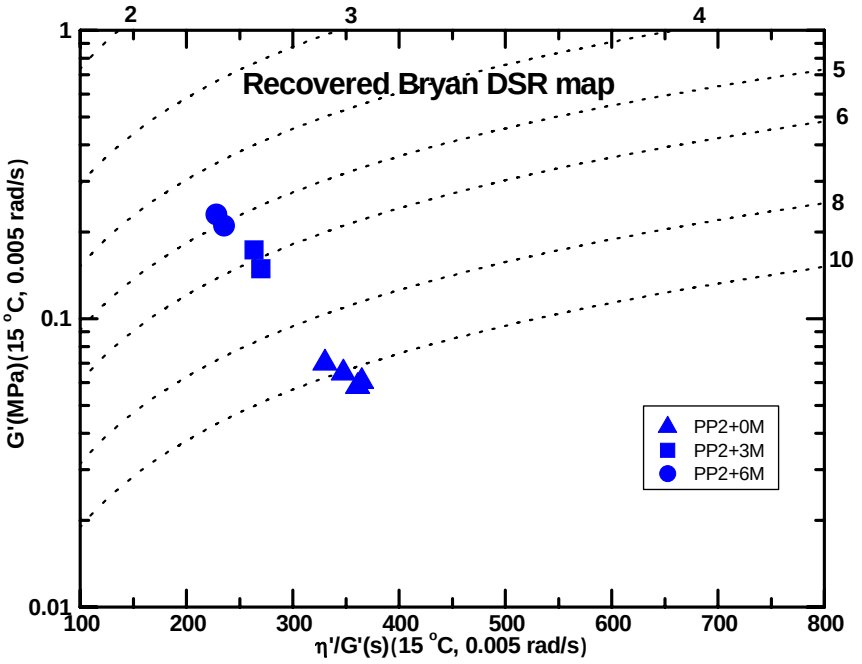

Figure B-27. DSR Map for Binder Recovered from Bryan Mixture.

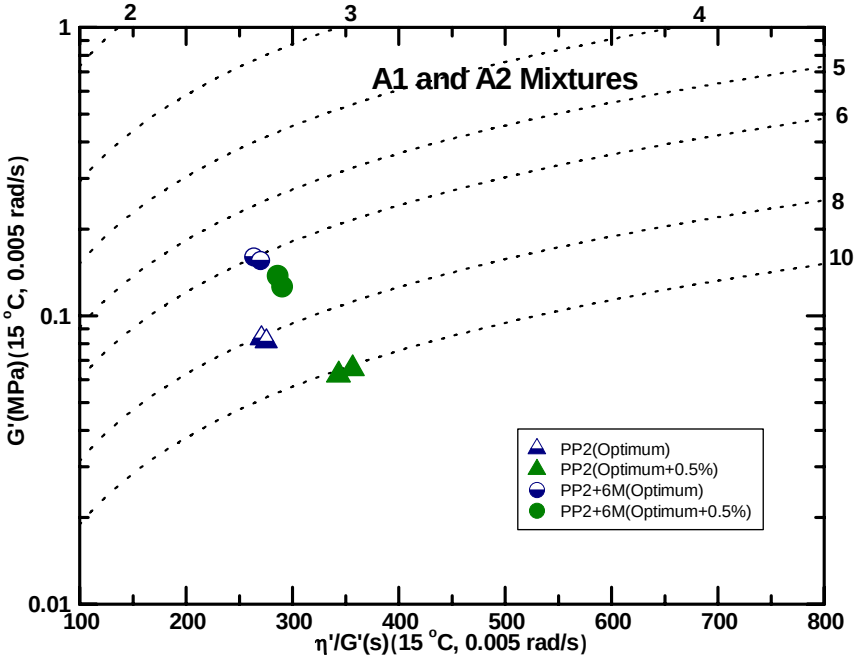

Figure B-28. DSR Map for Recovered Binder from A1 and A2 Mixtures.

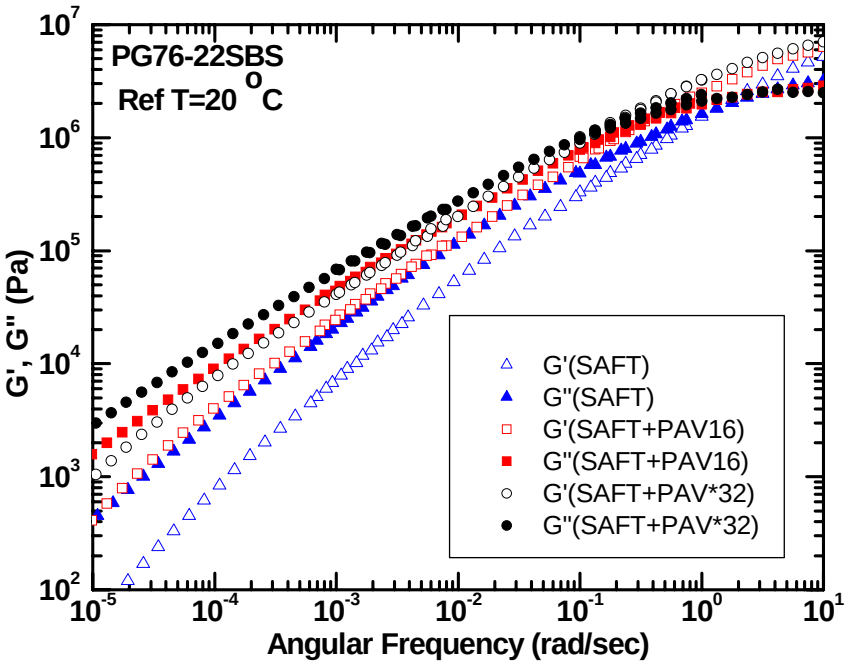

Figure B-29. Master Curves of Yoakum Neat Binder for G'(ω) and G"(ω).

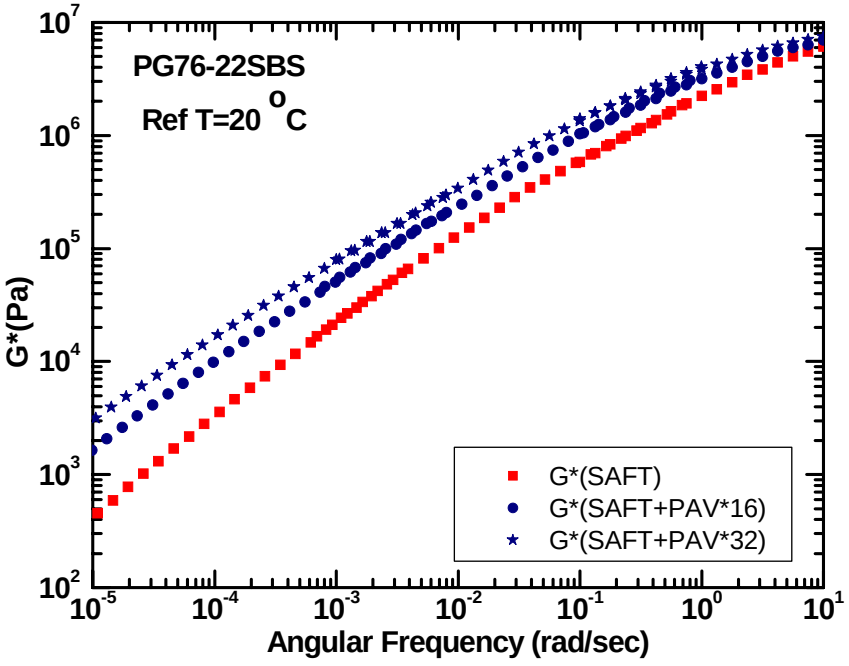

Figure B-30. Master Curves of Yoakum Neat Binder for G*(ω).

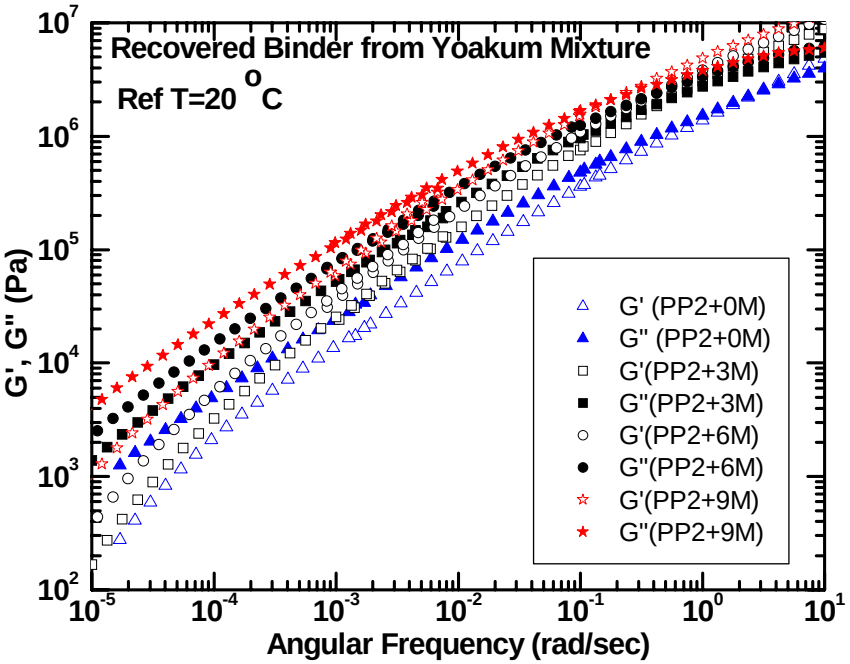

Figure B-31. Master Curves of Yoakum Binder for G'(ω) and G"(ω).

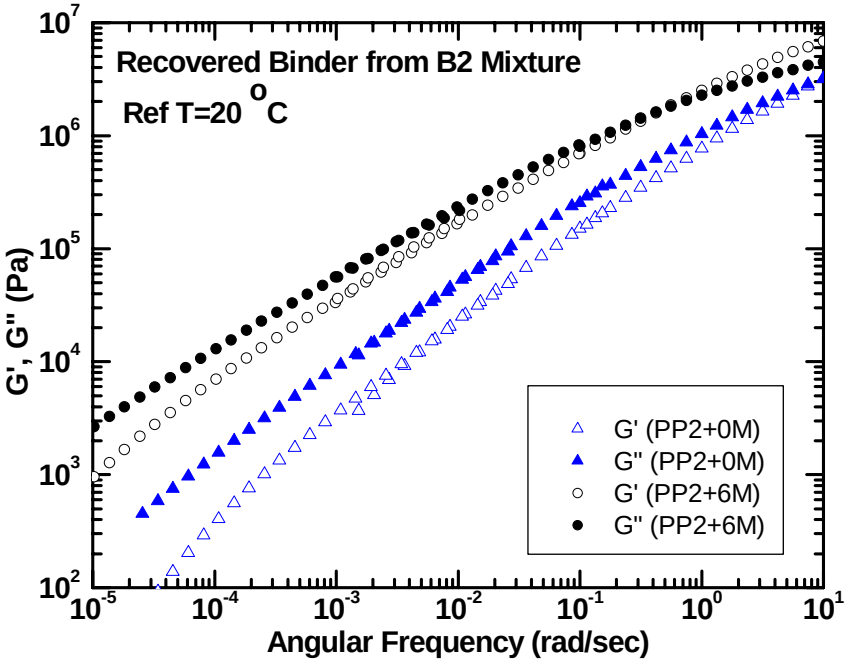

Figure B-32. Master Curves of B2 Mixture Binder for G'(ω) and G"(ω).

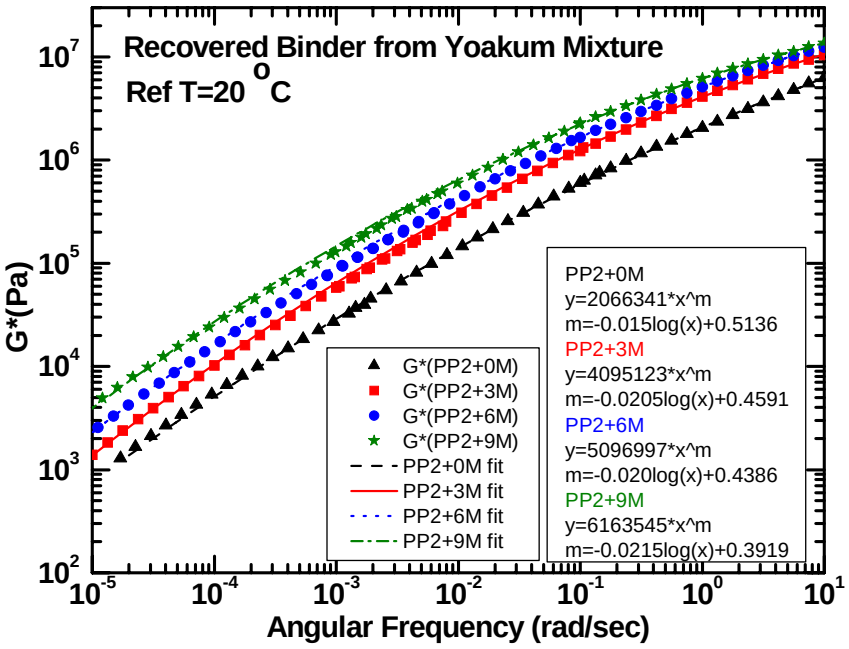

Figure B-33. Master Curves of Yoakum Binder for G'(ω).

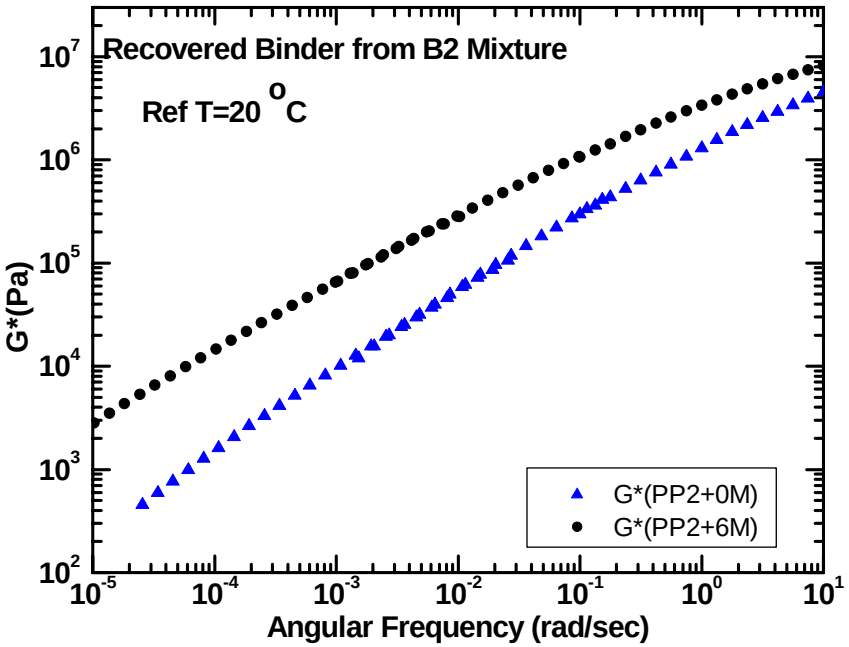

Figure B-34. Master Curves of B2 Mixture Binder for G'(ω).

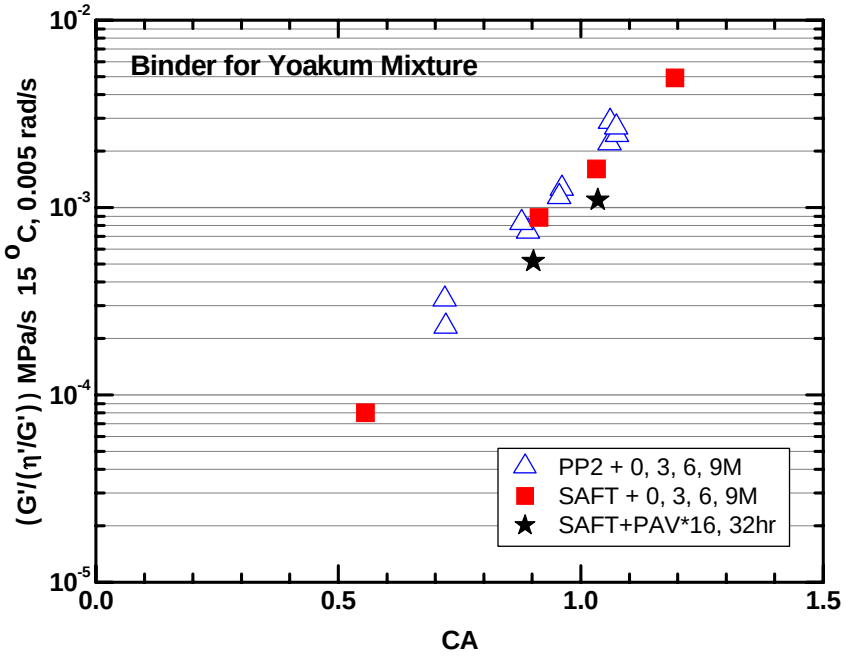

Figure B-35. DSR Function Hardening Susceptibility for Yoakum Binder.

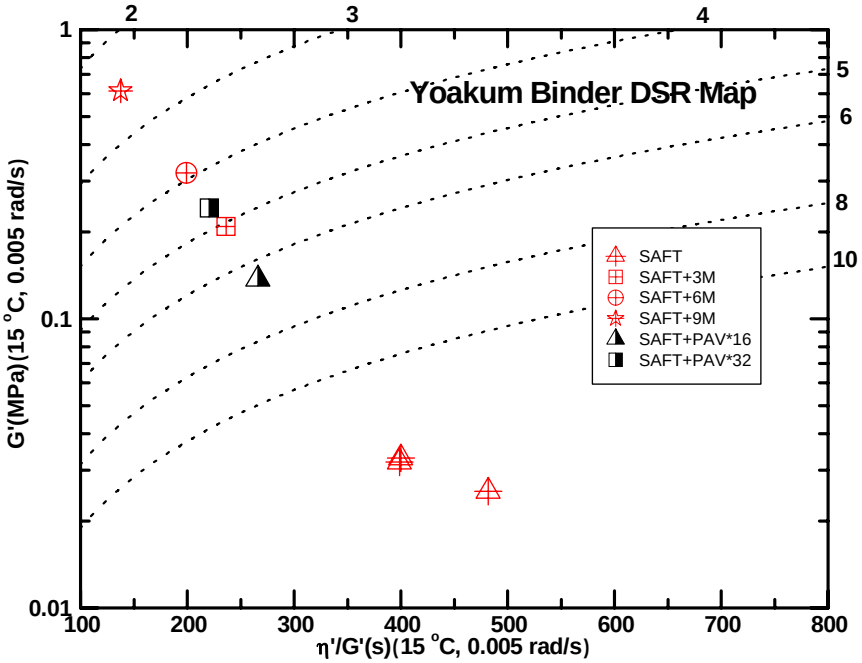

Figure B-36. DSR Map for Yoakum Binder (Thin Film Aging).

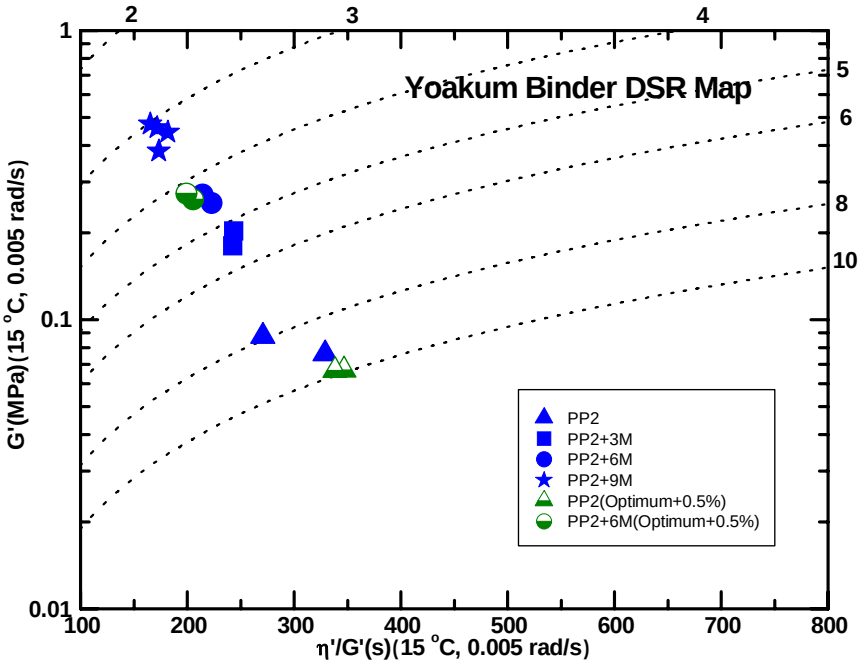

Figure B-37. DSR Map for Binder Recovered from B1, 2 Mixtures.

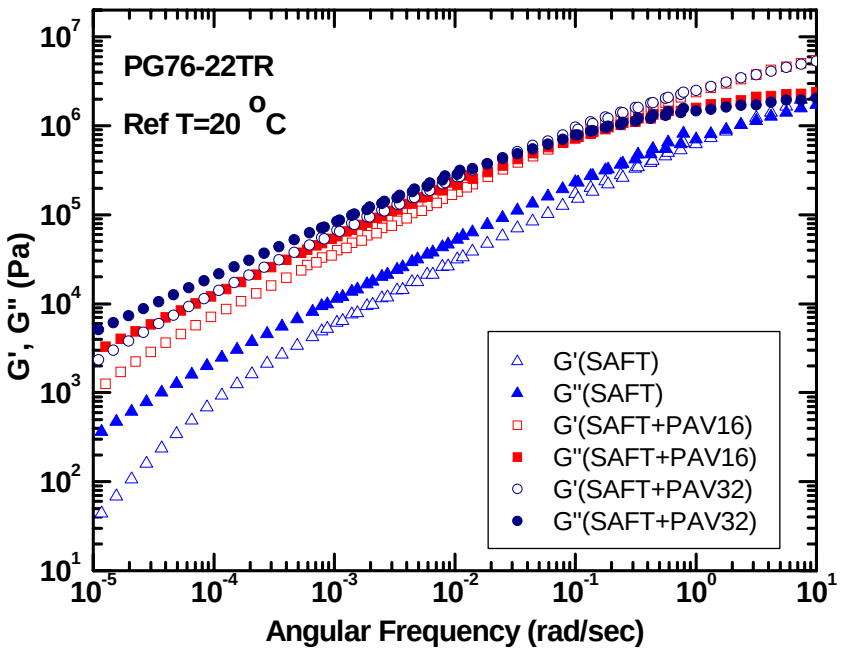

Figure B-38. Master Curves of C1 Mixture Neat Binder for G'(ω) and G"(ω).

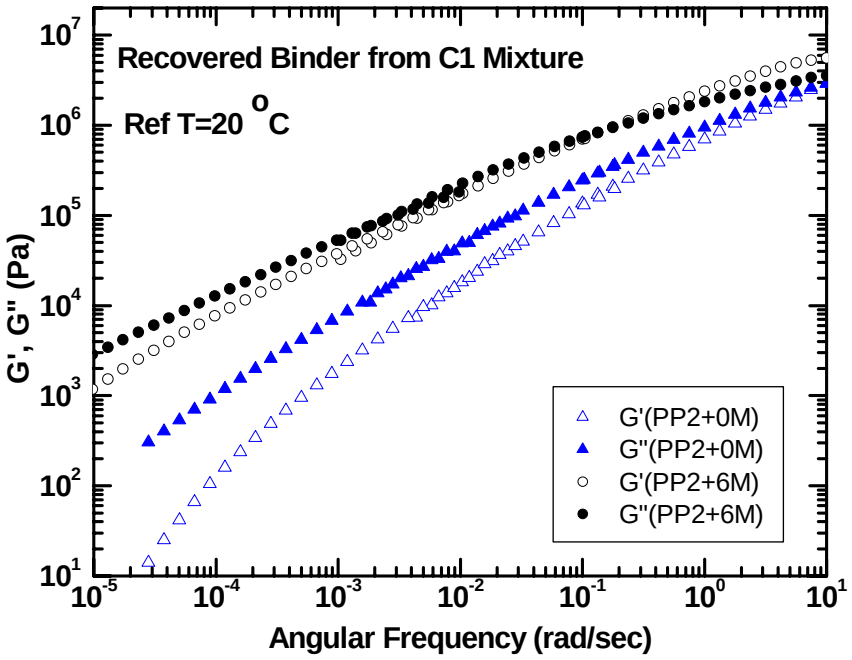

Figure B-39. Master Curves of C1 Mixture Binder for G'(ω) and G"(ω).

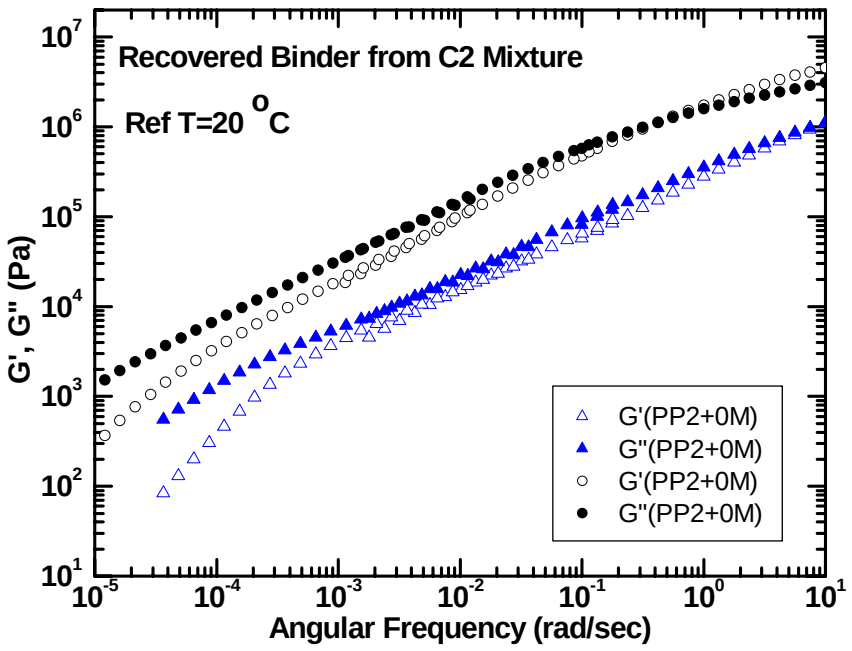

Figure B-40. Master Curves of C2 Mixture Binder for G'(ω) and G"(ω).

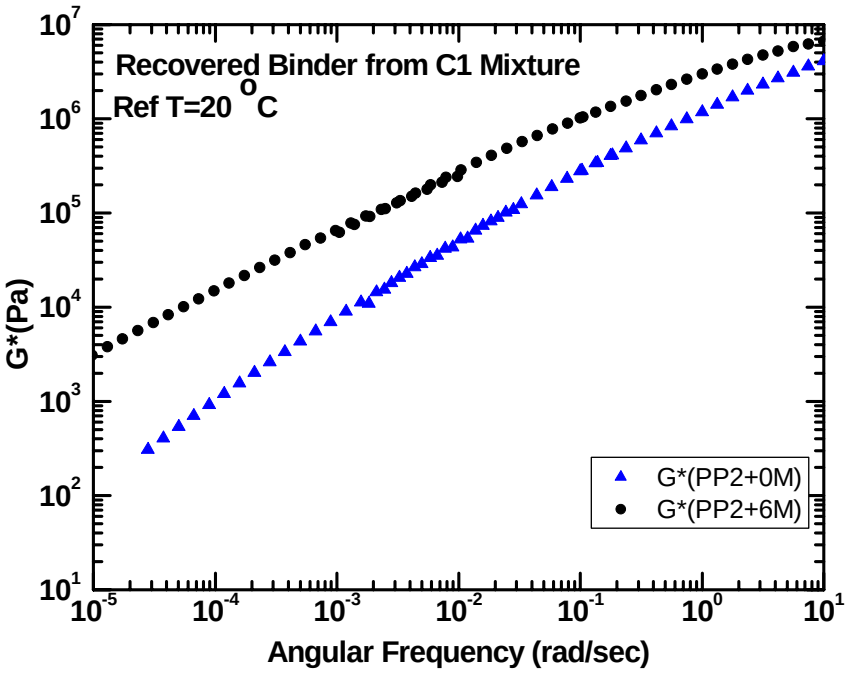

Figure B-41. Master Curves of C1 Mixture Binder for G*(ω).

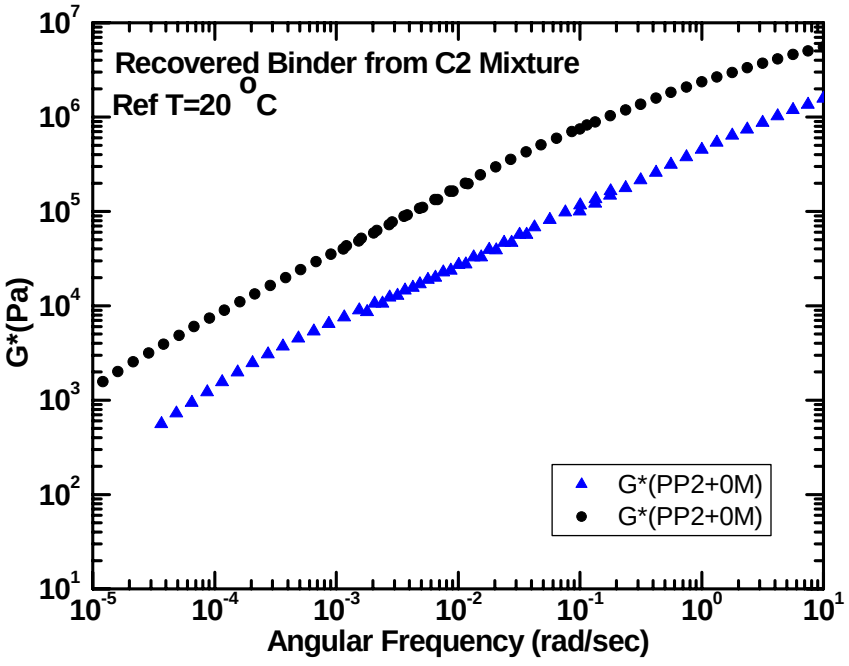

Figure B-42. Master Curves of C2 Mixture Binder for G*(ω).

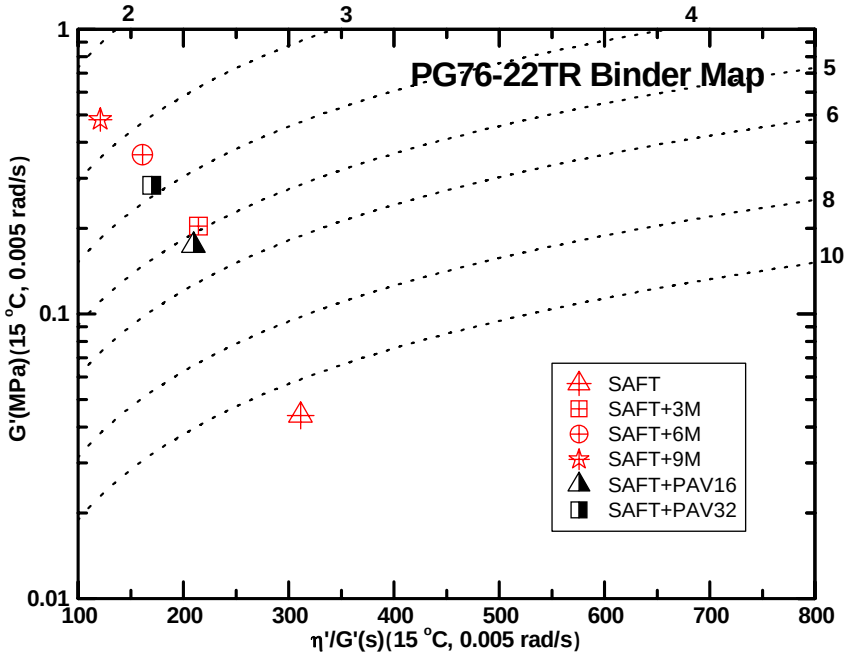

Figure B-43. DSR Map for C1 Mixture Binder (Thin Film Aging).

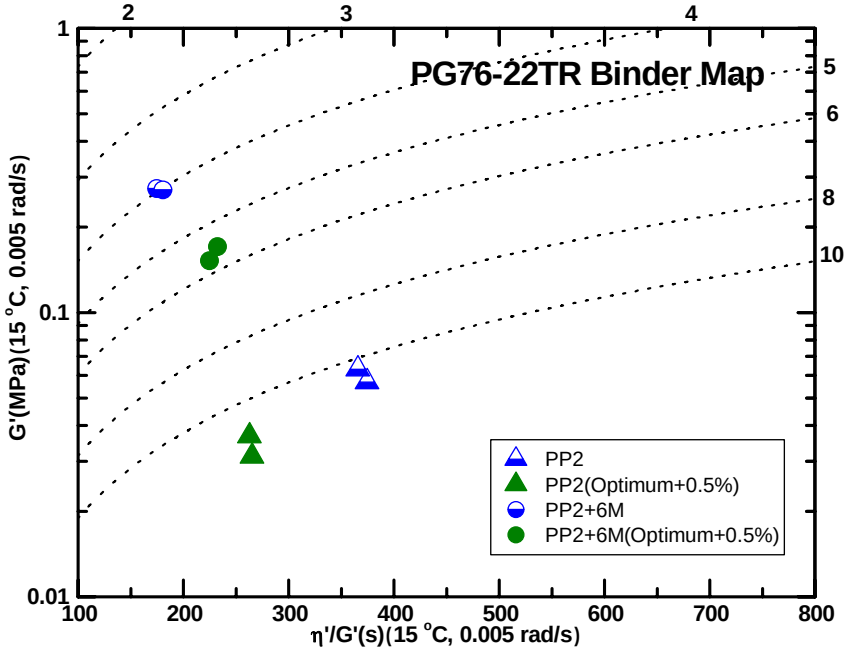

Figure B-44. DSR Map for Binder Recovered from C1, 2 Mixtures

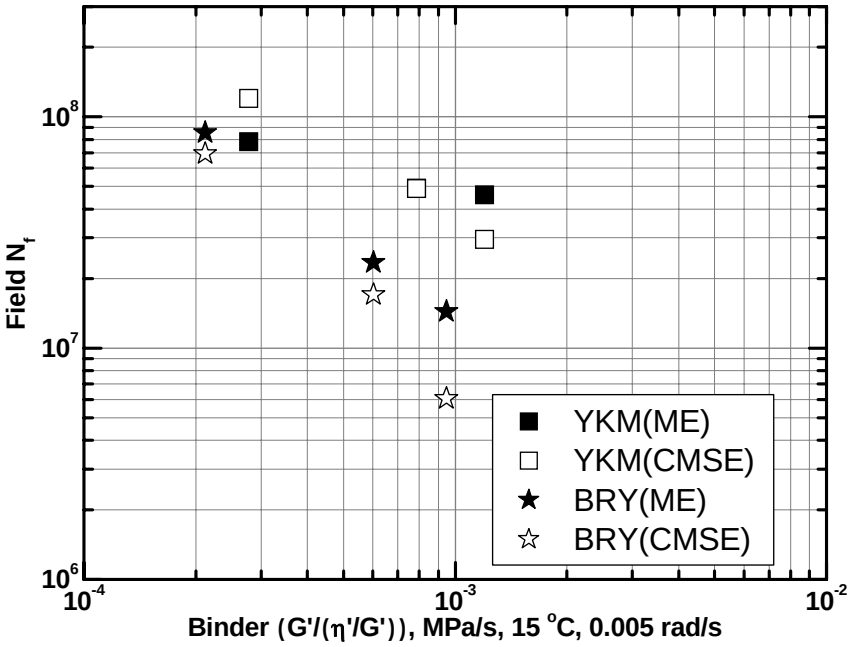

Figure B-45. Field N_f: CMSE versus ME.

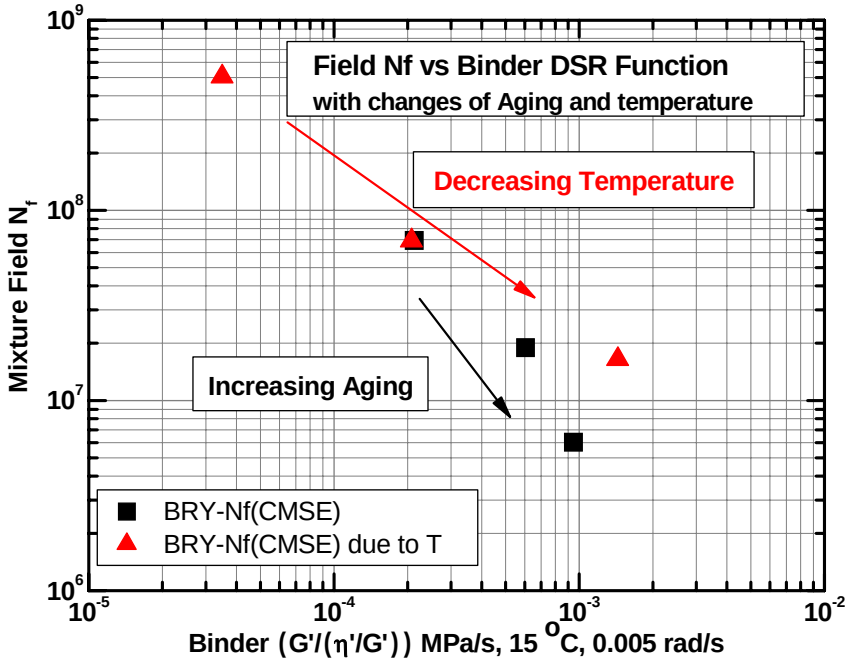

Figure B-46. Fatigue Life Decline due to Binder Hardening for Bryan Mixture.

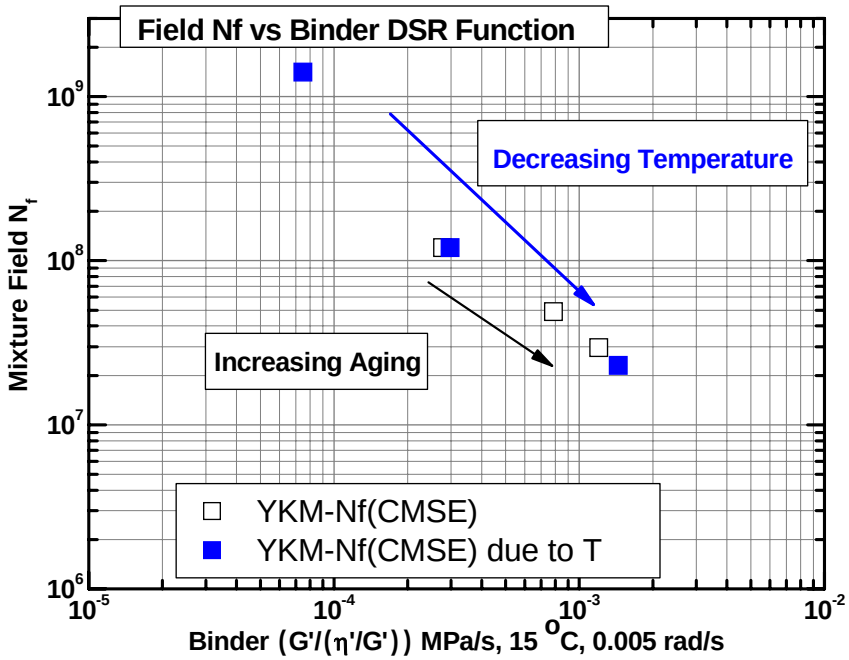

Figure B-47. Fatigue Life Decline due to Binder Hardening For Yoakum Mixture.

APPENDIX C
COPYRIGHT PERMISSION

To: Sung Hoon Jung
Texas A&M University

Dear Mr. Jung:

The Transportation Research Board grants permission to use in your dissertation your paper "Binder Oxidative Aging in Texas Pavements: Hardening Rates, Hardening Susceptibilities, and the Impact of Pavement Depth," coauthored with N. A. Al-Azri, K. M. Lunsford, A. Ferry, J. A. Bullin, R. R. Davison, and C. J. Glover, as identified in your e-mail of April 20, 2006, subject to the following conditions:

1. Please credit as follows:

   Presented at the 85th Annual Meeting of the Transportation Research Board, January 22, 2006, Washington, D.C., and accepted for publication in the 2006 series of the *Transportation Research Record: Journal of the Transportation Research Board* (forthcoming). Reprinted with permission of TRB.

2. None of this material may be presented to imply endorsement by TRB of a product, method, practice, or policy.

Every success with your dissertation. Please keep the *Record* in mind for future submissions.

Sincerely,

Javy Awan
Director of Publications
Transportation Research Board

VITA

Sung Hoon Jung was born on December 17, 1969 to Moo-young Jung and Gyung-ja Moon in Pohang, the Republic of Korea. He received his Bachelor of Engineering in chemical engineering from Soong-sil University in Seoul in February 1998 and his Master of Engineering in chemical engineering from Texas A&M University in College Station, Texas in May 2002. He continued to study for his Ph.D. in chemical engineering at Texas A&M University in May 2002. He graduated with his Ph.D. in August 2006. His current research interests include: binder oxidation and its effects on mixture fatigue performance; characterization of viscoelastic materials such as binders, HMAC mixtures and polymeric materials; material synthesis for better polymer modified binders; etc. He can be reached through the following address:

Department of Chemical Engineering, c/o Dr. Charles J. Glover
Texas A&M University
3122 TAMU
College Station, TX, 77843-3122